Light Flicker and Harmonic Modelling of Electrical Lighting

Lance Frater

A thesis presented for the degree of
Doctor of Philosophy
in
Electrical and Computer Engineering
at the
University of Canterbury,
Christchurch, New Zealand.

2015

ABSTRACT

Compact Fluorescent Lamps (CFLs) have emerged as cost-competitive, energy efficient direct replacements of the conventional incandescent lamp. However, little regard has been given to their widescale adoption in terms of the electrical network and power quality. Discrepancies have emerged over the CFLs light flicker sensitivity to voltage fluctuations and concerns at the level of harmonics they generate. This thesis develops an objective measurement method for light flicker, overcoming the limitations of the existing IEC flickermeter standard and develops models using the Harmonic State-Space (HSS) framework and Harmonic Domain (HD) for harmonic studies.

The new light flickermeter proposed, measures light directly to quantify flicker, thereby removing the dependency of the incandescent lamp modelled in the current flickermeter standard, IEC 61000.4.15. The light flickermeter methodology resembles the same functional blocks of the IEC Flickermeter to produce equivalent perceptibility levels. This allows for the direct comparison of the two procedures. The Light flickermeter along side the IEC voltage flicker are implemented in the experimental system and fully calibrated to the newly proposed CCU2/CIGRE flickermeter test protocol. The sensitivity of CFLs to common voltage fluctuations are investigated and the light flickermeter is utilised in the design of a new LED fluorescent tube replacement lamp.

A linearised Harmonic State-Space (HSS) framework is developed for the modelling of non-linear devices. The methodology includes basic Kirchhoffs voltage and current laws to realise a control block diagram approach to a device's operation. The HSS is centred around linear time periodic (LTP) systems and the use of harmonic transfer functions to model the switching behaviour (including Switching Instant Variation (SIV)) of converters. Importantly the models are suitable for both transient and steady state simulation. An example of a simplified CFL circuit is presented.

An automated sequential harmonic injection technique is developed for the experimental derivation of linearised harmonic admittance matrices of non-linear loads. This technique eliminates the traditional analytical based HD or HSS methods and creates a harmonic domain based model from the actual device. Models are presented for a number of consumer lamps. Detailed validation of these models are achieved under multi-frequency terminal conditions and through the illustration of self distortion by the system impedance.

This research paves the way in better understanding, management and coordination of flicker levels in electrical networks. The Light flickermeter apparatus provides a calibrated method for assessing light flicker sensitivity for both current and emerging technologies. The harmonic modelling methods are focussed towards lower powered devices and suited for studying their large scale use.

To Sarah
and Grandad

Harold Pemberton “Pem” Mayo
24 August 1917 — 03 July 2011

ACKNOWLEDGEMENTS

Foremost, I would like to express my gratitude to my thesis supervisors, Prof. Neville Watson and Dr. Alan Wood. Neville, thank you for your faith and the trust you placed in me, allowing me to choose my own research path, combining valuable experimental validation with theoretical foundation. Alan, thank you for making it harder, and introducing me to frequency domain modelling and eventually the HSS. Emeritus Professor Jos Arrillaga I am grateful for your confidence, encouragement and kind words.

I am truly indebted to the Electric Power Engineering Centre (EPECentre), for the financial support, but more importantly, for inspiring my passion of power engineering, as a subject of research and a career path. Thank you Joseph for your friendship and guidance.

I suffered greatly from anxiety and subsequently depression in my last few years of research. I nearly lost all the things I hold my dear to me: my marriage, my life, my family and friends. A huge thank you to the counsellors at the UC Health Center thank you Fiona, Graeme Warburton, Wendy, and Alex Mortlock. And also Steve Humm. I am thankful of Hugo's advice to seek help. The human mind is extremely powerful.

To those that came before me: Dr. Geoff Love, Dr. Bruce Smith, Dr. Graeme Bathurst, Dr. Hamish Laird, Dr. Norman Wereley, Dr. Thomas Keppler, Dr. David Hume, Dr. Christopher Collins and Chris Osauskas; I stand on the shoulders of giants.

To my colleagues, my friends, those whom I shared an office with, who came and went under me: Dave Smith (Danger Dave), Dr. Michael Hwang, Dr. Jordan Orillaza, Dr. Andrew Lapthorn, Clayton Mills, Hugo Vincent, Dr. John Stowers, Dr. William Kamp, Dr. Nick Murray, Dr. Simon Bell (MIA), Dr. Rob Turner, Blair Bonnet, Dr. Thahirah Syed Jalal (Mother Teresa), Dr. Bhaba Das (BP), Dr. Ali Farzanehrafat (that's illegal), Dr. Rowan Sinton, Ryan Van Herel (Harry Potter), Jeff Wei, Alejandro Castellanos Escamilla (Mexican Drug Cartel), Pramod Ghimire, James Ormrod, Dr. Nikki Newhan, Irvin Chew, Dr. Victor Lo, Patrick Chen, Rabia Nazir, Diwakar Bhujel, Ming Zhong, Kelvin Gong (kdog), Jennifer Wen, Vijay Bendre, Shreejan Pandey, Debbie Dick, Kalyan Malla, Parash Acharya, Yanosh Irani, Steffen Fischer, Laura King, Michael Frampton, Pierce Hennessy, Hantt Cao, Dr. Wade Enright, Dr. Stewart Hardie, Dr. Vocker Nock and Dr. Robert Eriksson (thank you for the invite to KTH Sweden).

You all harassed and made fun of me about my thesis, some were worse, Joseph! and some took the more amusing approach, namely Blair who launched www.haslancefinishedhisthesis.info and printed stickers to keep people up to date. It then redirected to www.lancehasfinishedhisthesis.info once I submitted.

Some of the best times were spent discussing and whiteboarding the worlds problems, the harmonic domain, electrical machines, transformers, control and generally ending up going back

to fundamentals. We spent many hours experimenting and conceptualising; Freaky Friday, HV Marshmallows, the allspark, IDMT relays, exploding wires, the countless Machines Lab and HV Lab Demo's to schools and tour groups, they all enlighten my passion for power and education. The Canterbury earthquakes lead to some depressing and frustrating times, thanks to all those that joined in celebration of each aftershock or tried to ride the wave.

Distractions helped me cope, I worked on many projects including; electric bikes/scooters/sidecars, electronics, smokers and hangi kegs, web development, axolotls and their axolittles, and took on many trades; car dismantler, brewer, concrete machine. I enjoyed my time as President of Fendalton Badminton Club, experimenting with black-light badminton and donated time to Badminton Canterbury.

I learnt (and gathered) so much from our technicians: Ken Smart (My go to man), Dave Healy, Jac Woudberg, Paul Agger, Edsel Villa, Scott Lloyd, and the late Ron Battersby as well as the computer staff: the late Pieter Kikstra (Best Computer Technician In the World), Mike Shurety, Dave van Leeuwen. You guys were always happy to answer my questions or have a discussion. You all contributed to me and my time at UC.

It was important that I picked up diverse range of contract work while studying. I am particularly thankful for the time spent with Shayne Crimp, Aiotec Ltd. working on the IEC certification of the Windflow 500 turbine. Thanks also to: Nick, Mighty River Power, Ashok, Vector, and the boys at Infact for the experience and expertise gained.

It is many years since I started and first hosted DC++, the Direct Connect Hub (UCDC), from my first year dorm in College House. A great community developed and provided a constant source of entertainment. The notorious hub, was taken down many a time but it (Nahub) some how ended up back in my office and under my administration. My legacy lives on in hubs still running around campus. whitestatic +whatsnew

A few quotes and wise words:

"If something doesn't work, you are doing something stupid"
"Everything has to be linear"
"Don't talk when you have no idea what you are talking about"
"Yanni your girlfriends here"
" 'The time has come,' the Walrus said, 'To talk of many things:' "

Finally I must thank my family and friends. For my friends especially Dr. Dan, Chris (Wobbler), Gina, Phil (Botros), Kris (KKK-Kris) and Ryan (Jesus), thanks for all the good times and distractions, being pirates, mountain biking and down-hilling. More than ever my Mum, for always giving me the advice that I can give up if I wanted to, and Dad for the love and support in every way. Thank you for allowing me to take on this challenge, did you even have a choice? Clint and Jac, Liam and Riley and little Bowen, Nikki and Tom, my Australian Mum and Dad, thank you. I am forever grateful of my South Island Mum, and Percy for taking me under your wing, inviting me to the family Bach, the one place I was truly free from my thesis. Kerry, the kids, and Glenn for getting the wolf pack together. Karen (Nurse,) and Gerrad I can't thank you enough, your care and support critical to my Ph.D. Scotty and Alice my little bundles of joy, you kept me going. A special thanks to Gerrad, Micheal and Blair for the time you spent forcefully helping me and reviewing my thesis.

Grandad, I admire your methodical thinking and distinction, you shaped the person I am today. A great mind of a different time. Grandad had great respect for education, even starting at the youngest of age. The Harold Mayo Kindergarten, Heretaunga, Hastings was named after him for his work and involvement. For you I climbed to the top.

My wife Sarah, I owe myself to you, I give you my heart, I give you my everything. You braved through my seemingly irrational behaviour, my messy house and disregard. I became a person I never wished to be, I am sorry. Your love and support throughout my life has only made this possible.

To Sarah and Grandad, I dedicate this thesis.

CONTENTS

GLOSSARY

NOMENCLATURE

$\mathbb{C}$	Set of Complex Numbers
$\mathbb{R}$	Set of Real Numbers
$\mathbb{Z}$	Set of Integer Numbers
T	Temperature
ω	Angular frequency
ω_0	Fundamental angular frequency
ω_n	Natural angular frequency
ϕ,ϕ_v	(Total) Luminous Flux to $V(\lambda)$, lm
ϕ_e	Radiant Flux, W
ϕ_v	Luminous Flux, lm
A	Time Invariant Dynamics Matrix
B	Time Invariant Control Matrix
C	Time Invariant Measurement Matrix
D	Time Invariant Direct Feedforward Matrix
E_v	Illuminance, lm/m^2
I	Identity Matrix
I_v	Radiant Flux, $lm.sr^{-1}$
L_v	Luminance, $lm/m^2/sr$
M	Highest harmonic order of the Output
N	Highest harmonic order of the Input
P_{lt}	Flicker Severity Index (Long Time 120min.)
P_{st}	Flicker Severity Index (Short Time 10min.)
s	Complex frequency, complex argument of Laplace transform
T	Fundamental Period
$V(\lambda)$	CIE spectral luminous efficiency function
X,$X(w)$	Harmonic domain vector of coefficients
ac	Alternating Current
dc	Direct Current
hvdc	High Voltage Direct Current

ABBREVIATIONS

ADC	Analogue to Digital Converter
AI	Analogue Input channel
AMIT	Amplitude Modulated Impulse Train
AO	Analogue Output channel
CFL	Compact Fluorescent Lamp

DAC	Digital to Analogue Converter
DAQ	Digital AcQuisition
DHD	Dynamic Harmonic Domain - Equivalent to HSS
EHD	Extended Harmonic Domain - Equivalent to HSS
EMP	Exponentially Modulated Periodic
FACTS	Flexible ac Transmission Systems
GI	General Input channel
GLS	General Lamps for Service
GO	General Output channel
HD	Harmonic Domain
HSS	Harmonic State Space
HTF	Harmonic Transfer Function
LFL	Linear Fluorescent Lamp
LTI	Linear Time Invariant
LTP	Linear Time Periodic
MEPS	Minimum Energy Performance Standards
PCC	Point of Common Coupling
SCR	Short Circuit Ratio
SI	Switching Instant
SIV	Switching Instant Variation
SVD	Single Value Decomposition

LIST OF FIGURES

LIST OF TABLES

Chapter 1

INTRODUCTION

1.1 GENERAL

Electric lighting has inspired the electrification of towns, cities and countries around the world. Artificial lighting has extended the usable hours of the day, created safer working conditions and provided comfortable living environments. The contribution of electrical lighting and the supporting electrical network is undoubtedly vital to our current way of life.

As the global demand for energy continues to increase, pressure mounts to reduce CO_2 emissions from carbon based fuels. In both developed and developing nations, the growing electricity demand is now being met by either developing or securing new energy sources to increase capacity, or by improving the way in which current resources are utilised through greater efficiency. The ability to build new generation capacity has been constrained in recent years due to imposed government polices, environmental constraints, and market risk through deregulation. Nearly all sectors of the industry are now responding to increase the efficiency of their electricity use. For consumers, greater efficiency reduces core energy costs. For network asset owners and operators, efficiency reduces system losses and can offset investment.

Lighting New Zealand residential homes equates to around 8 % of the total energy demand and around 14 % for public areas and businesses. It is estimated lighting annually contributes 2.65 million tonnes to NZ's greenhouse gas emissions. Similarly, throughout the world, lighting represents a considerable network load. Electrical lighting has significant potential to improve efficiency by the adoption of alternative, energy efficient lamp technologies. They offer substantial economic and environmental gains with relatively low capital investment.

Traditional incandescent lamps have remained relatively unchanged since their invention in the 19^{th} century and have long been known to be inefficient sources of electrical lighting; only around 5% of the input power is converted into visible light. Recently, Compact Fluorescent Lamps (CFLs) have emerged as cost-competitive, energy efficient alternatives to replace conventional incandescent lamps in their existing fittings. CFLs offer 4-5 times greater efficiency with an increased lifespan, typically over 6,000 hours compared to around 1000hrs for incandescent lamps. While the cost of CFLs is between three and ten times greater, the initial investment is recovered in a number of months and they continue to offer significant savings over their lifetime.

The adoption of CFLs by consumers has been aided by a dramatic reduction in cost and through numerous subsidised and promotional programs within New Zealand and throughout the world. Recently the EU released new minimum energy standards for electrical lighting. By 2020, a

phased approach will require manufactured lamps to meet increasing efficacy levels and is set to reduce energy Minimum Energy Performance Standards (MEPS) [5] are already in place in Australia and phasing out of the importation [7] and sale of low efficiency incandescent lamps is already underway [8]. New Zealand has formed a joint MEPS program with the Australian Equipment Energy Efficiency (E3) Programme [18].

The promotion of CFLs has also doubled as a medium to raise consumers' awareness of energy usage and educate them of the benefits of using energy efficient alternatives. As a result, the demand for higher efficiency appliances has accelerated, driving the redesign of existing devices to improve their energy efficiency and the development of new technologies to deliver greater performance and added functionality to consumers. As these technologies penetrate the distribution system its operation is changing in two ways:

- Firstly, distribution systems are becoming more active in the generation of their electricity through the installation of distributed generation, thereby being less dependent on bulk generation from major generating plants. For example, consumers are installing distributed generation in the form of micro windturbine, solar PV and micro combined heat and power directly within their premises.

- Secondly, conventional loads are being replaced by their more energy efficient alternatives. These are predominately linear loads such as resistive heating, incandescent lamps, synchronous and induction machines that are being replaced by more energy efficient and functional alternatives. Respectively, this has seen the increased use of heat pumps, compact fluorescent lamps and variable speed drives (VSDs).

Common to the modern alternatives is the use of semiconductors for control and power conversion. The non-linear behaviour of semiconductors increases the complexity over the existing linear devices. This makes the task of modelling and characterisation of loads increasingly difficult and more challenging for system operators.

Maintaining voltage quality (commonly referred to as power quality) in light of these changes is becoming of greater importance to the network. Although the power ratings of individual consumer loads are low, their accumulated effect at the points of connection can be considerable and the impact on voltage quality of the supply substantial. There is little indication that this trend will not continue into the future, meaning the electrical network will eventually become saturated with these non-linear type loads. It is therefore paramount that voltage quality levels are maintained to ensure adequate service quality for all connected consumers.

One of the more obvious effects of poor power quality is visible light flicker from electrical lighting. The light flicker phenomenon is the sensation caused by the variation of luminous intensity on the human perception system. For humans, light flicker generally results in annoyance and discomfort, however in some situations can lead to serious health hazards, such as loss of concentration or the triggering of epileptic seizures. Light flicker is caused by fluctuations of the system voltage and the subsequent variation of light output from electrical lighting. Within the electrical network these voltage distortions is simply referred to as flicker.

The complexities of the human physiological system and the stochastic nature of power systems have lead to the standardisation of flicker measurement in IEC standard 61000-4-15 [3]. The standard describes the function and design of a flicker instrument (a flickermeter) to analyse the

systems voltage waveform to quantify the flicker from a 60W incandescent lamp as perceived by the average human. Because CFLs use electronic ballasts, their non-linear behaviour has made modelling of their operation difficult. Equally their susceptibility to voltage disturbances resulting in visible light flicker is widely unknown and difficult to predict. With the adoption of energy efficient lighting the IEC flickermeter standard fails to quantify the actual light flicker experienced.

Harmonics are generated through the switching process of power electronic components. Harmonic current flowing back into the system distorts the system voltage and gives rise to increased system losses. In more serious situations, harmonics can lead to instabilities, increased aging or the malfunction of network infrastructure or customer loads.

In harmonic studies, low power consumer devices are traditionally ignored due to their insignificant current drawn from the system. Their highly variable and complex design means the accuracy gained by modelling of such loads does not warrant the extra computational requirements. On the other hand, large static power converters such as motor drives found in industrial plants, metal-smelting and HVDC links have been comprehensively modelled and included in harmonic simulations and studies [24, 53]. Despite the individual contribution of a single CFL being small, their cumulative effect can be considerable with their combined rating easily exceeding that of an HVDC link. In addition, the dispersed nature of these low power types loads makes possible mitigation of voltage quality problems difficult.

1.2 RESEARCH OBJECTIVES

Continuing changes to electrical networks has heightened the need to reassess the power systems' technical performance to maintain the same level of reliability and quality of power. Constant reconsideration of regulatory standards that govern the network operation are needed to ensure they conform to the current state of the system and changes likely in the foreseeable future. The primary objectives of this research are to develop an objective measurement method for light flicker and to develop models for both harmonic and flicker studies of modern electrical lighting systems. The power quality aspects of light flicker are reconsidered for modern lamp technologies and harmonic models are developed to simulate their network behaviour.

The widespread adoption of high efficiency lamps began to highlight the discrepancies between the measured flicker levels by the UIE/IEC 61000-4-15 standard and the actual levels experienced within the electrical system. The standard contains a model of a 60W incandescent lamp, limiting its measurement of flicker to this single lamp type; this the primary reason for the discrepancy. By removing the dependency on this single lamp, the quantification of flicker can be made directly from a light source, and for any lamp independent of its technology. Alternatively, by the same technique, comparison can be made between the susceptibility of the lamp technology to voltage fluctuations that may cause light flicker.

Complete and accurate modelling of a full power supply network is a formidable task. Its size, complexity and uncertainty requires careful consideration to formulate the most appropriate approach. Time domain simulation techniques are unsuitable due to the multitude of device models to create and the excessive computation necessitated by use of small time steps to accurately model the convertor switching behaviour. Frequency domain simulation techniques capitalise on the relatively linearisable frequency coupling characteristics of power electronic convertors. Through the use of linear algebra, highly complex systems including convertor

models can be condensed into single transfers and solved almost instantaneously or through the use of iterative methods. The frequency domain offers valuable insight into the device characteristics and can be formed analytically or by experimental techniques.

The propagation of flicker is well understood through many years of observation and statistical averaging. The prediction of light flicker originating from modern lamps, however, has been largely confined to experimental studies. Modelling the strong interconnection between the lamps supply voltage and its light output.

In summary the primary objectives of this thesis are:

- Develop a light based flicker measurement technique to overcome the limitations of the present IEC flickermeter standard.
- Implement the Light Flickermeter in an experimental test system for calibration and investigation of the flicker sensitivity of modern lighting technologies.
- Develop a linearised harmonic domain state-space model framework for the study of steady state and transient cases.
- Automate the experimental formulation of frequency coupling admittance matrices suitable for consumer based appliances.

This work is part of a broader investigation undertaken by the Electric Power Engineering Centre (EPECentre) at the University of Canterbury, commissioned by the Government and power companies (through the EEA) on the impact of the future distribution system on power quality. Parallel investigations are being carried out by co-researchers on the impact of heat-pumps, irrigation plants and renewable generating sources.

1.3 THESIS OUTLINE

This thesis is structured into two main parts, Light Flicker and Harmonic Modelling, as depicted in Figure 1.1. Central to these two areas are the electrical lamps, their construction and performance, and also an experimental system developed and utilised throughout the research. It was envisaged to extend the harmonic modelling techniques (HSS) for the prediction of flicker, however, the greyed out section Light Flicker Estimation was not included in the thesis.

Chapter 2 begins with a review of power quality aspects of electrical light flicker and harmonics. This is followed by a summary of commercially available lamp technologies, the techniques for standardised measurement of light flicker and the discrepancies in the IEC methodology identified. Finally a review of steady-state/transient frequency domain and harmonic modelling is presented, along with device representation and simulation solution methods.

Chapter 3 introduces the experimental system developed as part of this research. The system is designed as a general, low voltage, 3-phase test platform, capable of reproducing and measuring a wide variety of simulated system conditions. Industrial grade hardware is utilised in the design to achieve accurate and robust measurement conditions. A general overview of the software architecture to automate the testing procedures is given. In addition, the constructed light measurement equipment for the investigation of light flicker is detailed.

Chapter 4 proposes a light based flicker measurement technique. The light flickermeter resembles the methodology of the IEC voltage flickermeter and allows for direct comparison and calibration. Both flickermeters are implemented in the experimental system and calibration is performed to the proposed CIGRE Flickermeter Test Protocol [12] and the calibration requirements of the current standard[6].

Chapter 5 investigates the sensitivity of modern lighting technologies to voltage distortions that result in visible light flicker. Results demonstrate the application of the light flickermeter with different lighting technologies and illustrates the relationship between a lamp design and their flicker sensitivity. A prototype driver circuit for a new LED based fluorescent replacement lamp is designed for minimal flicker sensitivity.

Chapter 6 develops a linearised Harmonic State-Space (HSS) modelling framework for non-linear devices. The framework is based on single phase devices, preserving full convertor actions in both steady state and transient interaction using optimised tensor representation. An Example is given for a simplified CFL circuit.

Chapter 7 describes a sequential harmonic injection technique used to form linearised harmonic admittance matrices of non-linear devices. This technique is automated using the experimental test system introduced in Chapter 3 and frequency transfer matrices can be built for any consumer device. A key advantage is that the device can be considered as a 'black box' and the model is formed without an in depth knowledge of the devices operation. Models are presented for a number of consumer lamps and validated under multi-frequency terminal conditions and through the illustration of self distortion by the system impedance.

Chapter 8 concludes the research presented within this thesis and discusses possible future research directions.

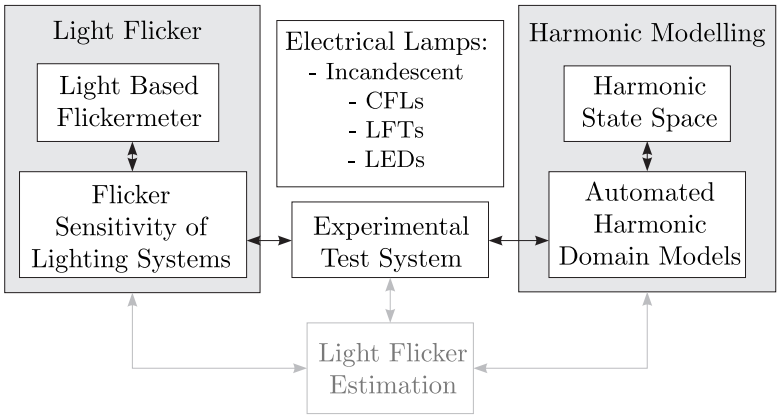

Figure 1.1: Thesis Structure: Light Flicker and Harmonic Modelling of Electrical Lighting

Chapter 2

A REVIEW OF FLICKER MEASUREMENT AND HARMONIC MODELLING TECHNIQUES

2.1 INTRODUCTION

The first electrical networks were constructed for the operation of electrical lighting. Many of these operated at DC and supplied incandescent lamps. It was not until 1886 that AC was first demonstrated as a means to distributing electricity for electrical lighting. Not long after, light flicker and harmonics were first reported. Light flicker was attributed to poor voltage regulation of the generator controllers. Harmonics were initially observed through transformer core saturation and the saturation of generator machine slots.

Electrical lighting went on to play an important role in the selection of the AC frequency of todays networks. In 1891, light flicker became an issue for the engineers at Westinghouse Electric Company. The selection of 60 Hz as a standardised operating frequency ensured that objectionable flicker was not observed from the lamp; more specifically, that the lamps AC power fluctuation could not be observed. In the same year, engineers at AEG in Berlin faced a similar problem, however, 50Hz was selected as their new fundamental frequency. The difference in frequency has been attributed to the predominantly open arc type carbon lamps used in America as opposed to the enclosed arc lamps found in Europe. The world's electricity networks have remained separated by these standardised frequencies.

The initial problems of light flicker were quickly resolved with improved control and load management. However, light flicker continues to cause serious yet isolated issues in modern electricity networks. Flicker is now commonly associated with large time varying loads and more recently, with distributed generation systems. The sources of harmonics have also grown with the proliferate use of semiconductors in the majority of modern devices, from large static power converters to low power consumer appliances.

The study of flicker and harmonics encompasses a wide range of topics, from the human biological aspects of vision, mental awareness and human perception, to the electrical network including load characteristics, interaction and propagation, to regulatory standards and governance. This chapter discusses these aspects, identifying the core concepts that form the basis of this research.

2.2 THE LIGHT FLICKER PHENOMENON

Light flicker is the phenomenon experienced by the human vision system in the presence of varying luminance intensity. For the observer, light flicker generally has a detrimental effect on the physiological system resulting in irritation and discomfort. Prolonged exposure to flicker leads to muscular eye strain and headaches, resulting in fatigue and loss of productivity. In more serious cases, fluctuations can cause loss of concentration or the triggering of epileptic seizures. An estimated $0.3 - 3\%$ of the population are photosensitive to rapid light variations [20].

Light flicker originates from within the power system; voltage fluctuations cause the variation of light produced by electrical lamps visible to humans. For consumers, light flicker is one of the most obvious indications of poor power quality. For engineers, light flicker presents one of the most technically challenging power quality problems.

As the aspects of flicker are discussed in detail throughout this thesis, the following definitions are made for clarity:

Voltage Fluctuation : variations in the system voltage [1]

Light Flicker : variations of illuminance intensity (light) perceived by a human observer

Voltage Flicker : light flicker resulting from voltage fluctuations.

2.2.1 Human Visual Physiological System

The human physiological system perceives light flicker involving complex mechanisms between the eye and brain. The human eyes retina contains two classical photoreceptors, cones and rods, that produce electrical pulses when struck by photons. A third photosensitive ganglion cell, only recently discovered, do not contribute to sight directly but are thought to support circadian rhythms and pupillary reflex. The pulses are combined and pass through the optical cord to the brain. Three kinds of cones form in the fovea area closer to the centre of the eye primarily function in the detection of colour. Rods are highly sensitive, functioning in lower light conditions and are concentrated around the peripheral of the retina. The peripheral has heightened sensitivity and acts as a natural protective mechanism to objects entering into the field of view. The amount of light reaching the retina is controlled by the dilation of the pupil. The brain's perception of variations in light is influenced by a number of aspects including; mental awareness and mood, the spatial environment, background lighting conditions, field of view, the rate, and magnitude, and waveshape. The human sensitivity is subjective, varying from person to person and across age groups and different demographics and therefore makes it difficult to quantify the impact light flicker has on human well-being.

The capabilities of the human vision system has intrigued the scientific and biological communities over the last century [46, 51]. Pioneering work by De Lange [17] conducted human flicker trials and observed what are called the Critical Flicker Frequency (CFF) and the Flicker Fusion Frequency (FFF) for a varying levels of light intensity modulation. The observer was subjected to a varying 2^o field of view under different background lighting. The critical flicker frequency

[1] As will be shown in following chapters, the resulting light flicker is dependent on lamp type, such that voltage flicker may cause light flicker in a certain lamp but not others.

is reached when the observer can no longer discriminate between individual brightness changes as the flicker frequency is increased. The fluctuations fuse together and a constant light is perceived. Later, Kelly [31] showed that for a greater field of view, flicker is perceived at higher frequencies. The small 2^o field used by De Lange subjected only the fovea view to flicker; further studies by Kelly [32] confirmed the peripheral vision has greater sensitivity which extends to higher frequencies.

The variation of critical frequency curves supports the fact that perception of flicker varies from person to person and that a standardised time-averaged perceptibility is required. It is possible for prolonged exposure to light fluctuations that fall below the region of perceptibility to result in eye strain. The person is usually unaware of the low fluctuating light levels, however can develop feelings of fatigue without explanation.

2.2.2 Sources and Propagation of Flicker

Within the power system, flicker originates from large fluctuating loads. The variation in current drawn by a load causes fluctuation in voltage across the system impedance. The supply impedance consists of transformers, transmission lines, generators and other network components. These allow the propagation of voltage fluctuations to other parts of the network, affecting customers both upstream and downstream of the distorting load.

Voltage flicker in its classical form appears as modulation of the fundamental voltage. The system voltage, either rectangular or sinusoidally modulated as is given here by;

$$v(t) = \sqrt{2}V \sin(\omega_0 t)(1 + m_f \sin \omega_f t) \tag{2.1}$$

where V, is the rms voltage at fundamental system frequency, ω_0, modulated by a sinusoid with amplitude, m_f, at a given frequency, ω_f. Based on the presumption light flicker is generated by the modulation of power dissipated in an electrical lamp, for example an incandescent lamp, the instantaneous power dissipated in the filament can be described as;

$$p(t) = \frac{v(t)^2}{R_n} \tag{2.2}$$

where R_n, is the filament resistance. Substituting in the voltage signal of (2.1) gives

$$p(t) = \frac{V^2}{R_n}\left(\sin^2(\omega_0 t) + 2m_f \sin^2(\omega_0 t)\sin(\omega_f t) - m_f^2(\sin^2(\omega_0 t)\sin^2(\omega_f t))\right) \tag{2.3}$$

Expanding and simplifying gives,

$$\begin{aligned} p(t) = \frac{V^2}{R_n}\Big(&1 + \frac{m_f^2}{2} - \cos(2\omega_0 t) + 2m_f \sin(\omega_f t) \\ &- m_f \sin((\omega_f + 2\omega_0)t) - m_f \sin((\omega_f - 2\omega_0)t) \\ &- \frac{m_f^2}{2}\cos(2\omega_0 t) - \frac{m_f^2}{2}\cos(2\omega_f t) \\ &+ m_f^2 \cos((2\omega_f + 2\omega_0)t) + m_f^2 \cos((2\omega_0 - 2\omega_f)t)\Big) \end{aligned} \tag{2.4}$$

This rather lengthy expansion can be separated into three distinct terms relating to the visual capabilities of humans: constant light, visible oscillating light and non-visible oscillating light. The non-oscillating terms of Eq. (2.4) are

$$p_c(t) = \frac{V^2}{R_n}\left(1 + \frac{m_f^2}{2}\right) \tag{2.5}$$

that represent the constant power being delivered to the lamp and thus the resulting constant light intensity. This is idealised light, suitable for lighting human spaces and results in no irritation. The visible oscillating terms are those which fall within the humans the perceivable frequency range, between 0 and 42Hz for the average human. Depending on the magnitude of ω_f, the direct, and sum and difference terms in equation 2.4 for both $\pm\omega_0$ and $\pm\omega_f 0$ can lead to a combination of visible terms;

$$\begin{aligned} p_v(t) = \frac{V^2}{R_n}\Big(& 2m_f \sin(\omega_f t) \\ & - m_f \sin((\omega_f + 2\omega_0)t) - m_f \sin((\omega_f - 2\omega_0)t) \\ & - \frac{m_f^2}{2}\cos(2\omega_f t) \\ & + m_f^2 \cos((2\omega_f + 2\omega_0)t) + m_f^2 \cos((2\omega_0 - 2\omega_f)t)\Big) \end{aligned} \tag{2.6}$$

Since m_f is typically small, the m_f^2 terms can be generally ignored. Besides the two modulated terms, $-m_f \sin((\omega_f + 2\omega_0)t) - m_f \sin((\omega_f - 2\omega_0)t)$, this leaves the largest signal $2m_f \sin(\omega_f t)$ that is of particular interest as it is the visible oscillating term resulting from the sinusoidal voltage modulation. The $\cos(2\omega_0 t)$ terms are omitted as $2\omega_0$ is always beyond the capabilities of the human perception.

The largest source and hence most commonly recognised source of flicker is the Electric Arc Furnace (EAF) used as part of the metal smelting process. EAFs are typically rated between 50-200MW and draw a highly variable load. The EAF process is initiated by lowering an electrode into raw and scrap material. After the initiation of a high current draw the arc length is adjusted via the electrode positioning. However, due to the randomly varying composition of the material in either liquid or solid form, the arc length — and hence the load — continues to vary. The process can be interrupted further by open or short conditions between the electrode and the material. The limited speed of the mechanical electrode control system means the current draw from the system is highly variable.

The source of flicker is not strictly limited to loads as intermittent or highly variable generation injecting power can contribute to flicker. For the majority of the 20th century, power generation was supplied by large, centralised generation plant, such as hydro or thermal stations. These plants have large inertial primary power sources (for example, the large head of water for hydro or the large boiler thermal mass of a coal fired station) and produce consistent output power. Of concern is the increasing penetration of wind and solar generation as their power output is highly governed by the available wind energy or radiant light energy hitting the panel. Wind Turbines have limited speed control of their mechanical pitch and yaw systems and can not control at the electrical flicker frequency rate. These renewable sources have little to no rotating inertia or storage and can not stabilise their output power.

In addition, many power quality, or voltage quality disturbances result in light flicker. Voltage

deprivation in the form of dips and over-voltage swells as well as interharmonic and subharmonic frequencies can cause light flicker. Harmonics on their own do not directly contribute to flicker but the modulation of harmonics with surrounding interharmonics can. In the majority of cases, power quality events are typically flagged and the phenomena handled categorically.

2.2.3 Flicker Quantification

The 1979 review, [57], Walker presented a collection of flicker sensitivity curves, see Figure 2.1, from scientific human based trials to industry adopted levels. This showed the great variation in the level of perception versus the frequency of pulsations.

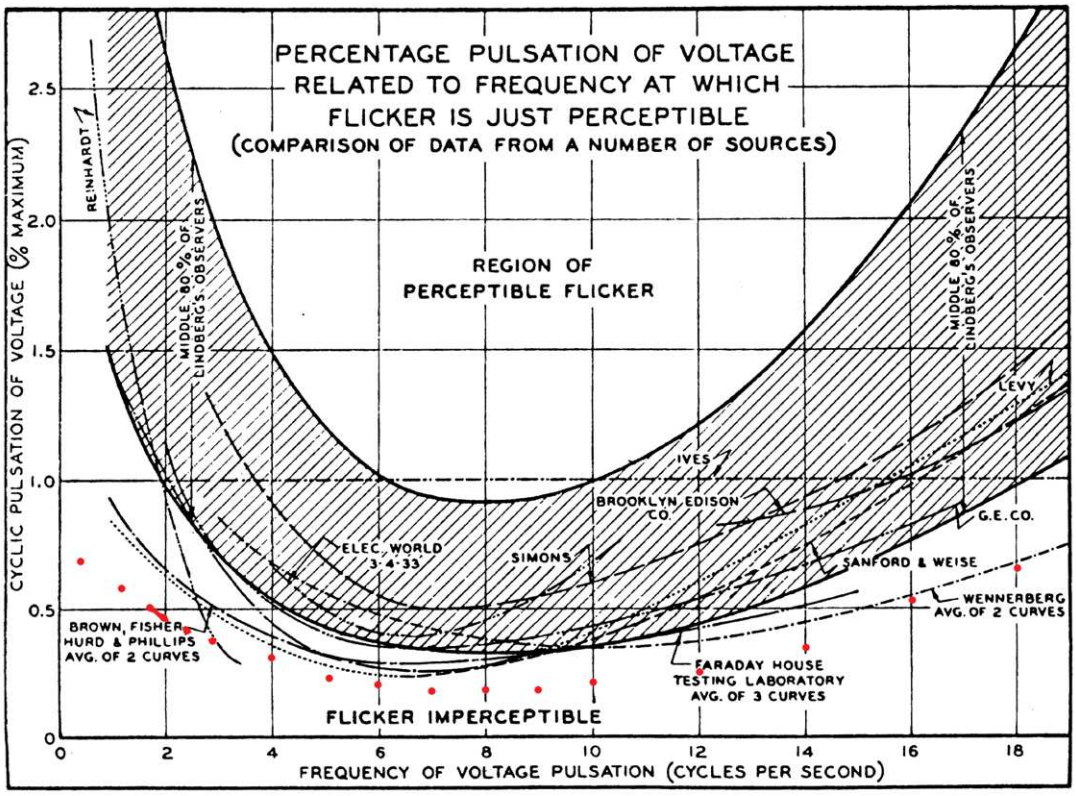

Figure 2.1: 1979 Walker [57] review of flicker sensitivity curves. Red markers indicating current IEC levels.

The complexities of the human physiological system and the stochastic nature of power systems lead to the standardisation of flicker measurement in power systems. In 1991, the UIE Disturbances Working Group formed to develop a unified international flicker measurement apparatus to standardise the quantification of flicker [16]. The working group combined experience from around the world including a number of existing flickermeters and techniques. At that point France, Germany and the United Kingdom had developed meters for flicker, Japan and the United States [2] had imposed limits on voltage fluctuations in their system.

Through studies of the lamp and human sensitivity to flicker [29] the UIE/IEC formed the 61000-4-15 standard [3] that has been adopted by a number of regulatory bodies including AS/NZS [6] and IEEE [4]. The standard gives the function and design of a flicker instrument that analyses

the systems voltage waveform to evaluate the flicker from a 60W incandescent lamp visible to the average human.

An example of a flicker levels is the $\Delta V10$ Japanese standard developed due to the high penetration of metal smelteries and a proportion of sensitive manufacturing plants. The $\Delta V10$ is a simplified method using a weighting curve with a peak at 10Hz as opposed to 8.8Hz found in the IEC standard. The $\Delta V10_s$ short term value is determined by the 1 minute RMS value of the weighted voltage fluctuation for which the limits as shown in Table 2.1 are applied.

Table 2.1: Japanese $\Delta V10_s$ Short Term Fluctuating Voltage Limits

	$\Delta V10_s$
Sensation Level	0.32%
Disturbance Level	0.45% =1 p.u.

The 4th maximum $\Delta V10_s$ from each hour are compared with these limits and the 1 hour results are averaged for comparison with the long term levels.

2.3 UIE/IEC FLICKERMETER

The IEC flickermeter was developed in order to standardise the quantification of voltage flicker. The flickermeter simulates a standard reference lamp and the human physiological and vision system to assess the light flicker severity from voltage fluctuations on the electrical network. The flickermeter produces a Flicker Severity Index, P_{st} known as *Short Time* and P_{lt}, *Long Time*. The P_{st} is determined from measurements made typically over a 10 minute period and the P_{lt} is calculated from 12 consecutive P_{st} values, equating to a 2 hour period. The perceptibility threshold, $P_{\mathrm{st}} = 1$ corresponds to where 50% of the population will be able to observe the flicker. Values of less than 1 mean fewer people notice the flicker and is considered acceptable; values greater than 1, results in over 50% of the population being irritated by the light flicker and is unacceptable.

The standard, [3], orignally designed for European 230V/50Hz, was based on a 60W incandescent reference lamp. In recent years, it has been adapted to other common system levels used throughout the world [49, 48], namely the American 120V/60Hz system [26], 100V/60Hz Japan, 230V/60hz, South Korea 220V/60Hz [10].

2.3.1 Functional Design and Methodolgy

The IEC Flickermeter describes functional and design specification for the flicker measuring apparatus to determine the correct flicker perception at any system level. It is intended to connect to the single phase voltage with a predefined nominal low voltage and frequency. Currently the standard only provides specification for 120V and 230V, 50Hz and 60Hz nominal systems, however, guidance is given to adapt to other system levels. The flickermeter consists of a series of five functional blocks as shown in Figure 2.2. The first block, 1, provides the normalisation of system voltage, the next 3, Blocks 2, 3, and 4, simulate the response of the lamp-eye-brain and the final block, 5, gives a statistical analysis of the perceptibly over the time period.

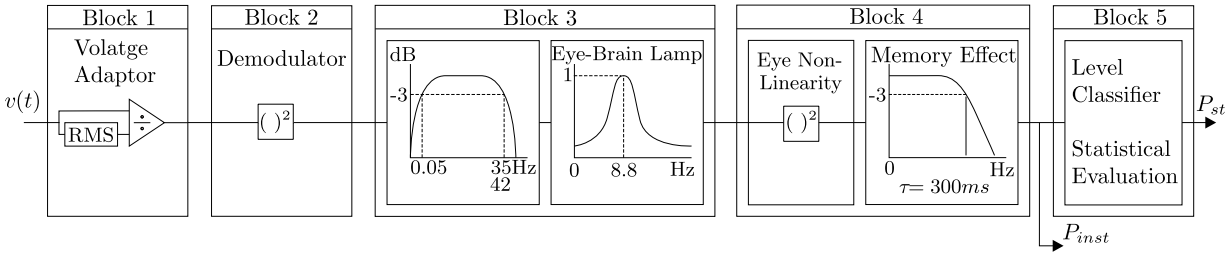

Figure 2.2: IEC Flickermeter [3] Functional Blocks

The Voltage Adapter, Block 1, normalises the input voltage, similarly to the Per Unit system, by scaling voltage input to its calculated RMS value. The RMS value is smoothed by a suitably long time constant low pass filter to ensure no abrupt changes in level. The block obtains the relative voltage change to the internal reference level pre-configured as the nominal system. It enables the evaluation of voltage flicker at all system levels (HV, MV, and LV).

Block 2 combines a demodulator to extract the modulated signal with a squaring function. This squaring of input signal is equivalent to the incandescent lamp power function described in Equation (2.2).

Block 3 contain weighting filters that describe the frequency sensitivity of the lamp-eye-brain combination to sinusoidal voltage fluctuations. The lamp, known as the reference lamp, is a coiled tungsten filament gas filled incandescent lamp rated at 60W. Composed of two second order filters, the weighting is given in the form:

$$F(s) = \frac{k\omega_1 s}{s^2 + 2\lambda\omega_1 + \omega_1^2} \times \frac{1 + s/\omega_2}{(1 + s/\omega_3)(1 + s/\omega_4)} \tag{2.7}$$

where s, is the Laplace operator.

Symbol	230V Lamp	120V Lamp
k	1.74802	1.6357
λ	$2 \cdot \pi \cdot 4.05981$	$2 \cdot \pi \cdot 4.167375$
ω_1	$2 \cdot \pi \cdot 9.15494$	$2 \cdot \pi \cdot 9.077169$
ω_2	$2 \cdot \pi \cdot 2.27979$	$2 \cdot \pi \cdot 2.939902$
ω_3	$2 \cdot \pi \cdot 1.22535$	$2 \cdot \pi \cdot 1.394468$
ω_4	$2 \cdot \pi \cdot 21.9$	$2 \cdot \pi \cdot 17.31512$

In addition, two selective filters are included; the first, a high-pass filter (1st order, $0.05Hz{-}3dB$) to eliminate non-fluctating terms, and the second, a low-pass filter (recommended 6^{th} order Butterworth filter, $-3dB@35Hz$ for $w_0 = 50Hz$, $-3dB@42Hz$ for $w_0 = 60Hz$). The non-fluctuating terms are those considered non-varying, including dc seen as the nominal level of luminance. The second filter ensures sufficient damping of the power frequency terms (100Hz and 120Hz) and those frequency terms beyond the capabilities of human vision system.

Block 4 models the non-linear response of the eye and the brain's memory effect. The weighted flicker signal is squared to simulate the non-linear eye-brain perception. Following this, a sliding mean filter (low-pass first order with time constant of 300ms) simulates the storage effect of the

brain. The output of block 4, is given as the instantaneous flicker perceptibly, P_{inst} a signal relative to the human perception of the light flicker.

Block 5 provides a statistical analysis to produce a single flicker severity index, P_{st}, for a 10 minute period. A Level Classifier is used to determine the time-at-level of the signal over the measurement period. This is achieved firstly by generating a histogram, placing the data into bins spanning the signal range of the flickermeter. Next cumulative distribution function (CDF) is formed and gauge points are used to calculate the severity index by equation (2.8). The smoothed gauge points, denoted by s, are found from equations 2.9-2.12 to alleviate sudden changes in the CDF.

$$P_{st} = \sqrt{0.0314P_{0,1} + 0.0525P_{1s} + 0.0657P_{3s} + 0.28P_{10s} + 0.08P_{50s}} \tag{2.8}$$

$$P_{50s} = (P_{30} + P_{50} + P_{80})/3 \tag{2.9}$$

$$P_{10s} = (P_6 + P_8 + P_{10} + P_{13} + P_{17})/5 \tag{2.10}$$

$$P_{3s} = (P_{2.2} + P_3 + P_4)/3 \tag{2.11}$$

$$P_{1s} = (P_{0.7} + P_1 + P_{1.5})/3 \tag{2.12}$$

2.3.2 Flickermeter Implementations

The IEC specification, aside from the statistical evaluation of block 5, describes the full analogue design of the functional blocks, filters and demodulators. An accurate analogue implementation proves difficult to construct. It requires all s-domain filters, demodulators and integrators to meet the design, while maintaining a measurable signal over the large dynamic range of voltage fluctuation levels to be quantified. As a result very few analogue flickermeters were actually built to a calibration standard. This became a decisive factor in the large allowable tolerance range for calibration.

The large dynamic range of the signals measurable by the specification required a range selector at the end of block 3 to control the signal gain. The manual range selection was set initially according to the amplitude of the expected fluctuations, meaning there was a chance signals would be clipped and resolution lost if the fluctuations were larger than anticipated.

Flickermeters are now fully digitised with functional blocks implemented in their software. They can be bundled in with many power quality analysers or smart meters alongside harmonic, unbalance, sag, and swell analysis.

2.3.3 Calibration

Over recent years the IEC flickermeter specification has come under close scrutiny as modern digital implementations do not produce consistent results in the field [45]. When stimulated by the same voltage distortion commercial flickermeters have been reported to produce different results. This is because it was originally designed for analogue operation and the calibration procedure is not comprehensive. It consists of only seven test points with a high compliance tolerance of $\pm 5\,\%$. It is therefore up to manufacturers to decide on instrument attributes such as sampling rates, digital resolution, filter design etc., which are not specified in the standard.

The CIGRE joint working group on power quality are working on a new test protocol for the IEC flickermeter. Currently in draft, the protocol specifies a number of tests which each verify an aspect of the meter's performance and accuracy [12]. Divided into four sections the tests verify accuracy to the existing standard, cases of no influence, unique cases of influence and simulations of complex waveforms characteristic of real world applications. The results of the CIGRE working group are expected to be included in the next revision of the IEC 61000-4-15 flickermeter standard.

2.4 ELECTRIC LIGHTING TECHNOLOGIES

Electric lamps are central to the study of light flicker and harmonic performance. The underlying technology, operation and circuitry forms the interface to the system, establishing the link between voltage fluctuations and light flicker. The numerous commercial lamp technologies are summarised in the following section.

2.4.1 Incandescent Filament Lamps

The traditional incandescent lamp has remained relatively unchanged since their invention by Edison in the late 19th century. The incandescent remains one of the most commonly used General Lamps for Service (GLS). The lamps' popularity has been due to its simplicity, low manufacturing cost and suitable attributes such as life time, colour temperature, and light distribution.

The incandescent lamp consists of a tightly coiled tungsten filament supported in an inert gas typically argon, and encapsulated in a glass bulb. Electrical current passes through the filament heating it to $2000-3000$K where the blackbody radiation emits photons across the visible range. A considerable amount of photons are emitted in the infra-red range with a small portion in the ultra-violet range. For this reason incandescent lamps have low efficacy converting only around 5% of the input energy to visible light spectrum. Due to the high temperature of operation, the tungsten evaporates and deposits on the inside of the bulb. This normal filament evaporation is the dominant failure mechanism of the lamp.

Halogen Incandescent Lamp

The halogen lamp incorporates a chemical reaction known as the halogen cycle that both improves the lamp's efficacy and prolongs its life. A halogen lamp contains a tungsten filament surrounded by an inert gas (typically argon) and a small amount of halogen encapsulated in a compact quartz globe. The halide, commonly iodine or bromine, forms the halogen cycle. More specifically, as the tungsten filament evaporates, the halide captures and redeposits it back onto the filament. This continuous recycling process prevents tungsten depositing on the inside of the bulb and sustains a higher filament temperature with greater efficacy. Operating the filament at higher temperatures produces excessive UV radiation, for which the quartz bulb is doped with a UV-absorbent material. The bulbs operate at either mains voltage AC or low voltage 12–24VDC necessitating the use of a power electronic convertor.

2.4.2 Discharge Lamps

Discharge lamps generate light by the excitation and ionisation of a gas which then emits radiation. The emitted spectrum depends on the composition of the discharge gas; for example, sodium and xenon gases produce visible light whereas mercury emits UV light. Discharge lamps are characterised into two categories, low and high pressure, based on the pressure of the gases.

2.4.2.1 Fluorescent Lamps

Fluorescent lamps are a type of gas discharge lamp that uses the principle of phosphor re-emission to generate visible light. Electricity is used to excite gaseous mercury in a low pressure tube, and as the mercury atoms return to lower energy states photons are released in the UV spectrum. The UV light excites a phosphor coating on the inside of the tube that re-emits light across the visible spectrum. The fluorescent technology achieves a greater efficacy than incandescent lamps, between 80–110 lm/W for linear fluorescent tubes and 40–80 lm/W for compact fluorescent lamps.

2.4.2.2 Linear Fluorescent Lamps

The linear fluorescent lamp is primarily used in commercial and institutional buildings where illumination of large spaces is required. The lamp consists of a long straight tube containing the low pressure mercury and an inert gas. The arc is formed between the two end caps and because the ionised plasma path exhibits negative resistance, a ballast is required to limit the current. The ballast also provides the starting circuitry for the lamp, heating end electrodes and developing a high strike voltage to initiate the arc. The traditional inductive ballast consisted of a large inductor (1H) in series with the tube; these ballast are being replaced by the more energy efficient electronic ballast that offer faster starting and life-time.

The rate at which mercury electrons are excited to the higher energy state is proportional to the instantaneous power being dissipated. The release of the photon occurs almost instantaneously as the mercury electron falls to the lower energy band. The phosphor re-emission occurs within $4ns$. These delays are considered insignificant when correlating the power input to the light output for the study of flicker.

2.4.2.3 Compact Fluorescent Lamps

The Compact Fluorescent Lamp (CFL) contains a fluorescent tube bent or twisted into a shape similar to the size of an incandescent bulb. In order to maintain the compact size, low cost electronic ballasts have been designed. Compact fluorescent lamps are based on same energy efficient discharge tubes found in fluorescent lighting. Similarly the ballast is required to limit the current flow in the discharge tube and for practically all CFL consist of a solid-state electronic ballast.

A number of concerns have been raised by consumers when replacing incandescent lamps with CFLs:

- Some lamps produce a 'cool white' colour not matching the 'warm white' colour of incandescent.
- CFLs can have a delayed start-up and/or take considerable time reach full brightness.
- They can fail to produce the equivalent rated light output.
- The electronic ballast can produce audible sound.
- Most CFLs cannot be used with dimmer switches.

A typical CFL ballast, as shown in Figure 2.3, consists of a single phase rectifier stage creating a DC bus from which a high frequency inverter resonates to control the fluorescent tube current. The ballast consists of four main blocks connecting the AC system to the discharge tube. The first block is likely to contain passive filtering for RF and/or power frequencies and in some cases fuse protection. The second block is a full bridge rectifier converting the AC voltage into a DC bus. The role of block three is to provide harmonic filtering for both the DC bus and the AC system. The final stage (block 4) is designed to start and operate the fluorescent tube. The lamp arc is started by heating elements at either end of the tube and striking a high voltage across the tube switched by a Diac. Once the arc is formed the current is maintained by a self-resonant inverter oscillating between 15 and 50kHz. This high frequency increases the tube efficiency by 10 - 20% but is above the power harmonic frequencies.

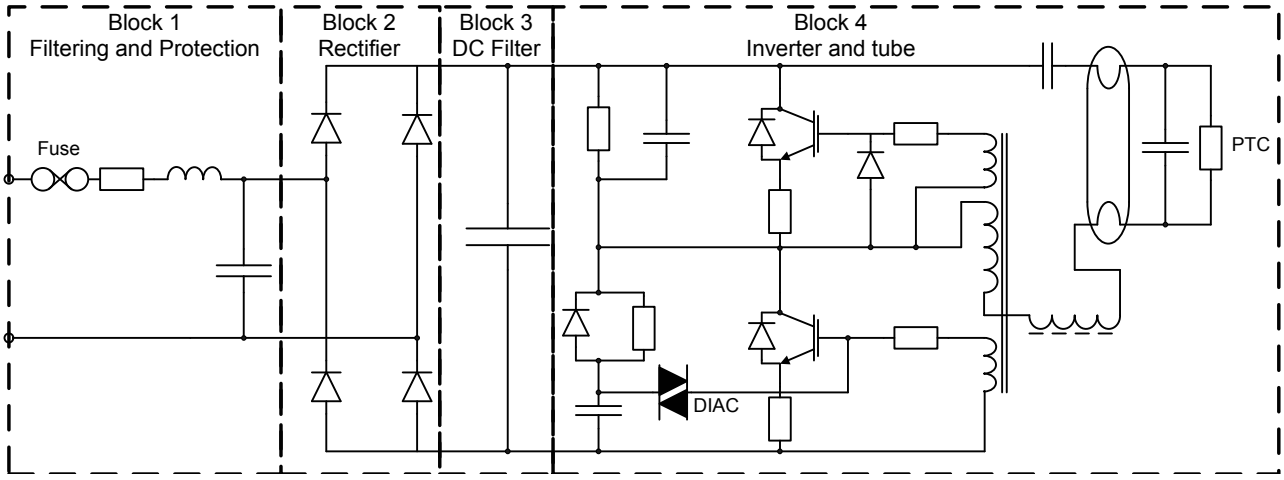

Figure 2.3: Typical CFL Ballast Circuitry Design

The filtering blocks 1 and 3 and the rectifier in block 2 determine the overall harmonic operation. The harmonic performance of readily available CFLs can be placed into four categories based on the circuit topologies of these three blocks [58]. Due to the diode rectification, some require EMC filtering to comply with national harmonic standards, while others omit this. During starting two filaments at either end of the tube are heated to create enough free ions for the plasma to be formed. Depending on the designed heating time, a delayed start-up can occur, on the other hand, insufficient heating reduces the life of the lamp.

From a manufacturer's perspective, the need to conform to performance standards typically involves additional manufacturing costs. In a highly competitive market profit margin is a key driver and lamp quality suffers. Unfortunately power quality is not of great concern to customers, and hence, manufactures are forced into producing lower quality simpler designs. The higher cost EMC filtering components originally designed into the lamp are first to be removed from the device. This is evident by the component place holders seen on the printed circuit. Other manufacturing trade offs include as the fluctuation of the bus voltage of the inverter circuit that can drastically affect the lifetime of the lamp. A larger variation reduces the life expectancy but generally produces a lower the harmonic current draw. The use of a positive temperature coefficient (PTC) resistor ensures the starting filaments are heating correctly before starting. This increases the life of the lamp, but causes a $0.2 - 1$ second delay from when voltage is applied to when the lamp produces light.

The lowest cost design shown below in Figure 2.4, is the non-filtered rectifier and typically produces a current THD of 150 - 200%. By adding passive filtering prior to the rectifier this can be reduced to between 100 and 130%.

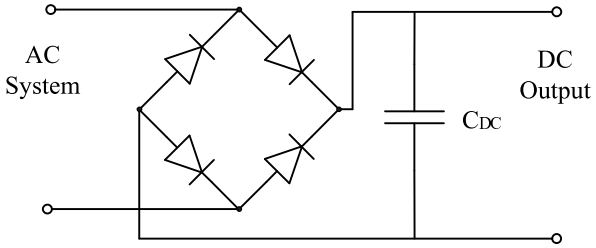

Figure 2.4: Simple Front End CFL Ballast Circuitry

A popular design is the valley-fill ballast shown in Figure 2.5. Diodes are added to the DC side filter to increase the conduction period and are able to reduce the current distortion to around 25 - 40% I_{THD}.

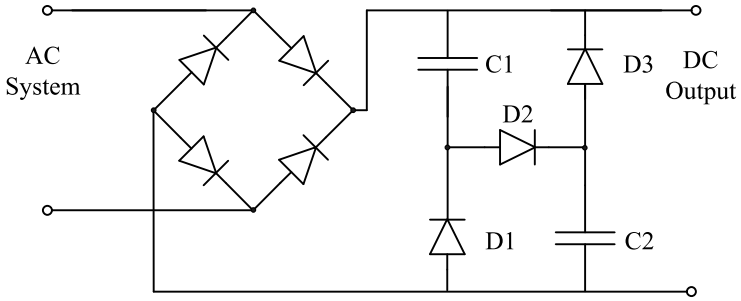

Figure 2.5: Valley-Fill Front End CFL Ballast Circuitry

By far the best performing yet most costly design employs active control, shown in Figure 2.6, to draw close to sinusoidal current at unity power factor. A dedicated IC is used in these designs to control the current and typically draw less than $5\%I_{THD}$.

2.4.3 Light Emitting Diodes (LEDs)

Over recent years extensive research of semiconductor materials has lead to the development of LEDs which cover a wide range of spectral wavelengths. In particular, those visible to humans

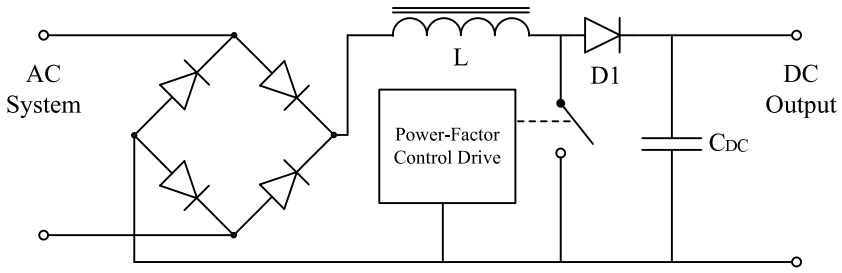

Figure 2.6: Active CFL Ballast Circuitry Design

(400nm-700nm) have followed Haitz's Law where the luminous flux (total light output) doubles every 18-24 months. Since the pioneering work in 1998 by Lumileds Lighting the commercialisation of high power LEDs has impacted on Haitz's law; a knee-point has emerged defining the moment when LEDs moved away from being indicator lamps to becoming powered sources of light [54].

The fundamental principles of LED operation have restricted the development of 'white' light LEDs suitable for lighting human environments. Although individual LEDs have been developed to emit narrow wavelength bands across the visible spectrum, white light can not be produced from a single substrate. This has lead to three general approaches to the generation of white light [50]. The first method mixes the light from three or more monochromatic substrates, usually red, green and blue (RGB). The mixing of individual colour LEDs presents a complex control problem to achieve the correct colour balance. This can result in the light appearing too blue, red or green. This approach can also lead to poor colour rendering where gaps in the light spectrum cause objects of the gap colour to appear washed out. The use of other colour LEDs can fill these spectral gaps but adds further complexity.

The other two methods use phosphor conversion technology, as found in fluorescent lighting. One method uses an Ultra Violet LED - all the UV photons are fully absorbed by the phosphor and more photons re-emitted at visible wavelengths. Greater efficacy can be achieved using a blue LED with a phosphor coating. A portion of the blue light is able to pass through the coating with the remainder re-emitted with green, yellow and red spectral wavelengths. The output light spectrum is greatly dependent on the phosphor material. Gaps in the light spectrum due to the phosphor coatings response present similar problems to monochromatic based lamps.

2.5 POWER SYSTEM HARMONIC ANALYSIS

The modelling of low power harmonic producing loads is important; suitable load models and simulation techniques are required to achieve accurate results. At the same time these approaches need to be feasible and computationally efficient to model large numbers of loads within a network. Three commonly used models for harmonic producing loads are introduced in this section; Harmonic Current Source, Norton Equivalent, and Harmonic Cross-Coupled Norton Equivalent.

Harmonic analysis techniques for modelling power systems have been extensively published [30] and implemented into many commercial software packages including PowerFactory, SinCal, PSCAD/EMTDC, and PSS to name but a few. Some techniques proposed included the use of the time domain, transfer functions or the Harmonic Domain. The Harmonic Domain solves for

the steady-state harmonics using either Gauss-Seidel type fixed-point iteration or Newton-type methods, and hence is classed as an Iterative Harmonic Algorithm (IHA).

The Harmonic Domain is the most rigorous method for describing a non-linear load and through its use of linear matrix algebra all harmonics in the system equations can be solved efficiently. The harmonic domain is simply a subset of the frequency domain where only the fundamental and its integer multiples are represented. In this form the problem set is reduced to focus directly on the quantities of interest. The simulation of the steady-state harmonics requires two key steps:

- The identification and derivation of non-linear load models and network components to define the system equation.
- To solve the system non-linear equation set by an iterative algorithm.

If the system can be linearised sufficiently well around a base operating point, the harmonic domain equations can be solved by a simple matrix inversion. A fundamental frequency load flow may be sufficient to set this base operating point. The accuracy of the solution relies on the correctness of the system model and the harmonic currents injected by the non-linear loads.

A suitable harmonic model must find a compromise between model complexity and the accuracy of the simulation. However, by over simplifying, or ignoring the characteristic operation of a device, the model can become inaccurate and origin of the errors difficult to identify.

Using the Norton equivalent model in the harmonic domain, the non-linear time domain interactions can be modelled by a first order approximation of the non-linear transfers and represented by a constant Frequency Coupling Matrix (FCM). The FCM allows the cross coupling of frequencies to be used to model the characteristic harmonics introduced by power electronic switchings of diodes, thyristors etc or natural non-linearities such as magnetic saturation or the operation of fluorescent tubes. Larsen was the first to present a linearised analytical model of a HVDC converter through the use of FCMs [34].

The Harmonic Current Source Model (shown in Fig. 2.7a) is most simplest and most widely adopted model for non-linear loads. The model consists of a fixed harmonic current source injecting the load characteristic harmonic currents into the busbar. A constant vector represents the current magnitude and phase at each harmonic frequency. This method is utilized widely (in harmonic limitation and allocation standards) and in many cases, reasonably accurate results can be achieved.

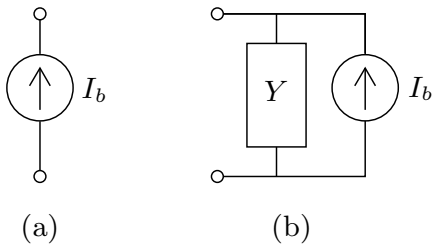

Figure 2.7: Harmonic Domain Models a) Harmonic Current Source Model b) Norton Equivalent and Harmonic Crossed Coupled Model

Because the harmonic injection is fixed the model fails to describe operation under varying terminal conditions or the interactions with the system components and/or other loads. The accuracy becomes unacceptable if the load is sensitive to the terminal voltage.

Both the Norton Equivalent (Figure 2.7b) incorporate the variation of the terminal voltage by the inclusion of an admittance component. The Norton Equivalent admittance can be modelled in the harmonic domain, where the admittance models the non-linear time domain interactions by a linear, or first order approximation. This is an effective technique if the small-signal operation of a device can be linearised around an operating point. This linear gradient represented by the Norton admittance term, can be consider constant [19] or if more accuracy is required, it can be varied with the operating conditions [53].

The Norton equivalent model represents the admittance independently seen by each harmonic frequency. In other words, Y is a vector containing the linear admittance between voltage and current of the same harmonic order. For the majority of non-linear devices the dominant relationship occurs between the voltage and current of the same frequency. The terminal current, I, is calculated by equation (2.13) and is the sum of the base case current (obtained at the operating point conditions) and the current deviation, caused by the voltage distortion across Y. In the simple case this can be solved independently for each harmonic order however if frequency coupling is included, all harmonics must be solved together; easily achieved using matrix methods.

$$[I] = [Y].[\Delta V] + [I_b] \tag{2.13}$$

I, ΔV and I_b are vectors of the relevant harmonic components. It is important to note that ΔV is the variation of the terminal voltage, specifically, $\Delta V = V_t - V_b$.

2.6 CONCLUSION

The IEC flickermeter describes one of the most complex, non-linear standardised measurement techniques used within power systems. Because of this, the study of flicker is generally not well understood and widely given lower priority. Flicker falls outside of the typical characteristics of the power system, its effects are not widely reported and issues are isolated. The detection of flicker goes beyond normal engineering concepts to involve the human physiological system; now its measurement includes the complexity of modern lamp technology and its full effect on the population is yet to be understood. There are many avenues for research in flicker to better its understanding. The most pressing matter is clearly the discrepancy in the lamp that the flickermeter models to derive flicker and lamps prominently used within the power system. Only once this is addressed can flicker be examined and understood in our current electrical networks.

The general guidelines describing the allocation and limits of flicker within the power system do not illustrate the complex nature of voltage fluctuations as a precursor to light flicker. Subsequently, the assessment of flicker is over simplified, limiting the accuracy to which voltage fluctuations can be allocated and managed on the system.

The implications of attaching megawatts of lighting loads, individually producing upwards of 130% total harmonic current distortion, are vast and warrant the need for accurate modelling techniques. Suitable modelling techniques are available for high power devices and harmonic

system simulation, however, the overall accuracy relies on the data available, its quality, and detail, and the underlying capabilities of modelling framework. To obtain detailed models for the masses of low power devices the techniques must remove the need for engineering interaction. That is, the engineer is not required to fully engage with the detailed operation and characteristics of each device. The model be fast to obtain, robust, and systematic, and most importantly provide a true representation of the devices operation.

Chapter 3

UNIVERSAL POWER QUALITY EXPERIMENTAL TEST SYSTEM

3.1 OVERVIEW

This chapter provides the design and operational overview of a universal power quality test system developed as part of this research. The test system was specifically built for the practical investigation of light flicker and the harmonic performance of electrical lighting. A general design approach enabled the simulation of a wide variety of power system conditions, to study and characterise the performance of consumer based electrical appliances. The functional design is based on a simple hardware platform, interfaced to a standard desktop PC. The software framework developed performs the automation of testing procedures, waveform generation and processing of measurements. An arbitrary waveform defined in software, is amplified to rated system voltage by up to 3 Chroma AC power sources. The system is capable of testing single phase (up to 4kVA) and three phase (up to 6kVA) loads, with accurate, concurrent measurements of voltage and current along with parameters measured by external transducers.

3.2 INTRODUCTION

The inception of solid-state consumer based electrical devices presents a multitude of unknowns and complexities regarding their operation and interaction with the electrical network. It has become nearly impossible to determine the behaviour of each individual device under complex voltage waveforms. In accordance, there is a lack of universal device models in order to predict behaviour for the wide range of voltage conditions found within the system.

In these cases, experimental testing is usually the first preliminarily step to initially comprehend, and understand the operation of the device. It is with this intention that the results can be grouped, based on devices characteristics or combined with circuit diagrams to develop an operational level understanding. However, the relationships between specific parameters can be complicated and are often non-linear. For example, relationships between real and reactive power are inherently non-linear, the transfer of terminal voltage to a DC bus voltage or angular rotational speed etc. are complex and non-linear. Particularly, for electrical lighting, the level of light flicker produced under voltage fluctuations is non-linear and such relationships are indeterminable based purely on its name plate details or technology type. Experimental testing, however, still involves extensive task to collect, test and characterise the vast array of device types, makes and models.

The relatively low power ratings of consumer appliances makes experimental testing practical under laboratory conditions. Consumer appliances are readily available, relatively low cost and give an ideal representation of the loads currently entering the system. In contrast, high power industrial plant and power system converters, such as hvdc or FACTS device, having high setup costs and power requirements, can not be tested within a laboratory environment. The analysis of such high power systems is largely confined to computer based simulation.

This chapter presents the design, construction and software of the low voltage 3 phase universal power quality experimental test system developed as part of this research. The system is specifically designed for the characterisation of low power consumer appliances, capable of simulating various power quality scenarios and system events in order to fully characterise the operation of a device. The description of the test system is introduced early in the thesis as its versatility was quickly realised, and incorporated into both the investigation of flicker and harmonic modelling.

The test system presented was first realised for the reproduction and study of light flicker. The system consisted of a single-phase supply with measurements of voltage and current and a number of general I/O channels used for the measurement of light and to generate a supply output waveform. It was built for the experimental requirements of the inherently single-phase flickermeter and measured light directly while generating complex voltage disturbances. The power quality testing capabilities of the system were quickly extended to the study of harmonics, voltage dips/swells, and inter-harmonics. This chapter presents the extended 3-phase system design that was built using the design principles of the initial single-phase test system. The new system has achieved greater accuracy and robustness while creating a more open platform for generalised requirements of power quality and device testing.

3.3 FUNCTIONAL OVERVIEW AND DESIGN APPROACH

The test system is designed as a general Automated Data Acquisition System for simulation of power quality events. The test system functional overview is given in Figure 3.1. The system provides a 3-phase fully independent measurement system, coupled with 3 single-phase AC power sources characterise the operation of electrical devices. The full functionality is realised using a standard desktop PC, fitted with a DAQ card, together forming the measurement, signal processing, automation and generation of complex PQ scenarios. The modular design approach allows for testing of the wide range of PQ events on common single- and three-phase devices. Measurement of additional operating parameters can be made by the connection of external transducers.

The role of the experimental test system is to create a controlled and isolated environment for the repeatable testing of devices. This is achieved by reducing, and/or controlling the number of system inputs and variables that influence the device operation. Primarily, this includes the environment in which the testing takes place, both electrical and physical, such as temperature, humidity or for example how external light will affect measurements. Control of these eliminates uncertainty in test measurements and gives complete control of the test environment to the operator.

Central to the operation of the test system is a generalised software testing framework written in the National Instruments (NI) Labview software environment. The software operates on a standard desktop PC and interfaces to the system hardware through a multifunction Data Acquisition (DAQ) card. The DAQ card performs the measurements of the electrical parameters

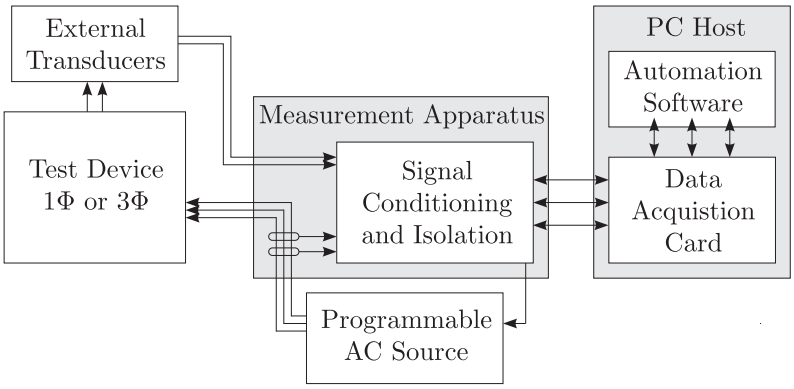

Figure 3.1: Universal Power Quality Test System Overview

through the measurement apparatus box that provides signal conditioning and isolation. The arbitrary voltage waveforms are developed in software and generated as an analogue signal by the DAQ card. This signal is then amplified by the Chroma Programable AC power sources supplying the load requirements in isolation of the grid.

The open hardware platform is developed using industrial grade instrumentation for robust and accurate measurement. Modular in its design, the hardware is reconfigurable and components can be replaced or later upgraded for higher performance or to increase functionality. Furthermore, the measurement apparatus is simple, performing only the basic signal conditioning and isolation without any signal identification or preprocessing of waveforms. This requires all signal processing be carried out within software. The software approach supports the rapid development of user defined testing procedures that are modular, reusable and can be easily upgraded to future requirements. The system supports the creation and measurement of low voltage, $120V_{rms}$ and $230V_{rms}$ 60/50Hz systems with PQ issues found throughout the world.

An important addition to this test system is the measurement of light from electrical lamps used for the assessment of light flicker. The second part of this chapter describes the design and construction of two lighting environments specifically designed for the measurement of light from common lamp technologies including full length fluorescent lighting, compact fluorescent lamps and LED lamps.

3.4 HARDWARE

The system hardware completes the closed form testing of the operation of a device, through generation of the appropriate test voltages, which are arbitrary defined in software, and the measurement of device response accurately by the computer data acquisition system.

3.4.1 Data Acquisition System

At the interface of the physical system and computer software is a National Instruments Multifunction PCI-6229 Data Acquisition (DAQ) card [38]. The DAQ card performs two functions, the digital to analogue conversion for the generation of an arbitrarily defined low voltage waveform to be amplified by the AC source, and the analogue to digital conversion for sampling of

the measurement signals. A summary of the PCI-6229 I/O is given in Table 3.1. The DAQ Card provides an industry standard measurement and control platform with documented performance with regards to noise immunity, EMC, measurement accuracy. The standardised interfacing allows for simple integration, assembly and modification of the system. The DAQ card platform provides the robustness and repeatability required for the test system and even with the relatively low specifications of the cards I/O, the bandwidth and resolution exceeds the requirements of power frequency signals.

Table 3.1: NI6229 Data Acquisition Specifications

Type	**Channels**	**Resolution**	**Range**	**Sample Rate**
Analogue Output	4	16bit	$\pm$10V	$\frac{833kS/s}{Channels}$
Analogue Input	32/16	16bit	$\pm 0.2V, \pm 1V,$ $\pm 5V, \pm 10V$	$\frac{250kS/s}{Channels}$
Digital I/O	48	-	TTL	1MHz

The PCI-6229 DAQ card contains 32 16bit analogue input (AI) channels, 4 16bit analogue output (AO) channels and 48 Digital I/O. The analogue input channels have a combined maximum sample rate of 250kS/s. Four double ended input channels (using 8 single ended channels in total) are reserved for the voltage measurement. A total of 8 differential channels (16 single ended channels) are used for the two current measurement techniques discussed later in Section 3.4.2.2. Furthermore, an additional 6 single ended channels is reserved for General Inputs (GI); their application and use are discussed in Section 3.4.2.3.

The PCI6229 contains a single ADC module, time-multiplexing the input channels to the ADC. The multiplexing of channels introduces a time delay, called the interchannel delay, occurring between the sampling of individual channels. The minimum attainable inter-channel delay is the reciprocal of the maximum sample rate in seconds or 1/250k seconds for the PCI-6229. This interchannel delay is generally acceptable being typically beyond the bandwidth of power frequency signals (upwards of 50th harmonic), however, any resulting phase delay can be corrected with post processing in software.

The 4 analogue output channels have a maximum combined update rate of 833kS/s. Each output channel is controlled by software to generate an arbitrary waveform; three outputs are needed for a 3 phase system. The 4 individual DACs are hardware timed through an internal clock, produce synchronised outputs. The output range, $\pm 10V$, matches directly to the input of the Chroma AC source.

The analogue input channels are operated in differential mode for connection to the SCMVAS (discussed in Section 3.4.2) and in single ended mode for the general input channels (see Section 3.4.2.3). Differential mode gives the best noise immunity for isolated signals. Single ended measurements are made with respect to the ground reference. The output channels are also generated with respect to ground reference of the DAQ card.[1] The PCI6229 contains internal circuitry for the calibration of the analogue input and output channels.

[1]The PCI-6229 analogue input and output channels supports a range of operating options that are configurable through software and/or hardware. *Consult the M series manual for full descriptions and configuration of modes.*

3.4.2 Measurement Apparatus and Signal Conditioning

The measurement equipment and signal conditioning units are housed together in a shielded metal switchboard case. The housing interfaces the potentially hazardous signals to the measurement by the DAQ card. Figure 3.2 shows the functional overview of the measurement apparatus, and in Figure 3.3 the internal layout of the physical components is shown. The breakout boards, signal attenuators, isolation units and current transducers units are mounted within a steel housing for increased noise immunity.

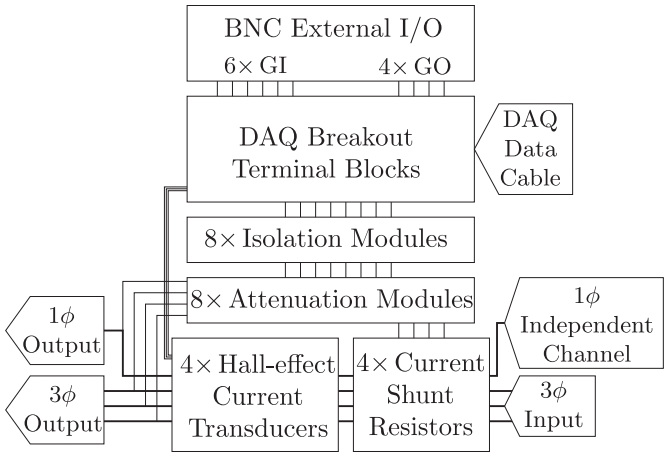

Figure 3.2: Signal Conditioning System Functional Overview

The layout of the measurement components, separates the high voltage mains rated system from the low voltage signal system as shown in Figure 3.3. The upper housed section contains the connection breakout boards and signal conditioning equipment and the lower section contains the high voltage cabling and terminals. The three-phase supply input enters the bottom right side of the case via modular individual terminal connectors, passing through the measurements (voltage and current) before exiting via the terminals on the front of the case. This orientation denotes the positive flow of power from the source to the load. The terminals for the additional voltage and current channels are mounted on the case front. Segregation is maintained within the housing with a clear isolation region between the two voltage systems. This reduces the risk of mains voltage entering the DAQ system and aims to minimise signal noise and interference from the high power system.

The PCI6229 DAQ card connects via two VHDCI 68-pin 1 metre cables to the internal breakout boards. The cable, SHC68-68-EPM, is a high-performance shielded cable for maximum noise rejection and low channel coupling. The input, output and digital channels are individually shield twisted pairs and separately bundled. The 2 breakout boards, National Instruments CB-68LPR, have right-angled cable connectors that mount directly to the cable access panel of the switchboard housing. Each CB-68LPR is mounted on insulated risers to the back mounting panel for adequate clearance. Termination of the I/O signals is made to 68 screw terminals on each board by the NI 6229 connection configuration. A 5V power rail, from the internal computer supply, can provide up to 1A per connector.

The primary voltage and current measurement channels use the Signal Conditioning Modular Voltage Attenuator System (SCMVAS) developed by Dataforth [13]. The SCMVAS is a high voltage analog signal conditioning system specifically designed for measurement and monitoring

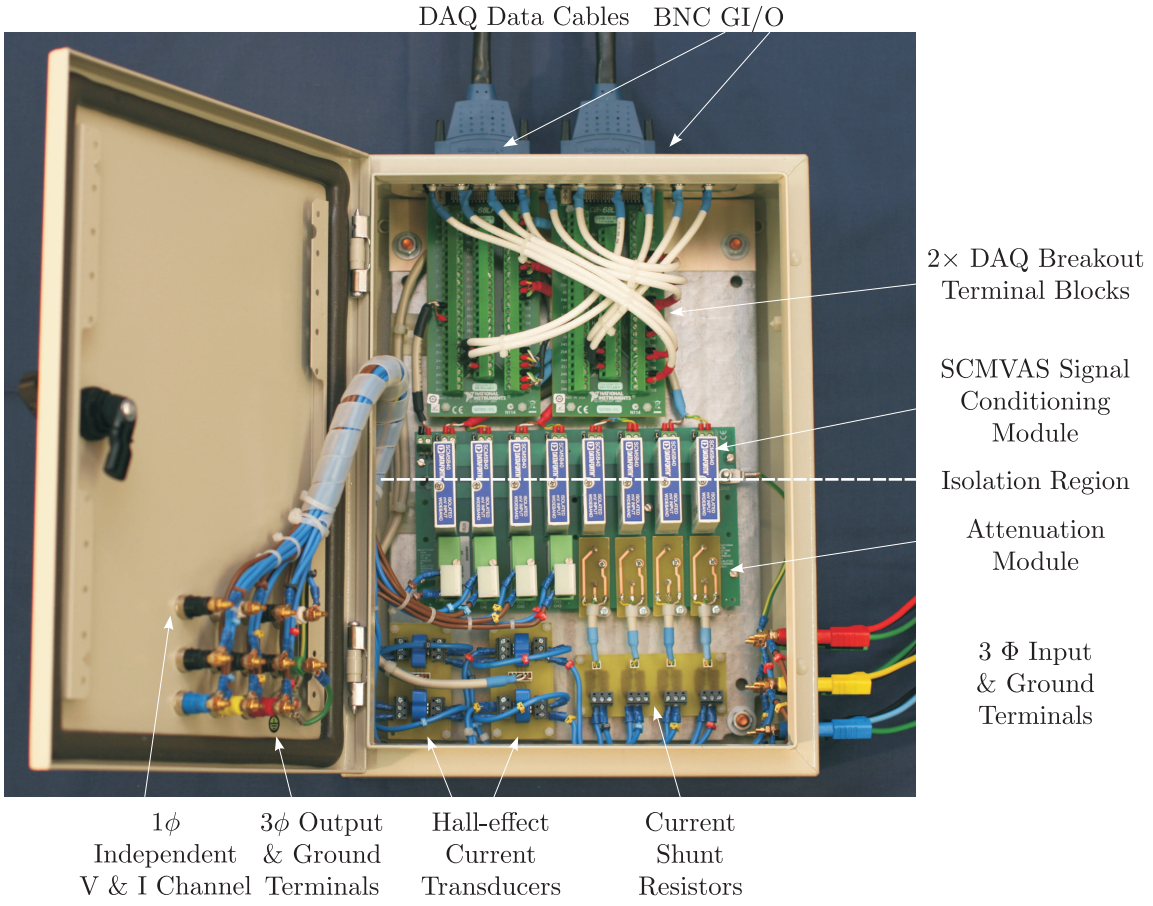

Figure 3.3: Measurement Apparatus Physical Layout

of high voltage potentials found in field measurement or industrial processes. The SCMVAS provides a configurable modular system, each channel consists of an attenuation module followed by an isolation module. A secondary current measurement is provided by Hall-effect current transducers.

The SCMVAS system consists an 8 channel back panel, with two module slots per channel. For each analog input channel, an attenuator module, SCMVAS-Mxxx, pre-conditions the signal, then an industrial 5B series signal conditioning module filters, and provides industry standard isolation, before converting the signal to a suitable range for measurement by the DAQ system. The modules can be configured for various input ranges. The backpanel is powered from the DAQ 5V supply and connects via dual channel twisted pair shield cable to the breakout board terminals.

3.4.2.1 Voltage Signal Conditioning

The signal conditioning of the voltage channels is provided by the SCMVAS and performs three primary functions; attenuation, isolation and analogue anti-aliasing filtering. The 4 voltage channels are configured completely independent within the SCMVAS. Each channel consists of an SCMVAS-M500 module [13], a 500:1 voltage attenuator and a 5B series SCM5B40-07 module [14], providing up to $1500V_{rms}$ isolation and a 10kHz anti-aliasing filter. The SCMVAS-

M500 and SCM5B40-07 mount directly on to the SCMVAS-PB8 backpanel. A summary of the SCMVAS-M500 and SCM5B40-07 specifications are given in Table 3.2.

Table 3.2: Voltage Signal Conditioning SCMVAS Module Specifications

Part	**Input Range**	**Output Range**	**Isolation**	**Accuracy**	**Bandwidth**
SCMVAS-M500	$\pm 500V_{peak}$	$\pm 1V_{peak}$	-	$\pm 0.03\%$	-
SCM5B40-07	$\pm 1V_{peak}$	$\pm 5V_{peak}$	$1500V_rms$	$\pm 0.03\%$ Span	10kHz (-3dB)

The SCMVAS-M500 is a high precision voltage divider, with an input impedance of $10M\Omega$. The high potential voltage inputs connect directly to the SCMVAS-M500 via covered terminals. The module has an input range of $\pm 500V$ spanning the typical range of voltages found within consumer appliances. The attenuated output, $\pm 1V$ range, is fed directly into SCM5B40-07 signal conditioning module.

The SCM5B40-07 is a single channel wide bandwidth analogue input module. The high accuracy, low drift modules provide $1500V_{rms}$ isolation with a 6th order low pass cut-off filter. The modules are powered from the 5V supply of the SCMVAS and maintain complete isolation of the field-side and computer-side power requirements. Further over voltage protection is provided for accidental continuous connection of $240V_{rms}$, critical upon failure of the attenuation module.

Voltage measurement is made directly at output terminals on the case front, to minimise the effect of cable impedance, connection resistance and the current measurement equipment. The SCMVAS voltage channels maintain an overall accuracy of 0.06% and $100dB$ CMRR at 50 or 60Hz. The single conditioning provides the directly analogue translation of the high voltage signal to a voltage level suitable for measurement by the DAQ card.

3.4.2.2 Current Signal Conditioning

The current measurement of DAQ system is performed by two concurrent techniques; the first using a shunt resistor, for high precision low current measurement and the second through a Hall-effect current transducer, for higher current waveforms.The channel configuration is shown in Figure 3.4 with a summary of the specifications given in Table 3.3. The current measurement of the 3 phase conductors is taken inline of the neutral conductors and between contacts of the additional current channel.

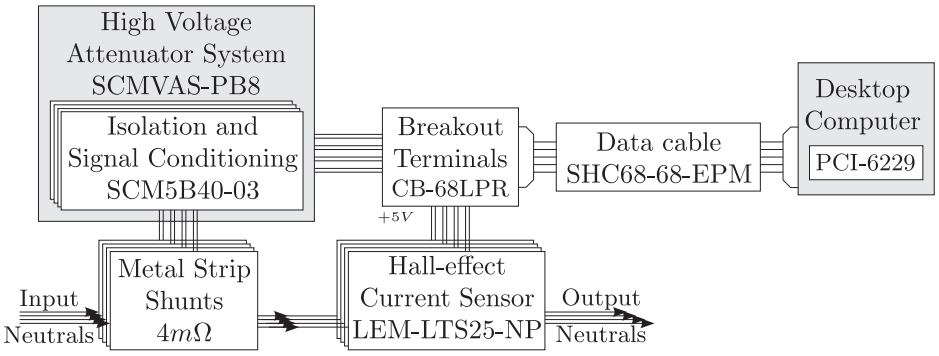

Figure 3.4: Signal Conditioning of the Current Measurement Channels.

Table 3.3: Current Measurement Channel Specifications

SCMVAS System					
Part	Input Range	Output Range	Isolation	Accuracy	Bandwidth (-3dB)
Shunt Resistor	$\pm 25A_{Max}$	$\pm 100mV$	-	0.1%	-
SCM5BB40-03	$\pm 100mV_{peak}$	$\pm 5V_{peak}$	$1500V_{rms}$	0.03%	10kHz
PCI-6229 AI	$\pm 0.2V$,$\pm 1V$, $\pm 5V$,$\pm 10V$	-	-	16bit	700kHz
LEM Hall-effect System					
Part	Input Range	Output Range	Isolation	Accuracy	Bandwidth (-3dB)
LEM LTS25-NP	$\pm 25A$ Nominal $\pm 80A_{Max}$	$0 - 5V$	3kV	$\pm 0.2\%$	0-0.5dB 100kHz 0.5-1dB 200kHz

Power Metal Strip shunt resistors were used for their high power rating, 2W per resistor, low tolerance 0.1%, low inductance and low temperature coefficient $\pm 50ppm/^oC$. Two surface mount metal strip resistors, $8m\Omega$, are configured in parallel ($4m\Omega$ effective) and mounted on the underside of a PCB. The 4 shunt current channels are signal conditioned by the remaining SCMVAS channels using the SCM5BB40-03 5B module [14]. The SCMVAS attenuation module bank is configured with a custom 1:1 attenuation module for direct pass through of the shunt voltage. The SCM5BB40-03 has a $\pm 100mV$ input range and equates a peak current of 25A through the shunts. At peak current, 25A DC current, the shunt dissipates $2.5W$ or $1.25W$ per resistor ($< 2W$ rating). The PCB track weight was further increased with copper wire inlay to carry the rated peak current. Also provided on the PCB are bypass jumpers to remove the inline shunt resistance from the circuit. If sustained inrush current or excess current is expected, then the shunt resistance should be bypassed.

The overall current resolution is $0.763mA$ per bit (16bit). This equates to the target minimum signal magnitude of $1mA_{rms}$ having 3.7bits of resolution at the 25A range. The resolution can be further increased by reducing the DAQ channel input voltage range, that is presuming the current remains within the specifications of the selected input range.

The LEM LTS25NP hall-effect current transducers were selected for the supplementary current measurement. The multi-range design of the LEM sensor can be manually configured passing the conductor through the active area up to 3 times, for nominal current range of 25A, 12A or 8A. The transducers connect to the breakout board by a dual channel twisted pair shielded cable, along with the +5V supply. Again the PCB track weight was increased using copper inserts to carry higher current and support inrush conditions.

3.4.2.3 General Purpose Input Channels

Six general purpose input channels are provided at the rear of the measurement box via BNC terminals. These provide connection for the measurement of external electronic signals as an addition to those already provided by the dedicated internal channels. They are suitable for connection of external transducers such as higher rated active or passive current clamps, voltage probes or for example, the light detector. The input connects un-isolated directly via coax cable to the breakout boards of the DAQ card input channels. Therefore isolation and conditioning of the signal must be performed by the external transducer. The input range and sampling rate of these channels can be controlled by the DAQ card through software.

3.4.2.4 Earthing

The presence of the mains voltage and the low voltage signal lines within the measurement box requires special care to avoid ground loops, circulating current and to control the flow of current under potential fault conditions. In the case of a phase to neutral fault, the AC source in built protection is required to operate. For the more serious case, a phase to chassis fault, the chassis is strongly bonded to the supply earth. This is to avoid the fault current returning through the shielding of the data cable, to the computer chassis/earth. The data cable shielding nor data lines are suitable for the level of fault current. The source protection is required to act and isolate the source. Earths for each input source is provided and are solidly bonded to the chassis earth, the case door, the instrumentation back panel and the SCMVAS system.

3.4.3 Programable Controlled AC Power Source

The Chroma 61500 series of AC programable power supplies [11] can generate up to $300V_{rms}$ AC, at a fundamental frequency range of 15Hz-1kHz and up to 424V DC. The 61500 series use solid-state PWM technology and are capable of recreating complex waveforms for appliance testing under controlled electrical conditions. The source has a bandwidth 2400Hz with $0.2\% + 0.2\%$F.S. accuracy and 0.3% distortion at 50/60Hz with a fully programmable output impedance. Built in DSP provides simple measurement and waveform synthesis. The output is protected by over-current protection and can deliver 6 times rated current during inrush.

The University of Canterbury has purchased 3 Chroma units during the course of this research with another unit on loan from Enermet NZ Ltd. (Landis+Gyr). The largest unit, 61505, can supply up to 4000VA at full rated voltage and fundamental frequency, the two 61504 units are rated at 2000VA and the final unit, 61501, has a rating of 500VA. All the units were selected as single-phase devices giving a number of possible configurations; the units can be used individually or combined in parallel for a high output power or configured in Y connection for a 3 phase supply. Two units can also be placed in series to increase the output voltage.

The functionality of the programmable source can be accessed via controls on the front panel or if fitted with an auxiliary PC interface board the unit can be controlled by a desktop PC. Basic measurement data are displayed on the front panel or on the PC and can be logged at around a 1s period to disk. The software provides access to the vast array of functions in addition to those available through the front panel. For example, the 'list mode' generates up to 100 timed voltage sequences containing dips, swells, ramps, frequency swings or transient spikes. Harmonic and inter-harmonic voltages can be composed and measurement made to the 40^{th} harmonic.

The PC interface board also provides an analog input for the control by a low voltage $\pm 10V$ user defined waveform. The analog input can be operated in either the AC *amplitude mode* or the AC *amplification mode*. In the *amplitude mode*, the input signal controls the RMS amplitude of the output waveform, at a user defined fixed frequency. In *amplification mode*, the input waveform is reproduced directly at the output, and becomes most versatile when amplifying a user synthesised waveform. Being DC coupled, practically any power quality waveshape, including step changes, inter-harmonics and frequency shifts can be generated to supply a load. A frequency dependent amplitude derating is recommended for frequencies greater than 10kHz.

3.5 SOFTWARE OVERVIEW

The primary control and automation software is written in the Labview software environment. Labview is an engineering package, focussed on test, measurement, and control of engineering systems. Labview was selected as it contains extensive libraries of mathematical and engineering based functions. It also provides a broad collection of supported hardware interfaces, drivers and has become an industry wide standard with third-party hardware support. Labview supports standard protocols TCP, GPIB, RS232, database support and web services all within a modern programming language. In addition, National Instruments release a number of application specific add on packages for Labview including a Report Generation Toolkit.Labview supports external code execution of many software languages and precompiled DLLs as well as interfacing to applications such as Matlab.

A Labview program consists of a number of Virtual Instruments (VIs) (or functions) connected together via data lines (carrying input and output variables). A VI consists of two parts; a front panel, containing a graphical display and user controls, and the block diagram, containing the program data flow diagram responsible for carrying out the program logic. The front panel and block diagram interface together using either controls, to pass user input information to the code, or by indicators, that displaying program variables on the front panel. SubVIs appear as blocks on the data flow diagram and act as functions, accepting inputs and processing outputs. Wires link the subVIs and functions to complete the flow of data in the program. Data abstraction and code reuse are available through the use of subVIs.

A unique aspect of Labview is the use of the dataflow architecture that gives a more intuitive approach to engineering test, measurement and control systems. The Dataflow architecture is a computer architecture that directly contrasts the traditional von Neumann architecture or sequential control flow architecture. Dataflow allows for the concurrent, parallel execution of code, analogous to the laws governing physical systems. Dataflow architectures do not have a program counter (or at least conceptually), the executability and execution of instructions is solely determined based on the availability of input arguments to the instructions. In other words, a section of code is executed once the required inputs become available. Inherently, dataflow architectures support parallel processing; code optimisation can be performed by the compiler to take full advantage of the parallel processing capabilities of modern multi-core processors.

3.5.1 Testing Framework

The software framework provides the supervisory controller to overview the automation of the testing procedures. The supervisory controller monitors the Data Acquisition/Generation and Data Processing sections of the program as shown in Figure 3.5. A classical test procedural logic is followed, as depicted in Figure 3.6 to sequence the multi-stage tests.

Each test consists of; an initialisation, setting the test details, a set of data generation instructions, detailing analytically the output waveforms for each test stage and a set of data processing instructions, used to compute a logic pass/fail result. In the final process the results are collected and presented to the operator.

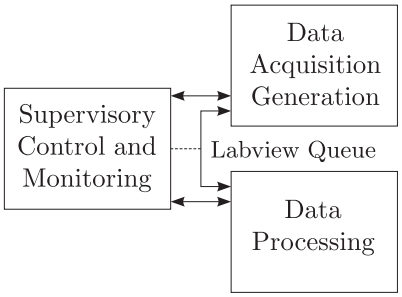

Figure 3.5: Supervisory Control of the Software System

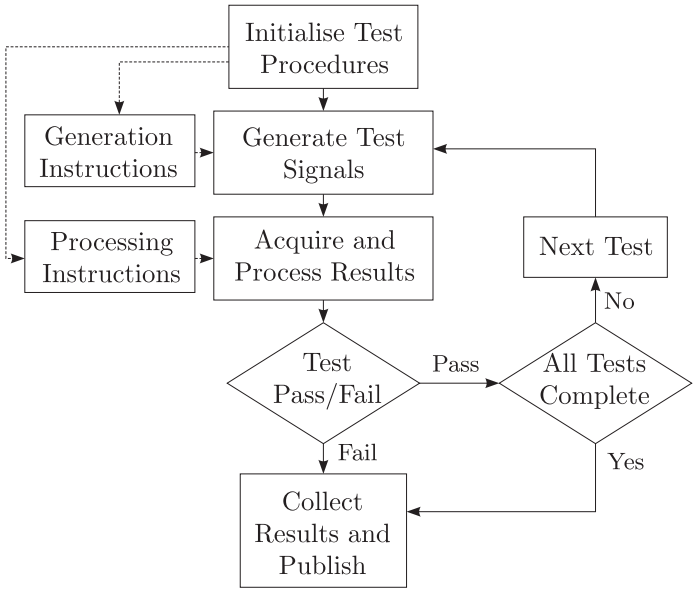

Figure 3.6: Control System Test Logic

3.5.1.1 Acquisition and Processing

The measurement and processing of the input data is handled by a classical Producer/Consumer architecture. The producer/consumer design pattern is based on the Master/Slave concept where the process that produces data is decoupled from the processing of data. This allows the two parts of the program to produce and consume data independently, at different rates. Higher priority given to the sampling of the input data and ensures that communication with the hardware is not delayed and interrupted. Data is therefore collected continually and processed in sequence.

Within Labview, this is typically achieved in two parallel loops, one that communicates with the hardware, producing data and the other performing the computation to the user requirements, consuming the data, as shown in Figure 3.7. The loop interfacing to the hardware is given higher priority than the consumer loop, as delays in connecting to hardware may result in loss of data. A delay in processing that will not compromise the results, is generally acceptable. The data is transferred between the parallel loop using a Labview Data Queue with First In First Out (FIFO) prioritisation to maintain the data sequence. During high processing load, data can continue to be added to the queue until processing time becomes available. In a general sense, the consumer loop must be able to process data quicker that producer produces it to avoid queue

overflow. The Labview compiler identifies and allows the execution of both producer/consumer loops in parallel.

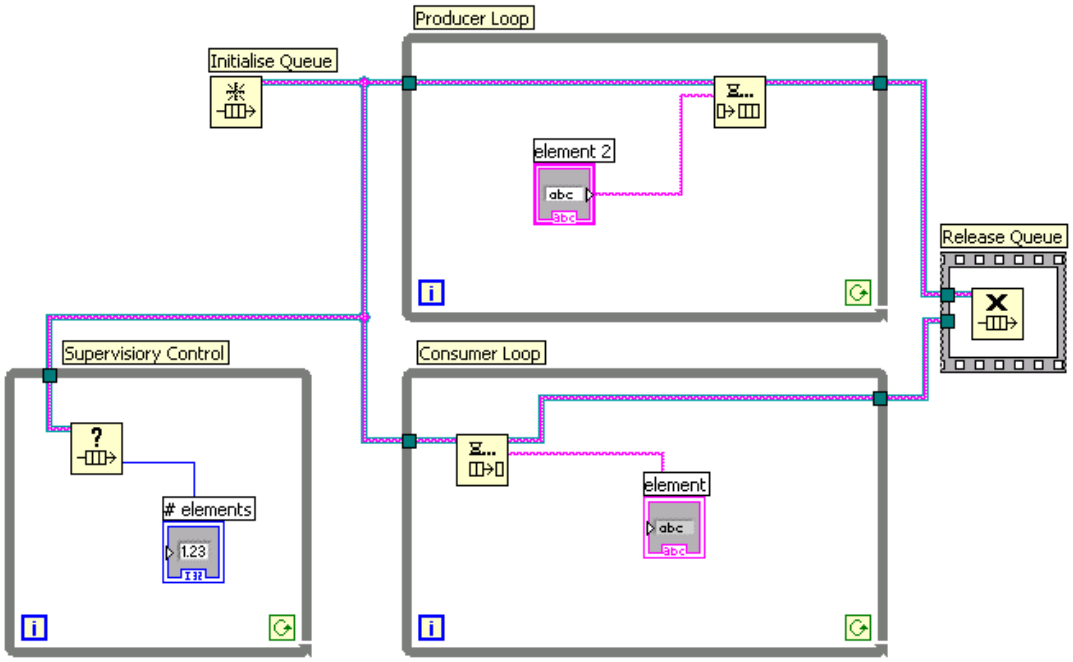

Figure 3.7: Producer/Consumer Data Acquisition Architecture in Labview

Data is produced by the sampling of the acquisition cards input channels and is collected in *Blocks* typically 2-4s in length (user specified). The DAQmx drivers provide the NI DAQ card with Direct Memory Access (DMA) to the computer RAM to improve the performance and avoid buffer overruns. The calibration is applied to the channels before adding the data block to the queue.

The consumer loop waits for data to be added into the queue by the producer loop by continuously polling the queues status. Once a queued block becomes available, the queue item is removed and passed to the data processing handler. The processing handle contains the code defined by user specific to the processing requirements. For example the handler may contain the flickermeter algorithm or an FFT to extract the harmonic information. How the data handlers operates and processes the data are described later in the relevant chapters.

3.5.1.2 Waveform Generation and Output

As mentioned previously the required output waveforms are analytically defined and calculated in software before being passed to the PCI-6229 card for analogue conversion. In order for the generation of complex arbitrary waveshapes the data must be continually calculated and generated in sequence. This is known as non-regenerative, where 'new' is always being generated at the output. In contrast, regenerative mode, uses a single data set and generates continuously by looping through the buffer. Regeneration reduces the data bandwidth, however is only

suitable for cyclic periodic waveshapes. Generation of non-periodic waveforms such as interharmonics would result in steps due to phase differences between the start and end of the data set, introducing unwanted distortion.

Non-regenerative mode is enabled by DAQmx drivers for the PCI-6229 analogue output channels. The waveform data is derived from analytical equations, with double floating point precision using a continuous time reference. Data is produced in 4-10s sections at the desired output level of the AC source before being scaled to the $\pm 10V$ output of the DAC.

3.6 LIGHT MEASUREMENT

Photometry is the measure of light, the visible part of the electromagnetic spectrum to the human eye. The precise measurement of light embodies the spectral sensitivity of the eye and accounts for spatial distribution, reflections and colourimetry, preventing the measurement environment from influencing the result. Two specific lighting environments, a photometric booth and an integrating sphere have been constructed for the measurement of light and are used in the development of a Light based Flickermeter described in Chapter 4.

3.6.1 Luminous Measurement Techniques

The measurement of total luminous flux (or visible total light output) forms the primary measure for lighting equipment. The CIE 84 [28] standard "The Measurement of Luminous Flux" describes two internationally recognised methods for realising the total luminous flux. The two instruments are the Goniphotometer and the Integrating Sphere (also known as the Ulbricht Sphere). In principle, the two methods integrate the spatial distribution of the lamp light output. An alternative technique is the point source method, used in optical benches for the measurement of luminance from a light source. For photopic measurement, the detection matches the normalised CIE spectral sensitivity of the human eye as discussed in Section 2.2.1 and detailed in the CIE standard [1].

In general, the equipment required to the maintain standard measures is highly specialised, costly and needs consistent calibration to maintain accuracy of $< 1\%$. For these reasons calibrated light measurement is typically only performed by national standard regulatory institutes.

3.6.1.1 Photometric Quantities and Measurement Techniques

The luminous flux ϕ_v is given by the radiant flux ϕ_e acting upon the CIE photometric detector. The photopic vision measure of the total lumens (SI unit: lm) is defined as

$$\phi_v = K_m \int_0^\infty \frac{d\phi_e(\lambda)}{d\lambda} V(\lambda) d\lambda \tag{3.1}$$

where $\frac{d\phi_e(\lambda)}{d\lambda}$ is the spectral distribution of radiant flux and $V(\lambda)$ is the CIE spectral luminous efficiency function.

The **luminous intensity**, I_v, is the the luminous flux emitted from a point source at a given angle. It is defined as

$$I_v = \frac{d\phi_v}{d\Omega} \tag{3.2}$$

where $d\phi_v$ is the luminous flux leaving the source and propagating in the element of solid angle $d\Omega$ containing the given direction. (unit: $\mathrm{lm.sr}^{-1}$)

The **Illuminance**, E_v, is a measure of the photometric flux per unit area or density of luminous flux incident on a point of a surface. Illuminance measured in Lux (lx) or lumens per square metre (lm/m^2) and is given by

$$E_v = \frac{d\phi_v}{dA} \tag{3.3}$$

where dA is the area of the detection element.

Luminance is a measure of the level of luminous flux, $d\phi_v$ propagating in a solid angle $d\Omega$ over an area of section dA. Luminance is also subject to the angle, θ, of incidence from the surface norm through the cosine law and is defined by the formula

$$L_v = \frac{d\phi_v}{dAcos(\theta)d\Omega} \tag{3.4}$$

(unit: $\mathrm{lm/m^2/sr}$)

3.6.1.2 Optical Bench - Lighting Booth

A optical bench measures luminous intensity and illuminance (at a fixed direction) of a source. A photometric detector positioned behind a series of baffles at a maximum practical distance from the source. The light source appears as a point source as seen by the detector. Multiple baffles are used to greatly reduce the influence of reflections and stray light. Objects near the detector have a greater effect and black matt paint can be used to reduce reflections. The point source methodology is prone to directional error and is therefore not suitable for the measurement of total luminous flux.

3.6.1.3 Goniphotometer

Total luminous flux is realised by the spatial integration of the luminous intensity. The goniphotometer performs the integration by systematically measuring the radiant flux on a spherical surface around the source. The goniphotometer consists of a photometer mounted on 3 axis arm, the detector is rotated spherically around the centered test lamp. The luminance detector maintains a constant radius, angularly encoding the spacial distribution. The total luminous flux is found by

$$\phi = \sum_{k=1}^{N} l_k/N \tag{3.5}$$

where ϕ is the total luminous flux, E_k is the luminance at each k^{th} location and N is the total number of measurements taken.

The disadvantage of goniphotometers, however, is the requirement of a large darkroom to both reduce reflectance and eliminate stray light. The goniphotometer requires high precision positioning system and lengthy measurement periods not suitable for flicker measurement.

3.6.1.4 Integrating Sphere

The Integrating Sphere (invented by Ulbricht [43]) provides the principle technique for the measurement of total luminous flux from a light source. An integrating sphere consists of a suitably sized hollow spherical cavity, with the test lamp positioned in the sphere center. A photometer placed at the sphere surface, measures the indirect luminance and by successive placement of a standard lamp within the sphere, the relative total luminous flux is determined. The measurement principle of an integrating sphere is considerably simple, however, careful design and construction is required to achieve desirable accuracy, throughput and repeatability of the sphere. The integrating sphere has other applications including; Reflectance and Transmittance measurement and for the generation of a uniform Lambertian light source. However, debate continues over the validity of the integrating sphere method, due to the errors introduced by non-spherical light distribution and indirect flux measurement.

More recently, Yoshihiro Ohno at the American National Institute of Standards and Technology (NIST) developed and realised the Absolute Integrating Sphere Method [39]. This method introduces an external luminance source into the integrating sphere in order to equalise the spheres response. The detector is exposed to the first reflection of the introduced flux of the external source. This method attempts to address the non-uniform reflectance of the sphere wall and effects of baffles and other structures within the sphere.

This section details the design and construction of an integrating sphere in guidance of the CIE 84 Technical report *'The Measurement of Luminous Flux'* [28]. The sphere provides the traceable calibrated measurement of the illumination behaviour of lighting sources. In comparison to the Goniphotometer, the integrating sphere provides a fast measurement procedure for flicker measurement without the large infrastructure of a darkened room.

Measurement Principle and Theory

Based upon the principle of multiple diffuse reflections, the integrating sphere is used to spatially integrate radiant flux, from an internal source of radiation. Derived from Ulbricht's theory, the test lamp radiant flux is uniformly distributed over the internal sphere surface by the Lambertian sphere coating. By the measurement of this uniform surface flux, the total luminous flux can be derived.

The near Lambertian coating of the integrating sphere, has low absorbtion and high reflectivity over the visible spectrum of interest. The reflection of light occurs multiple times within the sphere, evenly distributing the total light energy about the surface. The efficiency, or throughput of the sphere, is determined by the reflectance and diffused nature of the sphere coating, the size and number of ports, the size and location of baffles, and the shape of inclusions inside the sphere.

The sphere size is determined by the lamp under test, it must be suitably sized with sufficient distance between the lamp and the sphere wall to permit multiple reflections. For compact lamps the sphere diameter should be at least 10 times the active length and for tubular lamps at least

twice the largest dimension. The sphere should fully encompass the light source, ensuring no light from outside the sphere enters.

The measurement of total luminous flux is made by a photometer placed at sphere surface. The measurement is made indirectly behind a baffle. The baffle is sized to block the first incidence of light from test lamp falling on the detectors active area. The luminous flux is measured in comparison with a luminous flux standard lamp. The measurement is made by successively placing the light source and the standard lamp at the same location within the sphere.

An auxiliary lamp is incorporated within the sphere and is used for compensation of the lamps absorbance, and in calibration and monitoring of the spheres throughput. The auxiliary lamp compensates for the difference in fitting type of the test lamp in comparison with the calibrated standard lamp. The auxiliary lamp is positioned behind a small baffle, shielding the test lamps fitting from direct illumination and also covering direct illumination of the detector. All other inclusions within the sphere, the lamp supports, baffles, auxiliary lamp influence the measurement result should be kept as small as possible.

Integrating Sphere Theory

In theory, the total luminous flux, ϕ, is determined from the indirect luminance measure, E_{ind}, at the sphere wall by

$$\phi = E_{ind}\frac{1-\rho}{\rho}A \tag{3.6}$$

The infinite summation of the reflectivity, ρ, of the sphere coating gives the convergence term $\frac{1-\rho}{\rho}$. The luminous flux is spread over the area A of the internal sphere surface.

Equation (3.6) describes the idealised throughput of the integrating sphere, unfortunately, the effect of access ports, baffles, lamp supports and non-uniformity of the sphere coating results in a less than perfect throughput of the sphere. The throughput, k, known as the sphere factor, relates the indirect illuminance measurement to the luminous flux and can not be easily calculated [2]. The sphere factor can be more simply determined using by placing a standard reference lamp of known lumen output into the sphere. Using (3.7), k is determined from the standard lamps' known luminous flux ϕ_N and the indirect measure of illuminance at the sphere surface, $E_{ind,N}$.

$$k = \frac{\phi_N}{E_{ind,N}} \tag{3.7}$$

Then, from 3.6 and 3.7 the luminous flux of the test light source is determined by

$$\phi = kE_{ind} \tag{3.8}$$

or

$$\phi = \phi_N\frac{E_{ind}}{E_{ind,N}} \tag{3.9}$$

For a test lamp of similar size and spacial distribution as the standard lamp, 3.10 is applicable.

[2] Calculation of the sphere factor requires the 3D mapping of the sphere and its internal components, along with reflectivity, cosine distribution and spatial distribution of the lamp. Commercial software packages use Finite Element Analysis (FEA) or Ray Trace (RT) techniques

However, for most the consumer lamps, the size and directionality of the lamp varies. The casing and active area change the absorbance of the lamp fitting and hence throughput of the sphere. The auxiliary lamp introduced into the sphere determines the absorbance of the lamp fitting to compensate the lumen output.

The general procedure for measurement with the integrating sphere is as follows; the standard lamp is initially placed inside the sphere and remains turned off while the auxiliary lamp is turned on and the illuminance is measured as E_{nA} (uppercase denotes operational and lowercase denotes the lamp is off). The standard lamp is then turned on and the auxiliary lamp is shut off, after a suitable burning period, E_{Na}, is measured. The standard lamp is then replaced by the test light source and with only the auxiliary lamp on E_{hA} is measured. Switching off the auxiliary lamp, the test light source is energised and measured as E_{Ha}. The total luminous flux of the test source is calculated from

$$\phi = \phi_N \frac{E_{Ha}}{E_{Na}} \frac{E_{nA}}{E_{hA}} \tag{3.10}$$

The ratio of E_{nA} and E_{hA} is the absorbance factor of the test lamp fitting in comparison to the standard lamp.

3.6.2 Design of an Integrating Sphere for the Indirect measurement of Total Luminous Flux

An 828mm diameter integrating sphere was designed and constructed for the measurement of total luminous flux from consumer based lamps. The sphere supports photometric measurement for lamps of nominal active area of 83mm, up to a maximum 250mm length. This includes incandescent lamps, halogen lamps, compact fluorescent lamps and small linear fluorescent tubes. The geometric layout of the sphere design, including the detector, baffles and auxiliary lamp placements and permissable region of the lamps active luminous area is shown in Figure 3.8.

3.6.2.1 Design and Construction

The integrating sphere measures 828mm internal diameter and is constructed from 2mm Aluminium. The two halves of the sphere were formed using the metal spinning technique, over a large wooden former. Stretching of the material during spinning resulted in wall thickness of 1.4mm at the sphere openings. A mounting flange was attached around the hemisphere edges and the internal surface was prepared to uniform roughness before being applied with a spherical coating.

The two half spheres are mounted in a custom-made steel frame, for easy moveability. Each sphere half was bolted to an 8mm rigid backpanel plate attached to the framing. One sphere half is mounted to the stationary backpanel via the flange using 32 countersunk screws, the other half is similarly mounted to a panel that is hinged at the steel frame. This way, the sphere can be fully opened, giving access to the lamp mounting brackets, auxiliary lamp and baffles. Upon closing the sphere, locating pins in the backpanel ensure the sphere edge is correctly aligned, maintaining the form and minimising the sphere loss. Six hand grip bolts, spaced evenly around the sphere edge, tighten the two flanges together, ensuring a light seal in made. Furthermore,

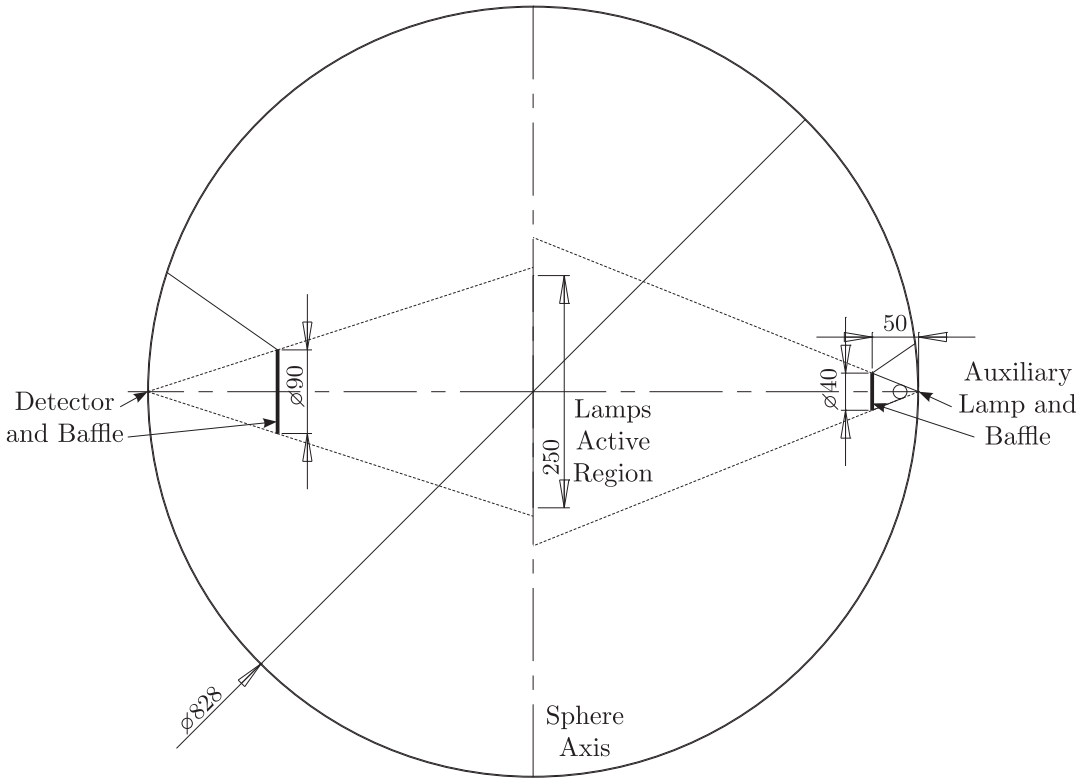

Figure 3.8: Geometric Cross-section and Ray Trace of the Integrating Sphere.

three light seals are used along the flanges, one inner white and two outer blacks, to provide a light seal along the sphere join.

The sphere contains 4 access ports; the detector port, auxiliary lamp port and two ports for lamp mounting positions. The detector and auxiliary lamp ports are both 50mm in diameter and the lamp mounting ports are 41mm⌀. On the outside of the sphere, at the detector and auxiliary lamp ports, shims to provide a flat mounting surface for the holders. A port reducer holds the detector in place at the sphere surface, another port reducer provides a GU10 fitting for the auxiliary lamp. The 90mm detector round baffle covers the detector and defines the permissible active area of the test lamp. Another baffle 40mm round directly opposite the detector covers the auxiliary lamp. Both baffles are held in place by thin metal rods attached to the outer sphere.

The lamp mounting fixture consists of two parts; the mounting post, which remains semi-permanent and the socket extension, containing the specific lamp socket. The electrical power supplied through a moulded 4 pin connection between the post and socket extension. The height mounting post is adjustable outside the sphere to position the active lamp area in the sphere center. The lamp mounting post can either be mounted from the top or bottom of the sphere and are used as different lamp burning positions. Pipe glans at the sphere exit points ensure a light seal is made.

Sixteen custom socket extensions for common lamp types were built. Tabs in the connectors lock the orientation at either 0° or 90° to the detector and ensure consistent placement of lamps. A photograph of the painted parts and fittings is shown in Figure 3.11 and summary of fitting types supported are given in Table 3.4.

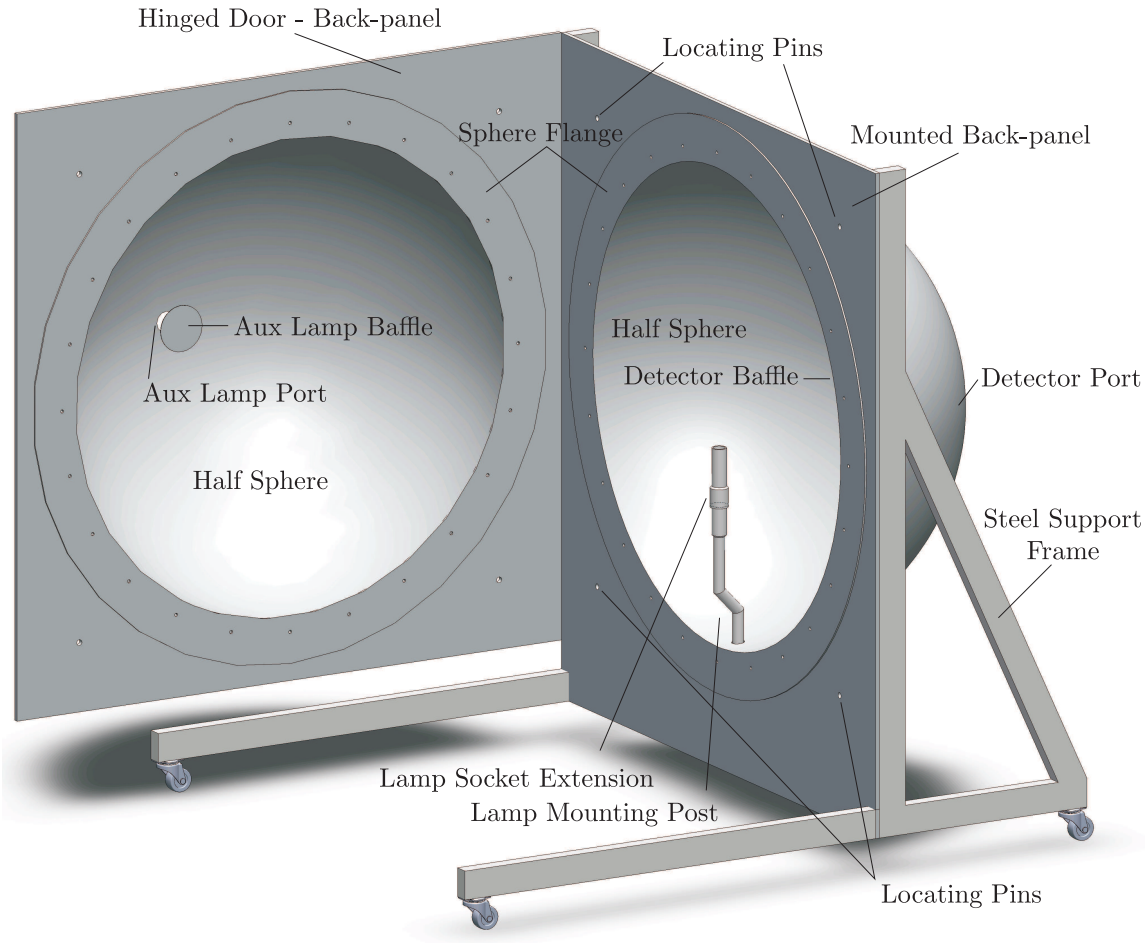

Figure 3.9: 3D Drawing - Integrating Sphere for the measurement of Total Luminous flux.

3.6.2.2 Lambertian Spherical Coating

The integrating sphere was coated in an optical spherical paint and constitutes to the most important parameter in the accuracy and throughput of the sphere. The Avian-B spherical coating from Avian Technologies USA applied is highly lambertian and exhibits non-selective reflectance of over 97% in visible range 350-850nm and greater than 92% from 250-1300nm. All the components inside the sphere that will reflect light are also coated. The sphere's throughput is critically dependent on the sphere coating and its application

To achieve the lambertian surface the Avian-B coating was applied with atleast 20 applications, slowly building the surface to a thickness of 0.5mm. The Avain-B coating is mixed 50:50 with pure ethanol and applied by a professional spray-painter to ensure an even coating to the sphere and components. The result, shown in Figure 3.12 is a highly diffuse, delicate, chalk like surface. The surface can not be cleaned or handled directly; gloves (powderless latex or cotton) must be worn when configuring the sphere to avoid contamination.

Figure 3.10: Photograph - Integrating Sphere for the measurement of Total Luminous Flux.

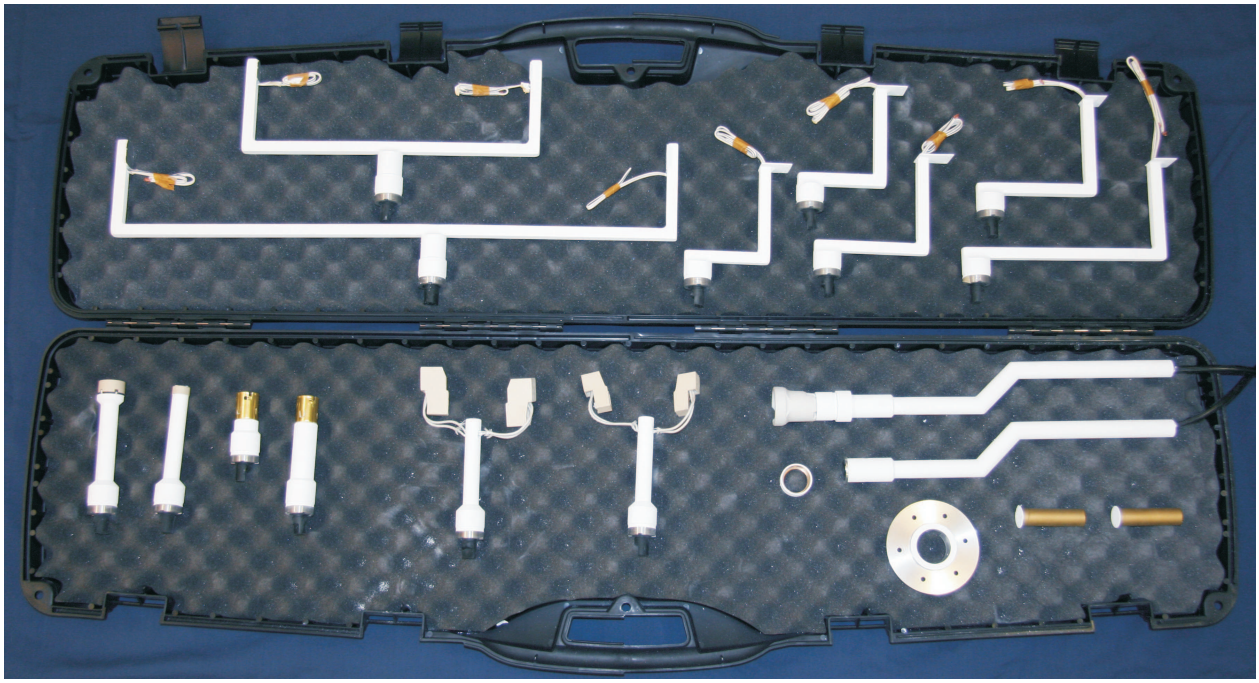

Figure 3.11: Painted Integrating Sphere Components: Lamp Fixtures, Baffles, Mounting Posts, Detector and Aux Lamp Holders.

Table 3.4: Lamp Types and Socket Extensions Built for the Integrating Sphere.

Description	**Fitting Type**	**Active Luminous Length or Tube Length**	**Orientation**
Bayonet GSL	B22	40-140mm [1]	Vertical
Edison Screw GSL	E27	40-140mm [1]	Vertical
Miniature Fluorescent Tube T5	G5	1ft	Horizontal
Standard Fluorescent T8, T12	G13	2ft	Horizontal
Compact Fluorescent 4 pin	2G11	190-380mm	Horizontal
Compact Fluorescent 2 pin	G23	130mm	Horizontal
Compact Fluorescent 4 pin	2GX7	195mm	Horizontal
Compact Fluorescent 2 pin offset	G24d, GX24d	110mm	Horizontal
Tungsten Halogen Lamps Mains Voltage	GU10	10mm [2]	Horizontal
Tungsten Halogen Lamps MR16, MR11 2 pin Low Voltage	G4, G5.3, G6.35	10mm [2]	Vertical
Tungsten Halogen Lamps 2 pin Mains Voltage	RX7s	80-110mm [1]	Horizontal
Metal Halide Lamps	RX7s, RX7s-24	80-110mm [1]	Horizontal

[1]Multiple extensions for range of lamp sizes
[2]Commonly directional lamps with fixed reflector

Figure 3.12: Avian-B Spherical Coating - Lambertain surface.

3.6.2.3 Luminance Detector

Luminance is measured in the integrating sphere and the lighting booth by the VL-3701 Photopic detector by Gigahertz Optik [22]. The detector spectral adaption to the CIE $V(\lambda)$ Photopic function is greater than 3% and meets Lux measurement requirements to DIN 5032-7 part 7 Class A. The detector has a 7mm ⌀ active area and is cosine corrected with less than 1.5% function deviation. Calibration by Gigahertz Optik gave an absolute responsivity of 5.639×10^{-10}A/lx with an error of 3.2%. A tungsten filament calibrated standard lamp was purchased for the

calibration of the sphere.

The detector as shown in Figure 3.13 is coupled with the P-9202-4 High Speed Photo-Current amplifier [22] to convert the detector current to a voltage for measurement. The single channel amplifier has high bandwidth 330kHz with a $1\mu s$ rise time. It has a 8 step sensitivity selector $300nA/V$ to $1\mu A$ at a maximum error of $0.2\% \pm 5mV$. The output connects directly to a general input of the measurement apparatus or through a second order low-pass RC filter was used for anti-aliasing the light signal.

Figure 3.13: Luminance Detector VL-3701 and Photo-current P-9202-4 Amplifier.

3.6.3 Design of an Photometric Booth for the Direct Measurement of Luminous Intensity

The photometric booth was design for the luminous intensity measurement of electrical lamp, primarily, to support the testing of full length fluorescent tubes. The booth, shown in Figure 3.14, is constructed as a photometric bench and consists of a tall cupboard to encapsulate the test lamp and detector. The booth is divided by a series of baffles with the lamp mounted on the left and the detector position in the furtherest external compartment. The light observed by the detector is confined using two baffles, the first in the center of the booth and the second at the entrance to the photometer compartment. The booth is painted internally with a matt black paint to reduce reflections. The detector compartment is covered with thick, light blocking, black material which is also used for the internal baffle. Lamp fixtures were made for bayonet and edison screw fitting in both vertical and horizontal burning positions. Mounts are provided for 3 full length fluorescent fitting in the various size requirements. The lamps are positioned with the viewable region at the center of the sphere to avoid measuring filament flicker at the ends of the tube.

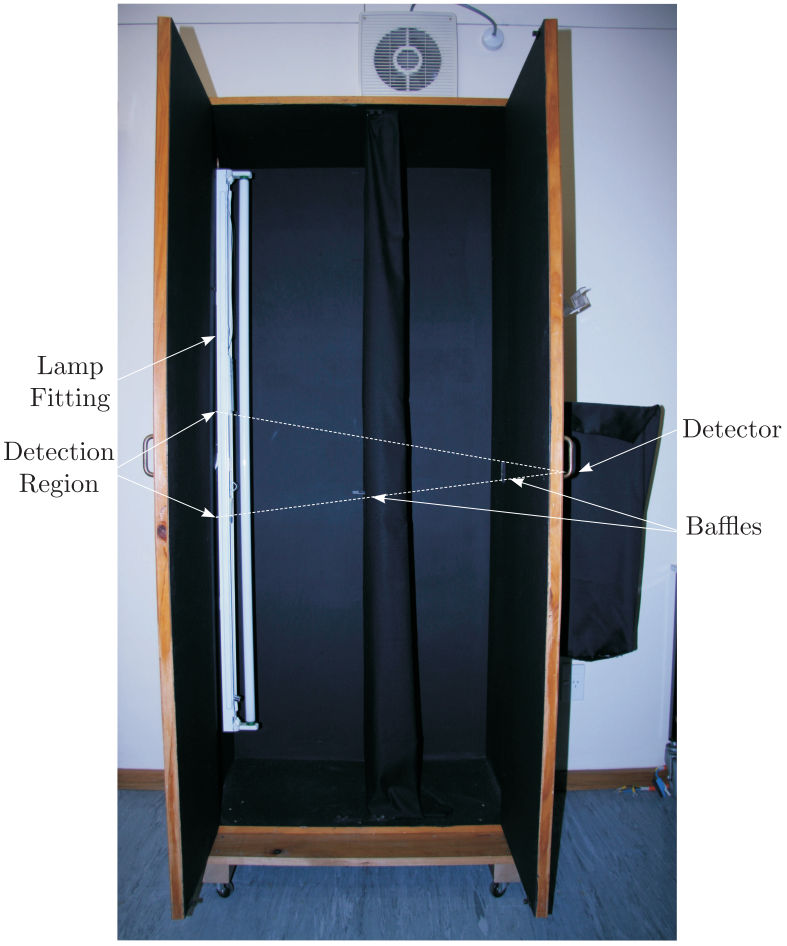

Figure 3.14: Photometric Booth for the Direct Measurement of Luminous Intensity

3.7 CONCLUSION

The experimental system provides a universal power quality test platform incorporated extensively throughout this research for the validation of light flicker and harmonic modelling. The system has been designed for testing consumer based appliances, both single-phase and 3-phase, for a wide range of test and power quality studies. Furthermore the use of the universal measurement system can be extended, for example, for the validation of power system hardware implementations and/or control strategies.

The test system has been automated within the Labview software environment providing a robust, repeatable platform. The user defined data processing and manipulation is performed by a standard desktop PC fitted with a Data Acquisition Card. The measurement apparatus contains 4 fully isolated voltage and current channels for the measurement of nominal power signals. It configured in 3 independent phases with an additional voltage and current channel. Six general input channels connect external voltage probes, current transducers, or other transducer types directly to the DAQ card for measurement. Up to 3 software defined analogue signals can be generated by the DAQ card for the amplification by Programmable Chroma AC power sources. The configuration of the AC sources can be used to generate highly complex waveshapes, for the reproduction power quality distortions and scenarios. An integrating sphere and lighting

booth were constructed for the measurement and analysis of light flicker from electrical lamps.

The versatility of the experimental system is utilised for both the experimental study of Light Flicker in Chapters 4 and 5. Experimental validation is also performed on the harmonic domain models developed in Chapter 7.

Chapter 4

LIGHT BASED FLICKER MEASUREMENT

4.1 OVERVIEW

This chapter proposes a new Light based flickermeter that measures the light levels directly, overcoming the current inaccuracies and enabling quantification of light flicker from any lighting source. This is achieved by removing the dependency of the 60W incandescent reference lamp used in the IEC flickermeter standard. The light flickermeter function resembles the same methodology used by the IEC Flickermeter to allow for the direct comparison procedures. Both the Light flickermeter and the IEC voltage flicker are implemented in the experimental system and fully calibrated to the proposed CCU2/CIGRE flickermeter test protocol.

4.2 INTRODUCTION

From the description of the existing IEC flickermeter it is clear the apparatus is incapable of measuring and quantifying the true flicker level present on modern electrical networks. The inclusion of the 60W incandescent bulb as the reference lamp in the flickermeter standard, limits the detection of flicker based only on this lamp type. Therefore, light flicker from those lamps which do not have the same 60W incandescent lamp characteristics or employ a different luminance technology can not be assessed by the standard. As an example, fluorescent based lighting installed in nearly every commercial and industrial premises and the widespread use of energy efficient CFLs in domestic dwellings, the current standard fails to assess the true flicker level present in the electrical network.

This presents a serious issue for transmission and distribution operators who's responsibility for the assessment and allocation of flicker on their systems is based on the IEC flickermeter standard. Without a coherent standard to quantify and base the management of flicker upon, system operators may impose unnecessary restrictions. Conversely, flicker levels may not be sufficiently managed and lead to increased complaints from affected customers. In both cases there are additional operational costs to the network following a normally expensive mitigation procedure.

Nonetheless the IEC flickermeter presents a clear, internationally recognised methodology for the current detection of flicker. It incorporates all the relevant mechanisms that contribute to the human perception of flicker. This includes; the measurement of voltage fluctuations in the power system, the voltage to luminance transfer through a electrical lamp, the eye-brain memory effect

and frequency response, and finally a time weighting statistical algorithm. The resultant flicker severity indices P_{st} and P_{lt}, align with the directives of the IEC Power Quality 61000 Series. The permissible emission and compatibility levels for customers and networks (respectively) can be coordinated by network operators to manage flicker within the system.

The industry requires a consistent standard that correctly represents the current system and has scope for foreseeable changes in lamp technology, such that system operators can accurately manage voltage fluctuations to minimise overall cost. This chapter proposes a new 'light flickermeter' that quantifies the perceived flicker level from the instantaneous light levels produced by a source. The 'light flickermeter' (as referred to hereafter) is logically based on the existing IEC flickermeter methodology. This allows for the direct comparison and calibration of the new light flickermeter to the existing standard. In addition the light flickermeter output, the sensitivity index, follows in accordance with the existing P_{st} and P_{lt} measurement and can continue to be utilised in the same way by the dependent international standards.

4.3 REVIEW OF THE IEC APPROACH TO FLICKER QUANTIFICATION

The IEC approach to flicker detection has been to measure the instantaneous system voltage and derive the relative light variation and effect on the human perceptibility. In doing so, the measurement of flicker could be made objectively from the AC voltage and made the meter practical for use in the power system industry. It is during this process, an estimate of the relative light change is calculated based on the 60W incandescent lamp.

The foundation research by the UIE Working Group developed a human perceptibility model. The model incorporated the observations of Rassbash, [47] along with some of the characteristics of existing flicker analysis methods. Rassbash's results were based on human flicker sensitivity trials, and like other similar observations of DeLange [17] and Barlow [9], the subject was exposed to controlled thresholds of luminance variation to a small section of the human retina. Rassbash's experiments, most importantly, furthered the perception of humans by studying the effect of combined stimuli (multiple pulses of differing waveshapes). He observed a non-linear square-law relationship of humans eye sensitivity and the brain's memory effect to combine and remember successive disturbances. The inclusion of the perceptibility model removes the subjective nature of human perception of light flicker.

Researchers have been able to develop alternative lamp models by the separation of the lamp characteristics and human response. This was firstly used in extending the IEC flickermeter from the 230V/50Hz subsystem to other system voltages. Sakulin, [48] used this approach in the early stages of extending the European 230V/50Hz flickermeter to the North American and Eastern Asia 120V/60Hz systems which were subsequently included into the IEC standard.

The most complete Light based flickermeter was developed by Gallo [21] at the same time but independently from this research. Gallo successfully developed an objective flicker measurement technique based on the IEC flickermeter approach. The characteristics of the incandescent lamp model were removed and the instantaneous light level was measured using a photodiode. The flicker severity was calculated using a DSP that was interfaced to a PC. A test system was developed for the calibration the flickermeter and was used to investigate the sensitivity of some modern lamp types.

4.4 THE LIGHT BASED FLICKERMETER

The light based flickermeter introduced in this thesis quantifies flicker by the objective measurement of light. The meter adopts the same internationally recognised and logical form of the IEC flickermeter as well as adapting from the 5 functional processing blocks. The stages of the voltage flickermeter process have been modified to achieve the corresponding function in the light flickermeter. Figure 4.1 shows the proposed light flickermeter (lower path) along side the IEC flickermeter.

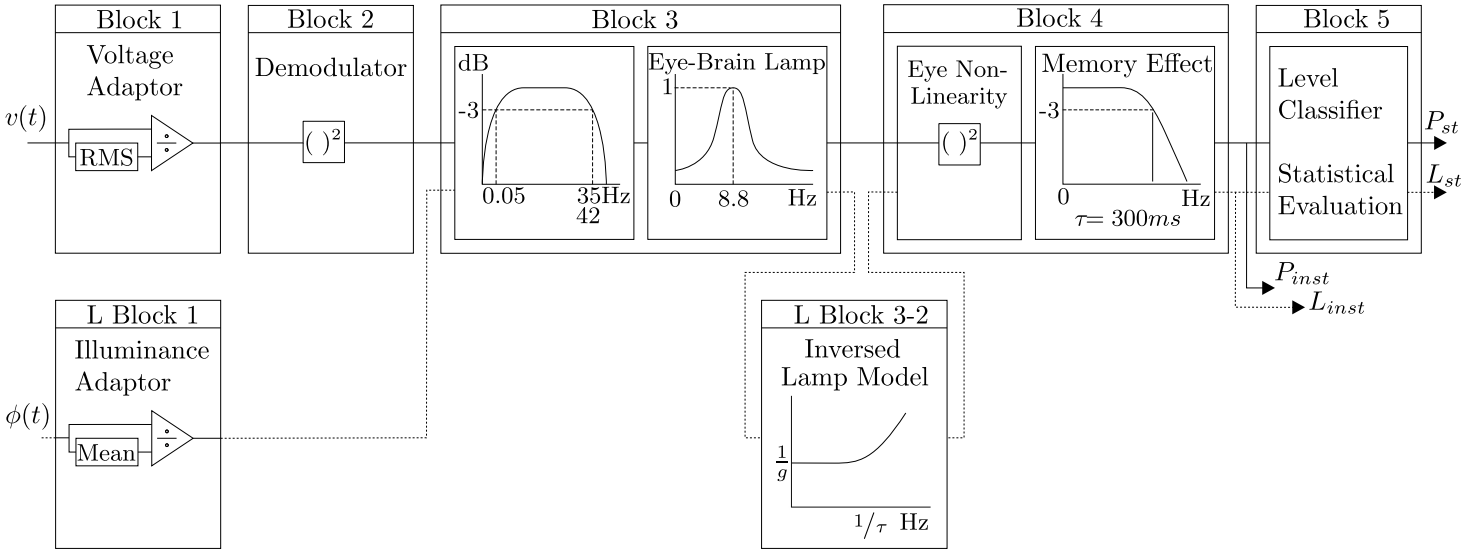

Figure 4.1: Proposed Light Flickermeter / IEC Flickermeter

The light flickermeter retains the objective human flicker perceptibility model of the IEC flickermeter and removes the dependency of the incandescent reference lamp. Additionally the light based flickermeter is adapted in order to directly measure the instantaneous light levels to quantify the human flicker perception. The stages of the voltage flickermeter process have been modified to achieve a similar function. At each stage of the voltage flickermeter process the signal representation is identified and formulated to the equivalent Light flickermeter process.

The human eye-brain sensitivity, memory effect and time weighting statistics, mentioned by the standard, are not dependent on the system reference voltage, frequency or lamp characteristics. The human characteristics model are universal and considered common across the world. Without specified demographics, the characteristics are averaged across all ages groups, genders and ethnicities. Also assumed in the models are normal mental awareness and emotional states. In this way, the light flickermeter assumes that the human perceptibility model within the IEC flickermeter is an accurate representation of the human flicker sensitivity. This is supported by the widespread use and acceptance of the IEC meter.

Shown in figure 4.1, the light flickermeter re-utilises Blocks 3, 4, and 5 of the existing IEC flickermeter. Block 1 is replaced with a Light Adaption Block while Block 2 is removed from the process. An inverse lamp model, Block 3-2, is added between blocks 3 and 4 to eliminate the reference lamp model. The following sections discuss in detail the modifications to each of the 5 functional blocks of the IEC flickermeter.

4.4.1 Block 1 - Light Adaptation

The original role of IEC block 1 was to normalise the input signal such that the flickermeter could be used across all system voltage levels. This is achieved by scaling the instantaneous voltage by a slow RMS value i.e. a RMS value filtered by a relatively large time constant. In relation to the original design, the newly proposed light adaptation block 1 normalises the input light signal which enables the detection of flicker from a light source of any brightness. However, the difference is that the input light levels are normalised to the constant or mean light intensity.

In practical terms the flicker severity measure is therefore independent of the detector position from the light source. This allows flicker testing to be performed using the point source discussed in the previous chapter. However, this does mean the detector must only be detecting light from the source under test.

4.4.2 Block 2 - Demodulator Power

Block 2 of the IEC flickermeter formed part of the reference lamp model. The normailised voltage from the original block 1 was squared, demodulating the RMS variation of voltage and hence power dissipated in the lamp (assuming that the incandescent filament resistance remains relatively constant).

In the new design, the voltage-power-luminance transfer is performed by the lamp which is now external to the light flickermeter process. Therefore the function of the original block 2 is removed and signal is passed directly from the light adaptation block 1 to block 3.

4.4.3 Eye-Brain-Lamp Filter - Block 3

Block 3 of the original IEC design comprises of three separate stages. The first two are a simple low-pass and high-pass filter combination to provide a cut-off for dc and high frequencies while the third stage is a lamp-eye-brain response. The third stage represents the lamp frequency response and the eye-brain sensitivity to light level fluctuation.

There is no direct output nor is it immediately clear where this estimation of light level fluctuation occurs. This is due the characteristics of the lamp being combined with the eye-brain frequency response in the same filter description. Therefore no measurable signal relating directly to the estimate of light exists during the IEC process, however its function is derived.

In the newly proposed light flickermeter an inverse lamp filter is used to remove the dependency of the lamp frequency response as light signals are directly measured. A suitable inverse lamp model is developed in the next section. The model filter response is explicitly added after the 3rd block to avoid numerical instability.

4.4.3.1 Inverse Lamp Model

The block 3 eye-brain-lamp filter is modified with an inverse lamp filter to remove the dependency of the 60W incandescent lamp. For a tungsten filament enclosed in a glass bulb, the filament temperature is modelled by an equivalent thermal circuit and given by the differential equation

$$P(t) = C_\vartheta \frac{d\mathrm{T}(t)}{dt} + \frac{\mathrm{T}(t)}{R_\vartheta} \tag{4.1}$$

where, the thermal input power, $P(t)$, equates directly to the electrical input power dissipated in the lamp. The temperature rise, $\mathrm{T}(t)$, relates to the thermal capacity, C_ϑ, of the filament and the thermal resistance, R_ϑ, representing the heat loss through convection and conduction by the gas, bulb and lead-in wires. This temperature is given as the rise above the ambient temperature T_a.

The transfer function written from Equation 4.1 relates the electrical power and temperature as

$$\frac{\phi(s)}{P(s)} = k_L \frac{R_\vartheta}{\tau s + 1} \tag{4.2}$$

where $\tau = C_\vartheta R_\vartheta$ equates to the lamps thermal time constant. This shows the filament acts as a low pass filter which naturally aids the lamps flicker reduction attenuating frequencies above $1/\tau$ radians/s. Typical lamp time constants vary between 20ms and 100ms and greatly depend on nominal voltage, encapsulating gas, bulb geometry, age, and filament length and thickness.

In [27], the relationship between the relative lumen output and the relative voltage is given as a nominal rated ratio,

$$\left(\frac{\phi}{\phi_{nom}}\right) = \left(\frac{V_{rms}}{V_{nom}}\right)^k \tag{4.3}$$

The ratio, $k = 3.4$, is noted approximately for standard tungsten lamps. The relative power, and voltage is given as

$$\left(\frac{P}{P_{nom}}\right) = \left(\frac{V_{rms}}{V_{nom}}\right)^n \tag{4.4}$$

where $n = 1.6$ is noted.

This indicates the presumption made in Equation 2.2 where the filament resistance, R_n, remains relatively constant over the voltage signal range is incorrect. Rearranging and in addition to linearising about the nominal operating conditions the linear relationship of P and ϕ,

$$\left(\frac{\phi}{\phi_{nom}}\right) = \left(\frac{P}{P_{nom}}\right)^{k/n} \tag{4.5}$$

$$\phi \propto \frac{k}{n} \cdot P \approx 2.125 \cdot P \tag{4.6}$$

Equation 4.6 determined as the gradient from the Differentiation of the nominal gain ratio as, k/n or approximately 2.125. Relating this to equation 4.2 the power to luminous flux transfer for the incandescent lamp is;

$$\frac{\phi(s)}{P(s)} = \frac{\alpha}{\tau s + 1} \tag{4.7}$$

where, α is the gain ratio from equation 4.6.

The lamp, a low-pass filter provides filtering of frequency above the $1/\tau$Hz. The inverse incandescent lamp model 4.8 is therefore the direct inversion of equation 4.7. The filter zero is BIBO unstable, special implementation of this filter is required to ensure the correct gain and roll-off

frequency is retained from the original filter. The pre-filtering of the cut-off filters ensures that the instability of the lamp filter is not excited

$$\frac{P(s)}{\phi(s)} = \frac{\tau s + 1}{\alpha} \tag{4.8}$$

The lamp model and its inverse were both experimentally obtained for the selected calibration lamps. The gain and the time constant, τ, were verified systematically to ensure complete and accurate calibration of the light flickermeter.

4.4.4 Block 4 - Eye-Memory Response

The original block 4 of the IEC flickermeter mimics the observed memory effect of human by a squaring multiplier and a first order sliding mean filter. This block bears no relation to the reference lamp or the measurement of light thus makes it suitable and does not need to be modified for the proposed design.

4.4.5 Block 5 - Statistical Evaluation

Block 5 of the IEC flickermeter is designed to provide a statistical analysis for the time-at-level measure i.e. the time period spent for a human perceiving fluctuating light that caused annoyance. It outputs a perceptibility index for the observation period which describes the level of irritation sustained. This block does not depend on the lamp model nor the light measurement and thus it is not modified for the proposed design.

4.5 OPERATIONAL COMPARISON TO IEC 61000-4-15

The IEC flickermeter and the proposed light flickermeter become equivalent when the 60W incandescent reference lamp is placed in front of the Light Flickermeter. As shown in Figures 4.3, 4.4 and 4.5, exciting both the lamp and the IEC flickermeter with the same input voltage, the light flickermeters operation can be compared and calibrated.

The light flickermeter and the IEC flickermeter were implemented side by side in the test system software as described in Chapter 3. Both were stimulated by the same input voltage, for illustration, 1% 8Hz square-wave modulation. These results show that prior to the input of block 4 the signal appear different as indicated in Figures 4.3. Figure 4.3(a) is the input to the IEC flickermeter, the voltage waveform, Figure 4.3(b) is the measurement of light produced by the 60W standard lamp. Figure 4.3(c) has been normalised by its RMS Value and Figure 4.3(d) normalised to the averaged light level. Figure 4.3(e) shows the demodulated (squared) waveform from the output of Block 2. Since the Light flickermeter does not contain a block 2, Figure 4.3(f) is unchanged from Figure 4.3(d). Following the filters of Block 3, the IEC flickermeter signal becomes identical to the Light Flickermeter signal once it passes through Light Block 3-2 the inverse lamp filter, as shown in Figure 4.4(a). After Block 4 the waveforms remain similar as shown in Figure 4.4(b). And finally the CDF developed in Block 5 of the two waveforms (shown in Figure 4.5) are practically identical, giving the same P_{st} and L_{st} results.

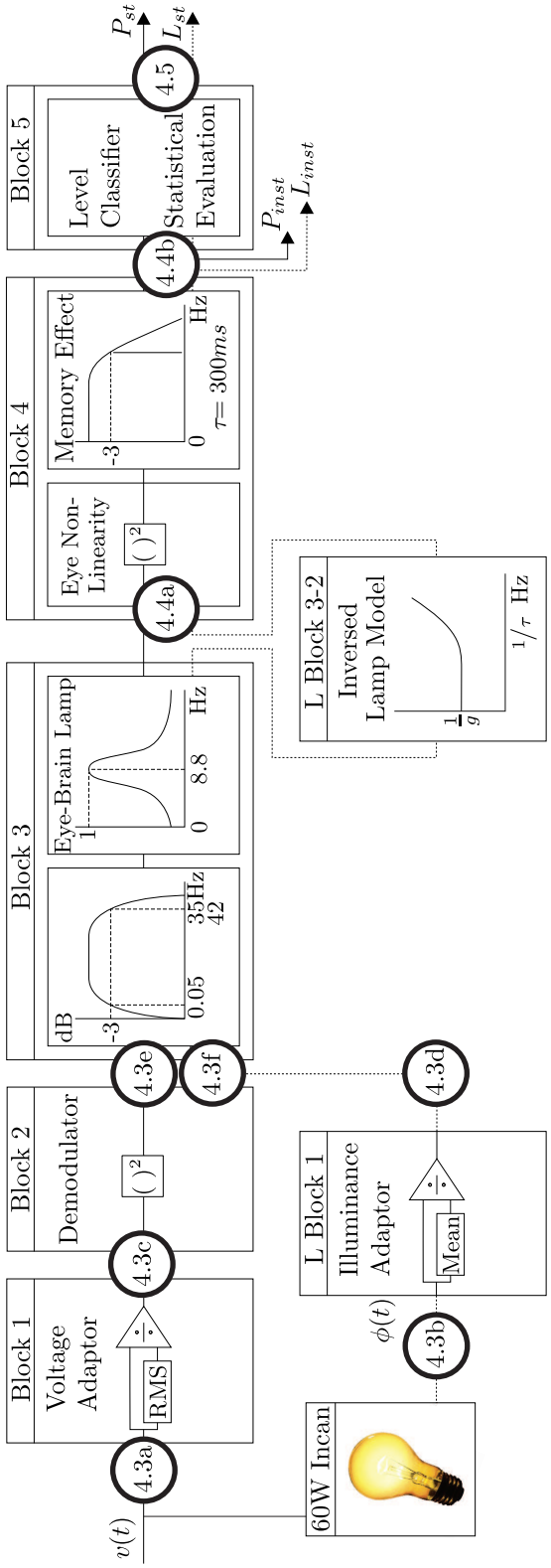

Figure 4.2: Comparison of Light Flickermeter and IEC Voltage Flickermeter indicating waveform locations as plotted in Figures 4.3, 4.4, and 4.5

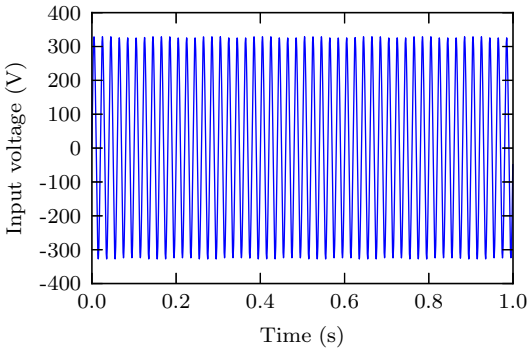

(a) Input Voltage Block 1 IEC Flickermeter

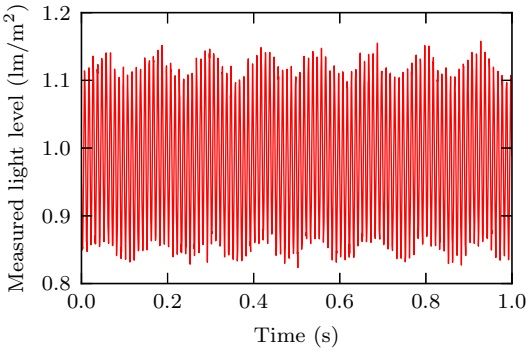

(b) Input Light Block 1 Light Flickermeter

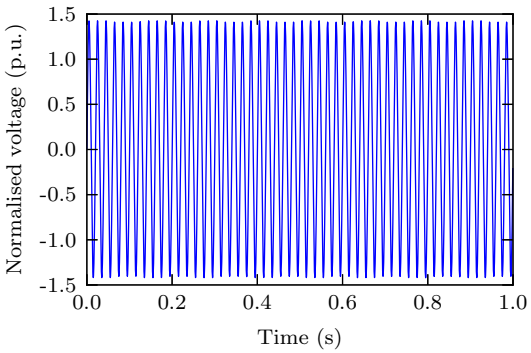

(c) Normalised RMS Output Block 1 IEC Flickermeter

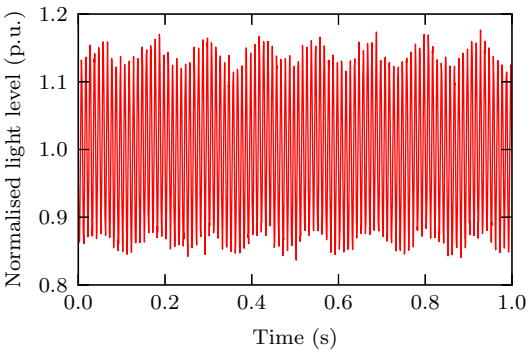

(d) Normalised Light Output Block 1 Light Flickermeter

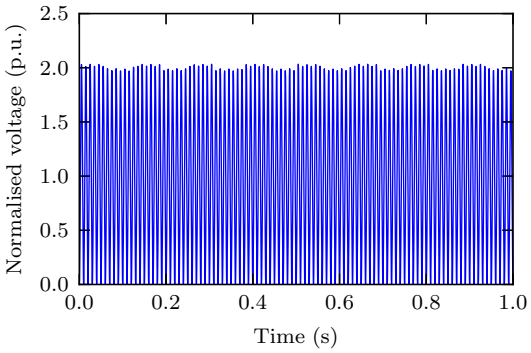

(e) Demodulated Output Block 2 IEC Flickermeter

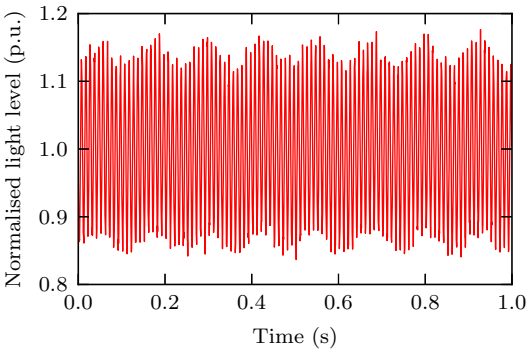

(f) Normalised Light Output Block 2 Light Flickermeter

Figure 4.3: Operational Comparison of Light Flickermeter and IEC Flickermeter: 1% 8Hz square-wave modulation. Input voltage waveform, Incandescent 60W Lamp Light, Output waveforms of Block 1 and 2 at locations indicated in Figure 4.2.

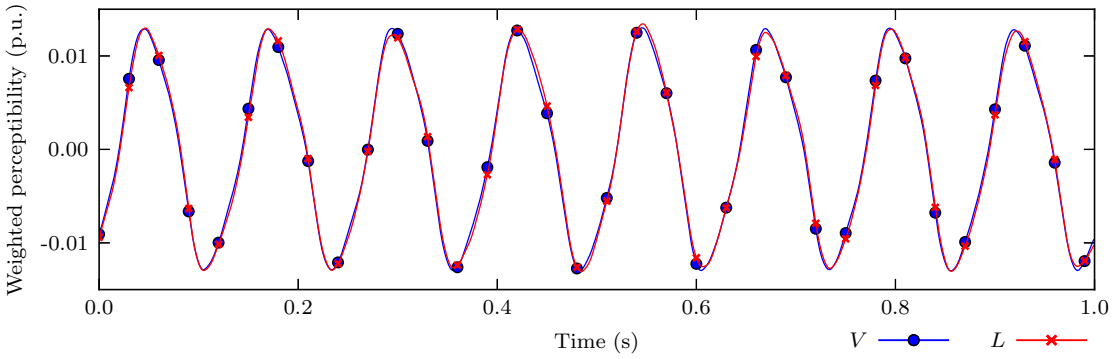

(a) Weighted Perceptibility Output Block 3 IEC Flickermeter and Light Flickermeter

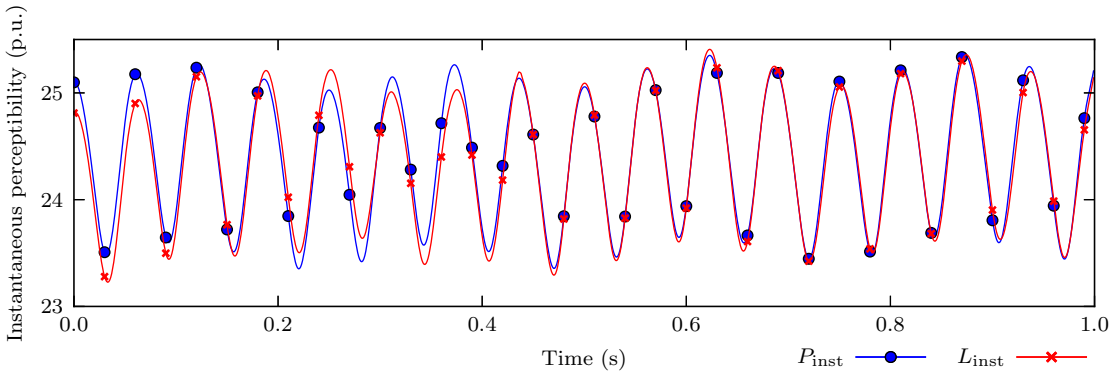

(b) Instantaneous Perceptibility Output Block 4 IEC Flickermeter and Light Flickermeter

Figure 4.4: Operational Comparison of Light Flickermeter and IEC Flickermeter: 1% 8Hz square-wave modulation. Waveforms of Block 3 and Block 4 as indicated in Figure 4.2.

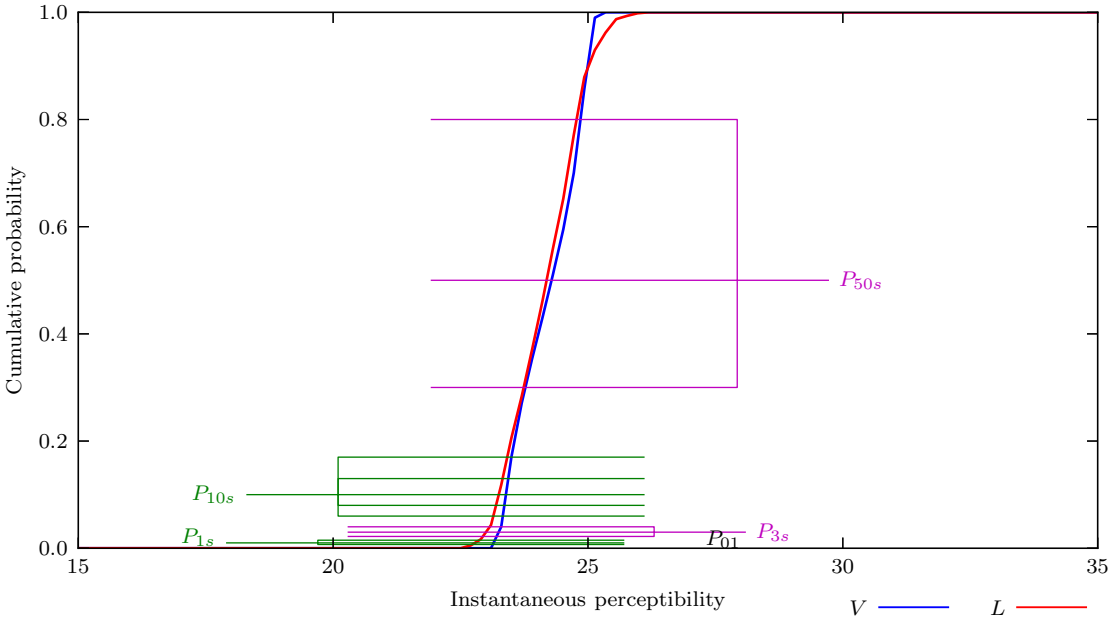

Figure 4.5: Operational Comparison of Light Flickermeter and IEC Flickermeter: 1% 8Hz square-wave modulation. Block 5 CDF with gauge points indicated

4.6 CALIBRATION

In recent years the IEC flickermeter specification has come under close scrutiny as modern digital implementations do not produce consistent results in the field when stimulated by the same voltage. This is because it was originally designed for analogue operation and the calibration procedure is not comprehensive. It consists of only seven test points with a high compliance tolerance of +/-5%. It is therefore up to the manufacturers to decide on the instrument attributes, namely, sampling rates, digital resolution, and filter design, which are not specified in the standard.

The CCU2/CIGRE joint working group on power quality developed new test protocols [12] for the IEC flickermeter. A portion of these are adopted into the latest IEC Flickermeter standard. The test protocol specifies a number of tests that each verify a certain aspect of the meter's performance and/or accuracy. The tests verify: accuracy to the existing standard, cases of no influence, unique cases of influence, and simulations of complex waveforms characteristic of real world applications.

Three instrument test classes were devised to define the unit's accuracy and capabilities. Class 1 is mandatory for all flickermeters to meet the specifications [3]. Classes 2 and 3 indicate the instrument is tested to the CCU2 Test protocol and define the specified operational range and accuracy of the test compliance. The Light Flickermeter and IEC flickermeter were calibrated to Class 3 of the Test Protocol. The following presents only a selection these results. The lamp model parameters for the two calibration incandescent lamps, for the 230V/50Hz and the 120V/60Hz nominal system, are given in Table 4.1.

Nominal system	α	τ (s)
230V/50Hz	1.923	0.019
120V/60Hz	1.923	0.021

Table 4.1: Verified Standard Lamp model parameters

4.6.1 CCU2 Flickermeter Test Protocol 2: Rectangular Modulation

Test 2 performs the calibration to the rectangular voltage fluctuations as presented in the IEC Flickermeter standard [3]. The modulation levels indicated were generated and applied to the standard incandescent lamps. The P_{inst} was calculated from the voltage measured and the L_{inst} calculated from the measured lamp light output to be within 8% of $P_{inst}/L_{inst} = 1.0$.

4.6.2 CCU2 Flickermeter Test Protocol 3: Sinusoidal Modulation

Test 3 performs the calibration to the sinusoidal voltage fluctuations presented in the IEC Flickermeter standard [3]. Again the modulation levels indicated were generated and applied to the standard incandescent lamps. The P_{inst} was calculated from the voltage measured and the L_{inst} calculated from the measured lamp light output to be within 8% of $P_{inst}/L_{inst} = 1.0$.

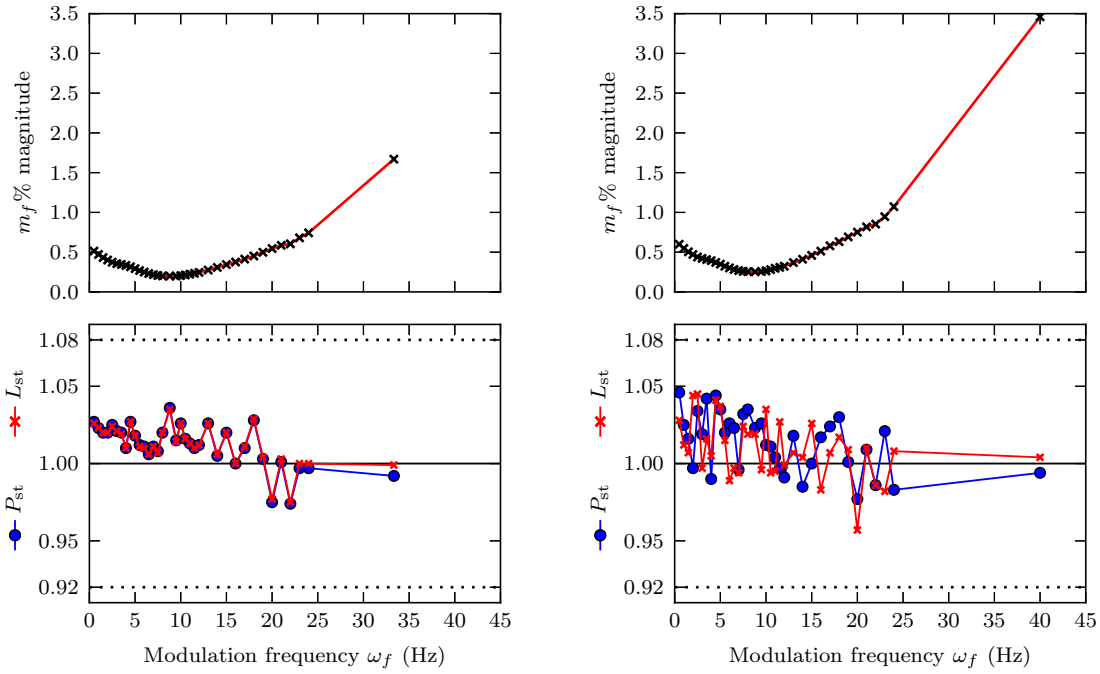

(a) 230V 50Hz Nominal Voltage

(b) 120V 60Hz Nominal Voltage

Figure 4.6: Test 2. Light Flickermeter and IEC Flickermeter Response to Rectangular Modulation. (upper: Modulation Level. lower: Calculated P_{inst} and L_{inst})

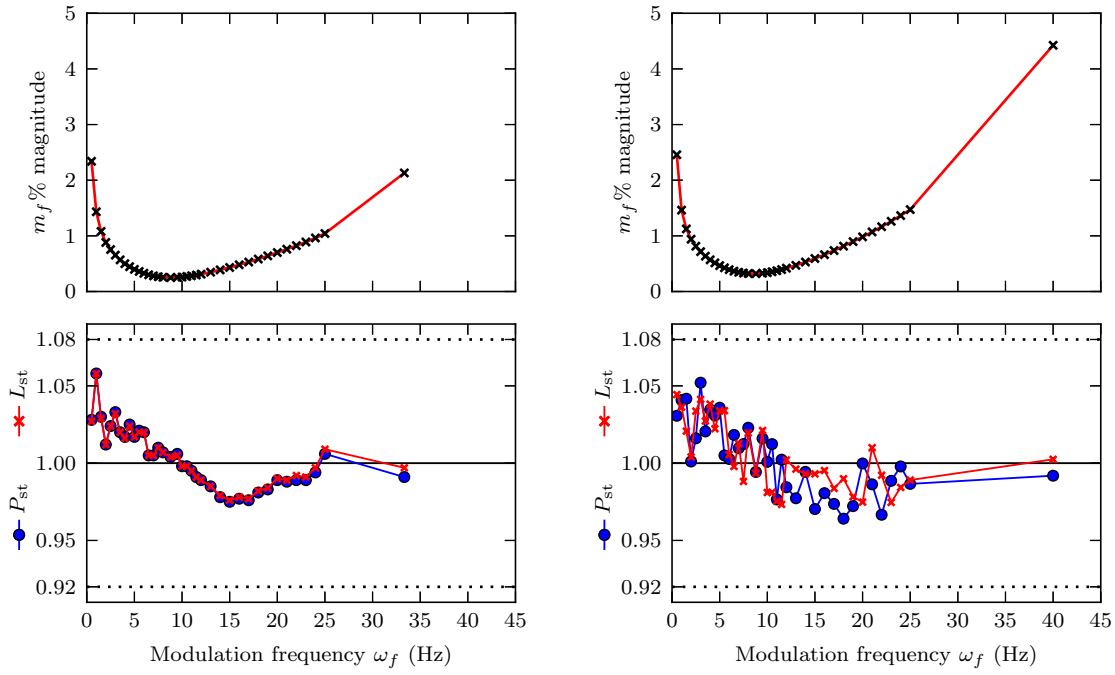

(a) 230V 50Hz Nominal Voltage

(b) 120V 60Hz Nominal Voltage

Figure 4.7: Test 3. Light Flickermeter and IEC Flickermeter Response to Sinusoidal Modulation.

4.6.3 CCU2 Flickermeter Test Protocol Test 4: Mains Frequency Variation

Test 4 verifies the flickermeter performance to variation of the mains frequency. For Class 3 this requires the 2.0% change in fundalmenal frequency while applying rectangular modulation at 8.8Hz to measure a $P_{st}/L_{st} = 1.0 \pm 5\%$. The results for the 230V/50Hz system are given in table 4.2.

Fundamental (Hz)	P_{st}	L_{st}
50 -2% = 49 Hz	1.03	1.03
50 +2% = 51 Hz	1.03	1.03

Table 4.2: Test 4. Light Flickermeter and IEC Flickermeter Mains Frequency Variation.

4.6.4 CCU2 Flickermeter Test Protocol Test 5: High Frequency Influence

Test 5 checks the flickermeter bandwidth to ensure high frequency disturbances are correctly blocked from measurement. This non-influence test ensures correct filtering so that high frequency aliasing does not affect the meter during normal operation or when flicker is present. For Class 3 a 10% voltage is swept from 100Hz to 2kHz at a 5Hz/s slew rate. With no distortion the flickermeter should measure a maximum $P_{inst}/L_{inst} < 0.2$. The same sweep is performed with a 8.8Hz voltage modulation and the measured maximum $P_{inst}/L_{inst} = 1 \pm 5\%$. The results as expected are given in Table 4.3.

	P_{inst}	L_{inst}
No distortion	0.003	0.003
Distortion at 8.8 Hz	1.036	1.035

Table 4.3: Test 5. Light Flickermeter and IEC Flickermeter High Frequency Influence, CCU2 Protocol

4.6.5 CCU2 Flickermeter Test Protocol Test 6

Test 6 verifies the linearity of a flickermeter over the specified range. Class 2 defines meters to be linear for short time perception from 0.2 to 4.0 p.u.; Class 3 from 0.2 to 20.0 p.u. This test ensures sufficient perceptibility levels in the statistical analysis of Block 5. Figure 4.8 show the linearity of both flickermeters between 0.2 and 4.0 p.u.[1]

4.6.6 CCU2 Flickermeter Test Protocol Test 8

When an interharmonic beats with either a harmonic or another interharmonic flicker can result. Test 8 simulates the interaction of a harmonic with an interharmonic separated by 10Hz. In effect this ensures the bandwidth of the input electronics and of Block 1 to allow for high frequency interharmonic pairs to be measured. Table 4.4 shows the test points of a harmonic

[1]Both the Light Flickermeter and the IEC Flickermeter were calibrated to Class 3. 0.2 to 20 p.u. For presentation purposes linearity for 0.2 to 4.0 p.u. is shown.

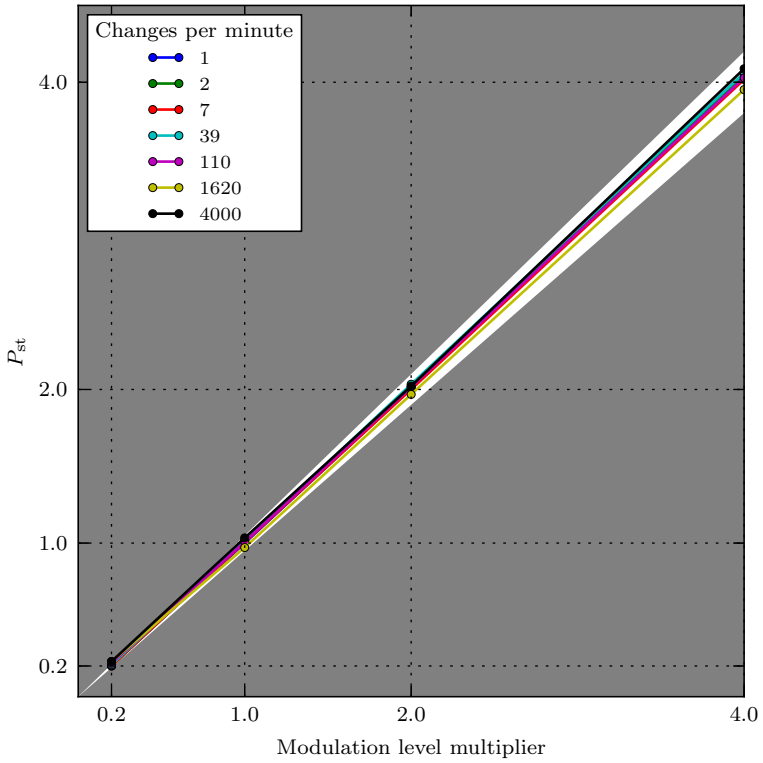

(a) Voltage - IEC Flickermeter

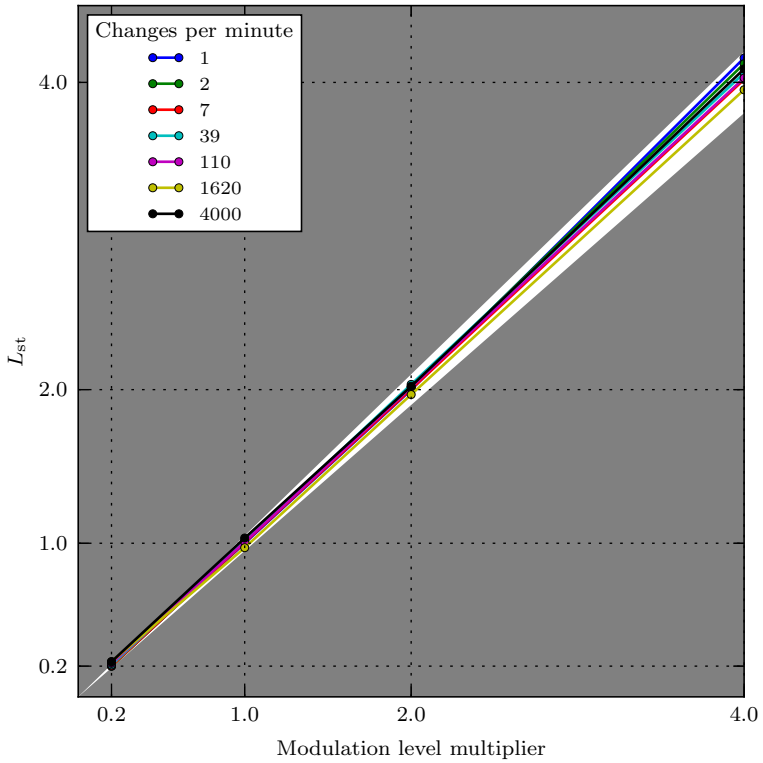

(b) Light Flickermeter

Figure 4.8: Test 6. Light Flickermeter and IEC Flickermeter Linearity 0.2 - 4.0 p.u. The grey area marks the 5% error region.

and $+10Hz$ interharmonic applied at 3% with the nominal voltage to both flickermeters. The $P_{\text{inst}}/L_{\text{inst}} = 1.0 \pm 5\%$ results demonstrate fulfilment of the test.

Frequency 1	Frequency 2	P_{inst}	L_{inst}
150 Hz	160 Hz	0.989	0.986
250 Hz	260 Hz	0.987	0.986
350 Hz	360 Hz	0.987	0.986
550 Hz	560 Hz	0.987	0.986
650 Hz	660 Hz	0.987	0.986

Table 4.4: Test 8. Light Flickermeter and IEC Flickermeter Interharmonic Pairs, CCU2 Protocol

4.6.7 CCU2 Flickermeter Test Protocol Test 9: Phase Jumps

Phase jumps occur on networks during switchings of feeder, faults or line disconnects, EAF and static switch of large loads or capacitor banks. The phase jump test was extended to include a greater number of jump angles. The phase jumps are tested at 5° angles $0 - 360°$. The phase jump occurred from the zero crossing of the fundamental voltage. The P_{st}/L_{st} was recorded with the jumps occurring at 1, 3, 5, 7, and 9 minutes of the 10 minute period. Figure 4.9 shows the alignment of the light flickermeter and shows how the flicker level varies with the angle of phase jump.

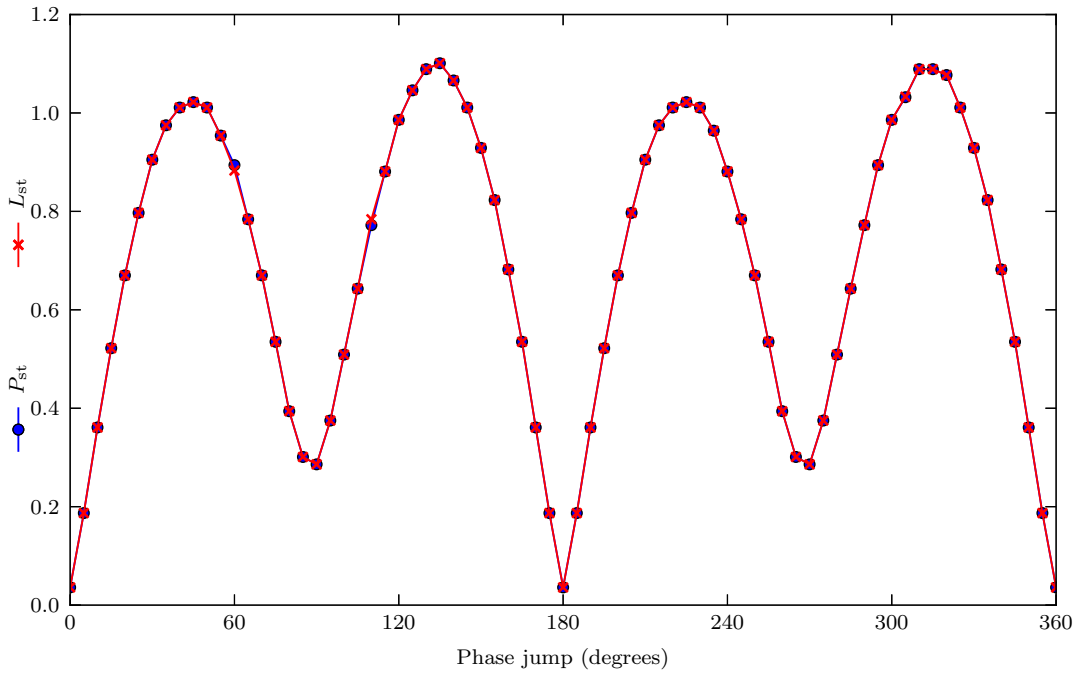

Figure 4.9: IEC and Light Flickermeter Phase Jump

4.7 OPERATIONAL CONSIDERATIONS

The light flickermeter is highly susceptible to external light sources being detected by the light detector, therefore, careful consideration needs to be given to the operation of the device. It would be impractical to used the light flickermeter without a tightly controlled environment. At the greatest sensitivity (near 8.8Hz), the light variation only needs to vary by as little as 0.196% to be considered noticeable and borderline irritable flicker. In a practical example if a person was to walk past and block a portion of the detectors vision, the change in light level would be detected and measured as flicker. The issue here is that the measured flicker did not originate from the power system nor the light source but the local environment. Similarly, if the light detector observed stray light from a constant light source, such as sun light, the flickermeter would measure a lower relative light fluctuation and hence a lower flicker level. It is not possible for an international standard as such, to compensate for the local environmental considerations. The light flickermeter is best suited to controlled laboratory environments.

While the use of the point source light measurement method is applicable, the ageing of some lamps, can cause visible light fluctuations in various parts. Particularly in discharge lamps, the leaking of internal gases can result in swirling gases or flickering near the electrodes. The most ideal apparatus is an integrating sphere, where the total lamp output is integrated over all spherical angles[2]. Extensively aged lamps, and likewise malfunctioning lamps, should be avoided. Lamps should ideally be generalized to ensure results are comparable. That is to select lamps which are neither the best performers or the worst.

4.8 CONCLUSION

This chapter has identified the shortcomings of the IEC approach to the detection of the light flicker beyond the incandescent lamp. By modification of the IEC approach, a light based flicker measurement technique has been developed. The quantification of flicker levels directly from the instantaneous lighting level eliminates the dependence on a reference lamp thereby expanding its capabilities to other lighting sources.

As the use of highly non-linear and highly variable efficiency lighting systems increases in the domestic market, the current flicker standards will fail to evaluate the perceivable flicker present on the electrical network. This has been the case in commercial and industrial sectors for sometime where energy efficient fluorescent lighting is standard.

While the light flickermeter is intended to be useful in its own right, the technique allows for the investigation of other lighting technologies to voltage disturbances and is the subject of Chapter 5.

[2]The integrating does not strictly integrate over all spherical angles. The lamp supports, baffles, auxiliary lamp, and surface coating all obstruct the full integration. Further information on the integrating sphere operating principles can be found in section 3.6.1.4

Chapter 5

FLICKER SENSITIVITY OF ELECTRICAL LIGHTING

5.1 OVERVIEW

Having developed a fully compliant Light-based flickermeter capable of testing new lighting technologies in Chapter 4 this chapter will demonstrate the flicker sensitivity of this technology. First a comparison between compact fluorescent lamps and incandescent lamps for flicker production under common power quality disturbances is presented. Secondly, a LED lighting system designed to eliminate flicker, is developed and tested.

5.2 INTRODUCTION

The widespread adoption of high efficiency lamps has highlighted the discrepancies between the measured flicker levels by the AS/NZS 61000-4-15 standard and the actual levels experienced by humans. Using a unique method of flicker detection, the actual instantaneous light levels produced by a lamp are analysed. This overcomes the limitations of the flickermeter standard and is used to demonstrate the sensitivity of the light CFLs produce in the presence of power system disturbances such as; interharmonics, phase jumps, dips and swells some of which are not normally associated with flicker.

Compact fluorescent lamps (CFLs) have recently emerged as cost-competitive, energy efficient alternatives to replace conventional incandescent lamps in their existing fittings. Traditional incandescent lamps have remained relatively unchanged since the invention in the 19^{th} century and have long been known as inefficient sources of electrical lighting. With current global pressures towards energy efficiency, CFLs offer 4-5 times the efficiency using fluorescent technology.

However, because CFLs use electronic ballasts, their subsequent non-linear behaviour has made modelling of their operation difficult. Equally their susceptibility to voltage disturbances resulting in visible light flicker is widely unknown and difficult to predict. This has given rise to discrepancies between the measured flicker levels by relevant international flicker standards and the actual flicker present on the system. The following sections presents a comparison between compact fluorescent lamps and incandescent lamps for flicker production under common power quality disturbances.

LED lighting is an emerging technology that is rapidly being deployed due to its benefits. The most efficient white LEDs now achieve light outputs in LED lighting can deliver in excess of 100

lumens per watt of electrical input power, surpassing the efficiency of fluorescent tubes. With suitable drive circuitry they can be made immune to electrical disturbances, as well as providing dimming and controllable colour rendering. To show what can be achieved a new multichip LED lamp with spectrum adjustment, mounted in a four foot fluorescent fitting, with ballast replaced by driver electronics has been developed. In Section 5.4 this LED lighting system is compared with a commercial white LED fluorescent tube replacement as well as with a white fluorescent tube, all mounted in the same four foot fitting, with conventional inductive ballast.

5.3 FLICKER SENSITIVITY OF COMPACT FLUORESCENT LAMPS

Given the vast array of CFLs present on the market, extensive testing lead to the selection of 4 CFL lamps presented in Table 5.1. These lamps and their flicker sensitivity represent the similarities and differences found across the bulk of CFLs, manufactures and power ratings currently on the market. These results are not meant to form a complete comparison of the CFLs available but are to demonstrate the application of the light flickermeter presented in the previous chapter.

ID	Brand	Circuit Topology	Cost	Rated Power (W)
Eco 20w	Ecobulb	Modified Valley-Fill	Medium	20
Eco 20w	Ecobulb	Modified Valley-Fill	Medium	13
Elite 20W	Elite	Valley-Fill	Low	20
Tornado 24W	Phillips	Filtered Rectifier	High	24

Table 5.1: Selected CFLs for the flicker performance comparison.

5.3.1 Rectangular Voltage Modulation

Figure 5.1 shows the 2 CFL subjected rectangular voltage modulation. The level shown is the modulation required to reach the perceptibility limit of $L_{st} = 1.0$. A lower result indicates increased sensitivity to rectangular modulation at the particular frequency. It can therefore be said that a level of modulation below the curve would result in acceptable light flicker and for modulation levels above the curve unacceptable flicker would be observed. The results clearly shows the Incandescent lamp response (equivalent to the IEC flickermeter) is incapable of quantifying the visible light flicker from CFLs. The IEC flickermeter and incandescent lamp produce measurable flicker up to 150Hz while CFLs produce significant flicker at higher modulation frequencies.

5.3.2 Single Interharmonics

Figure 5.1 shows the same 2 CFLs supplied with a single interharmonic voltage distortion. Again the level indicated is the magnitude required to reach the perceptibility limit of $L_st = 1.0$. In this case the IEC flickermeter and equivalent incandescent lamp only produce measurable flicker from single interharmonics up to 100Hz. CFLs are generally less sensitive (by a factor of 2) up to interharmonics of 100Hz however the sensitivity extends beyond with similar response to frequencies beyond 500Hz.

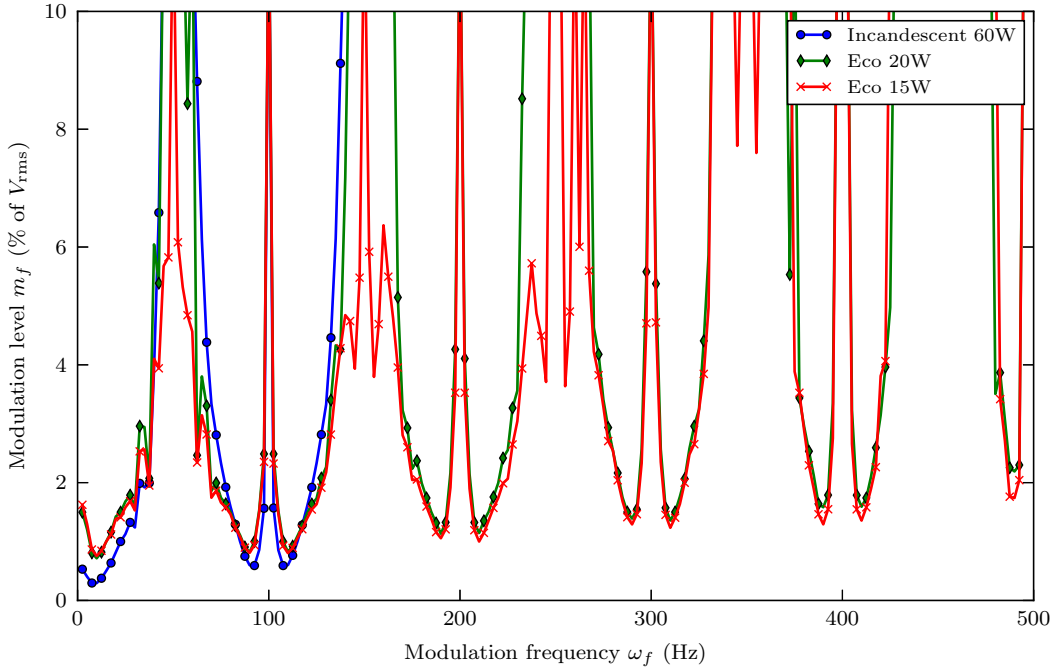

Figure 5.1: Voltage modulation level perceptibility threshold $P_{st}/L_{st} = 1.0$. 60W Incandescent, Ecobulb 15W and 20W.

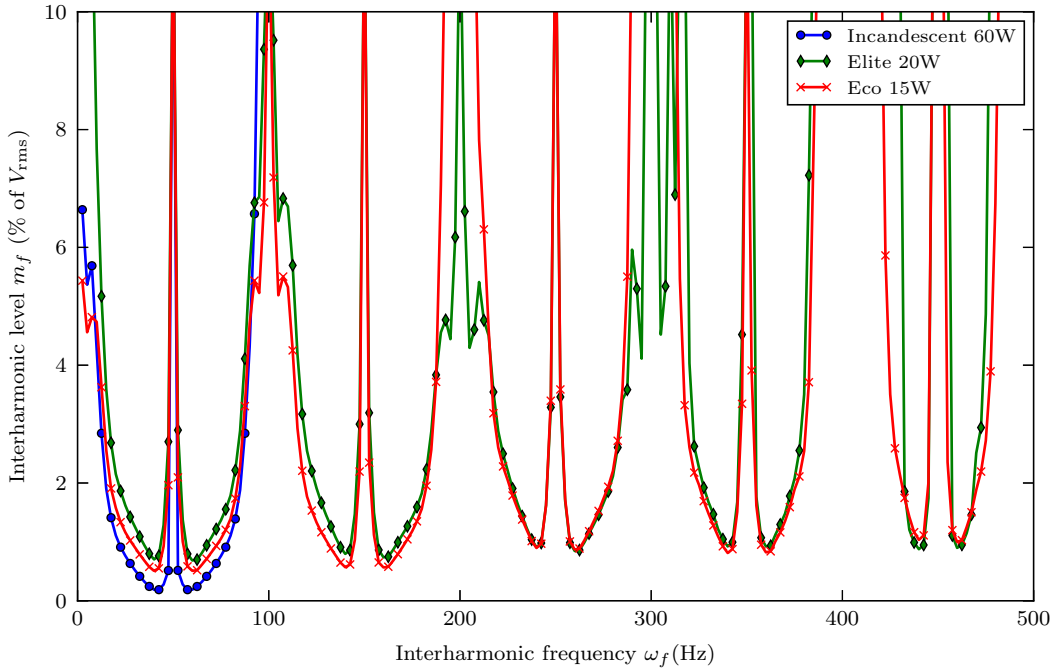

Figure 5.2: Incandescent Lamp and CFL Sensitivity to a Single Interharmonic Voltage, Magnitude required for the Flicker Threshold $P_{st}/L_{st} = 1.0$.

5.3.3 Voltage Dips and Swells

In this example the test lamps and incandescent lamp were subjected to a multitude of different voltage dips and swells. The results, shown in Table 5.2, indicate a similar perform of CFLs to 0% when compared with incandescent lamp flicker. For the 40% 1s dip the CFLs performed slightly better but for the voltage swell to 120% they were marginally worse.

	0% 0.02s			40% 1s			120% 0.5s		
Number of events	1	3	5	1	3	5	1	3	5
Voltage	1.32	2.57	3.01	1.32	2.57	3.07	1.53	2.98	3.35
Incandescent	1.32	2.57	3.02	1.32	2.58	3.08	1.50	2.96	3.35
Eco 20W	1.35	2.60	3.02	1.32	1.73	2.10	2.18	3.13	3.65
Eco 15W	1.35	2.64	3.09	1.19	1.66	1.93	2.18	3.08	3.60
Elite 20W	1.38	2.63	3.03	0.72	1.02	1.18	2.17	2.98	3.59
Tornado 24W	1.32	2.57	3.02	1.24	1.74	2.02	2.17	2.98	3.60

Table 5.2: 10 minute P_{st} levels for 1, 3, and 5 occurrences at simulation.

5.3.4 Phase Jumps

The phase jumps were applied in the same sequence as described in Section 4.6.7, jumping as the fundamental voltage crosses the axis at 1, 3, 5, 7, and 9 minutes of the 10 minute period. The IEC flickermeter and incandescent lamp results are presented for comparison in Table 5.3. CFLs appear generally unaffected by the jump in phase and is a result of their narrow conduction period and storage. Further investigation of the phase jump performance is required.

$\theta_2 - \theta 1$	V P_{st}	Incandescent	Eco20W	Eco15W	Elite20w	Torn24W
30∘	0.977	0.962	0.122	0.051	0.064	0.121
45∘	1.170	1.102	0.156	0.089	0.088	0.173

Table 5.3: Light Flickermeter Perceptibility to Phase Jumps of Test Lamps.

5.4 CASE STUDY: DESIGN OF NEW LED LIGHTING AND DRIVER FOR LIGHT FLICKER ELIMINATION

The new 4ft LED lamp has been designed to be mounted in existing 4ft fluorescent fittings. By using existing fittings and wiring in commercial buildings, the cost of retro-fitting the LED lamps can be reduced. Existing fluorescent fittings include ballast circuitry to start and operate the fluorescent tubes; this must be removed and replaced with a new driver circuit. A 1W range of surface mount LEDs were selected as they offer excellent price per lumen and are produced in a wide range of colours including 'white' (using a 'royal blue' LED). The forward voltage drop is typically 3.15V at 25°C with light output of 23-100 lumens per watt, depending on colour. In this case 80 lumen per watt (minimum at 25°C) white LEDs were used, with a typical colour temperature of $6500K$ and a colour rendering index (CRI) of 70. The voltage drop and efficiency both fall with increased junction temperature.

The LED lamp consists of the following three series LED strings: 48 white, 12 blue plus 12 cyan, 12 red plus 12 red/orange. Using a common anode connection, three strings can be accommodated using the 4 available contact pins on a standard fluorescent fitting. The two colour correction strings were chosen based on the findings of previously reported work [23]. In order to mix the light as well as possible, the sequence of LEDs along the lamp is ordered as follows: red-orange, white, cyan, white, red, white, blue, white and so on. A single heat sink runs along the back of the circuit board for cooling.

Fluorescent lamp: A TL-D 36W/840 white tube was used. At 36W and 30°C an output of 3000 lumens, or 83 lumens per watt, is quoted, with a colour temperature of 4000K and a CRI of 85.

Commercial LED fluorescent replacement lamp: An EverLED E25T8-48-S4N was used. This has a rated power of 25W and a quoted output of 2900 lumens, with a CRI of 85. This lamp consists of 36 white LEDs in a series string, in parallel with which is placed a pair of 10uF capacitors. In each end cap is a full bridge rectifier, ensuring that the lamp can be placed either way round in a fluorescent fitting and work correctly. Figure 5.3 shows one end of each of the three lamps. The sequence of different LEDs is clearly visible.

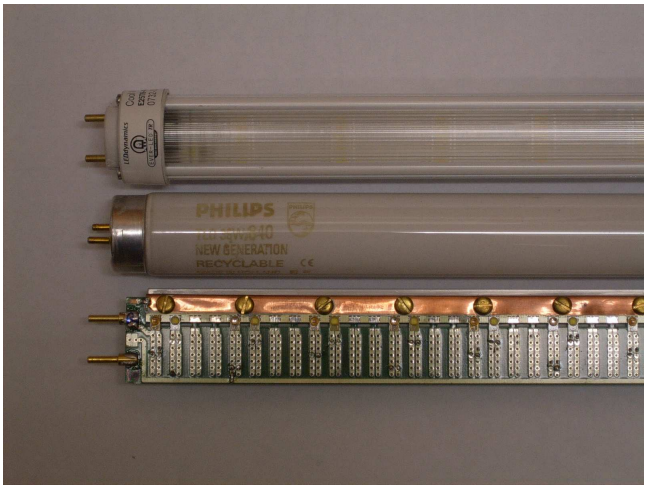

Figure 5.3: End section of the three lamps and construction of LED Lamp

5.4.1 Drive Circuitry LED lamp

The LED lamp drive circuitry consists of two parts: a 230VAC 50Hz rectifier stage (Figure 5.4) followed by three constant current drive circuits (one for each of the three LED strings) (Figure 5.5) on the DC bus. This allows for independent control of each LED colour string. The mains input passes through a fuse and EMC filter and then a full wave bridge rectifier.

The rectifier is followed by a Unity Power Factor Correcting (UPFC) boost converter, based around the IR1150 integrated circuit. The boost converter works in continuous inductor current conduction mode with a switching frequency of about 100 kHz. The active switching device is a 560V SPD02 CoolMOS power MOSFET. The IR1150 control circuit measures the inductor current and controls the duty cycle such that the current follows an approximately sinusoidal profile. A 600V CS0106 SiC Schottky device is used as the catch diode.

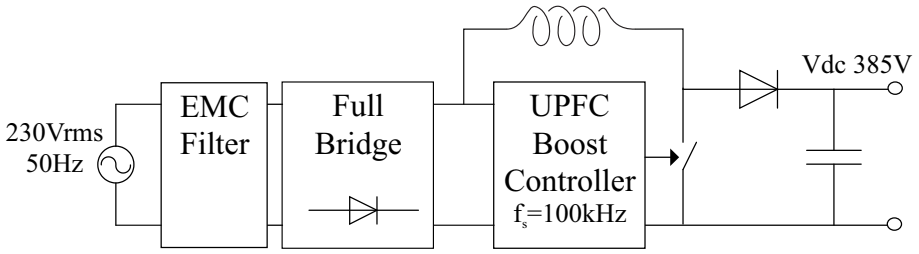

Figure 5.4: Unity Power-Factor Rectifier

The DC reservoir capacitor was chosen as $33\mu F$, with the DC bus controlled at a nominal $385V_{dc}$. With 48 white LEDs in series, the voltage drop of the string is approximately 150V. At an LED power input of 36W the forward current is hence around 240mA. This gives a theoretical hold-up time of a little over 30ms, or 1.5 cycles.

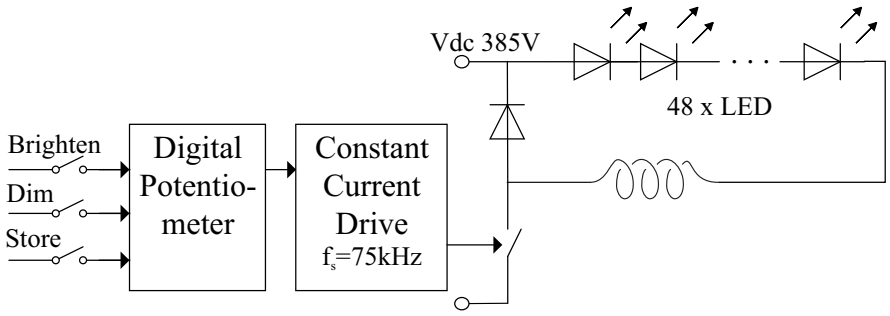

Figure 5.5: LED Constant Current Driver

The LED driver stage (Figure 5.5) takes the form of a buck converter, acting as a switching constant current source with the LED string as load, based around the MLX10803 LED driver integrated circuit. This integrated circuit monitors the inductor current (again operating in continuous conduction mode at around 100 kHz) and compares it with a reference level, derived from a voltage reference through a digital potentiometer, and alters the duty cycle appropriately. Three digital inputs control the wiper position of the potentiometer and hence the brightness of the lamp. As the RMS and average currents are of the same order as in the input boost converter, a similar MOSFET and catch diode are used as in the input circuit. At rated power, losses are less than 3W.

Fluorescent lamp: The electromagnetic ballast has an inductance of 1.2H and a series resistance of 49 Ω, measured at 50Hz - by 150Hz the resistance has risen to 76Ω. With a sinusoidal 50Hz voltage of 230V rms applied to the lamp, the inductor current is 0.41A, yielding losses of about 8W and power of about 35W into the lamp itself. Commercial LED fluorescent replacement lamp: The LED replacement lamp uses two of the same electromagnetic ballasts in series (2.4H, 98Ω at 50Hz). With a sinusoidal 50Hz voltage of 230V rms applied to the lamp, the inductor current is 0.20A, yielding ballast losses of about 4W and power of about 23W into the lamp itself.

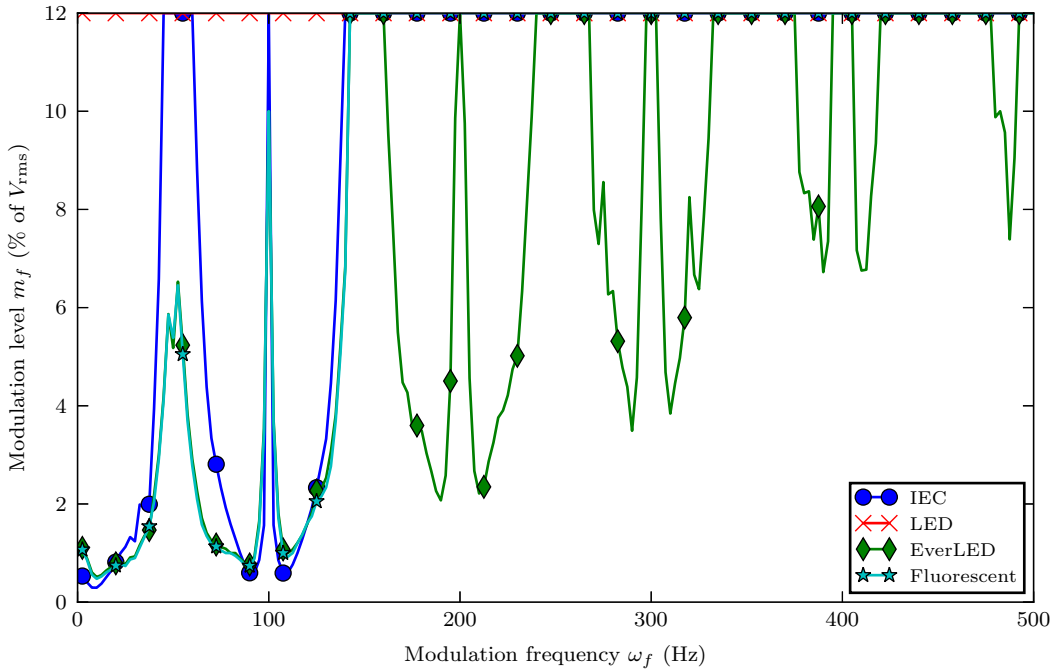

Figure 5.6: LED Lamp and Fluorescent Tube Sensitivity to a Rectangular Voltage modulation, Magnitude required for the Flicker Threshold $P_{st}/L_{st} = 1$.

5.4.2 Flicker Performance Results

Figure 5.6 shows the amplitude of RMS supply voltage modulation required to produce unacceptable flicker for the various lamps, including an incandescent bulb, versus frequency. The modulation level was restricted to 10%, at which point no perceptible flicker was seen with the new lamp, though the EverLED and the fluorescent cases were similar, requiring less than 1% modulation in the 5 to 30Hz region.

Table 5.4 shows flicker perceptibility results for three typical supply disturbances - a 20ms dip to 0% (i.e. a missing cycle); a 1s dip to 40% of nominal voltage; a 0.5s swell to 120% of nominal voltage. In each case the value of Pst is given where 1, 3 or 5 of the same event occur within a 10 minute period. The new lamp does not exhibit perceptible flicker under any of the test conditions, whereas all the other lamps make the user aware of the supply problems. Figures 5.7 and 5.8 compare the light output levels for the three lamps during the missing cycle and 1s 40% dip events, respectively. The fluorescent lamp drops out during both of these disturbances and takes 2-3s to restart afterwards. The EverLED output falls to zero and to a very low level respectively, but of course restarts immediately. The new lamp experiences little variation in light output.

The hold-up capability of the new lamp was tested by applying a supply voltage drop to zero and measuring the time taken for the light output to drop noticeably. As shown in Figure 5.9, the period is approximately 50ms, or 2.5 cycles.

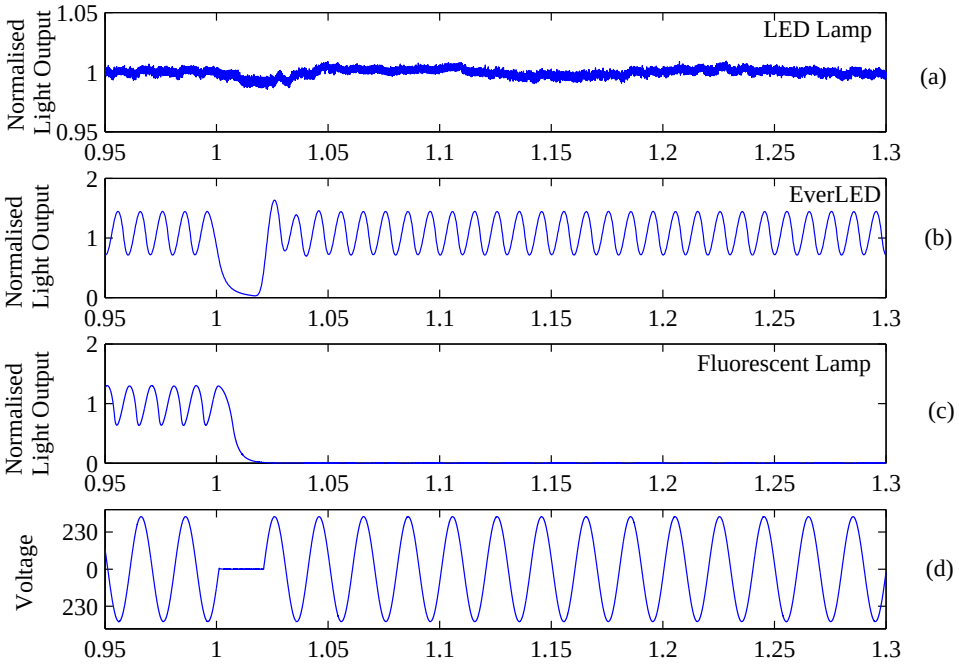

Figure 5.7: Normalized light output and supply voltage during missing cycle. 0% voltage for 20ms.

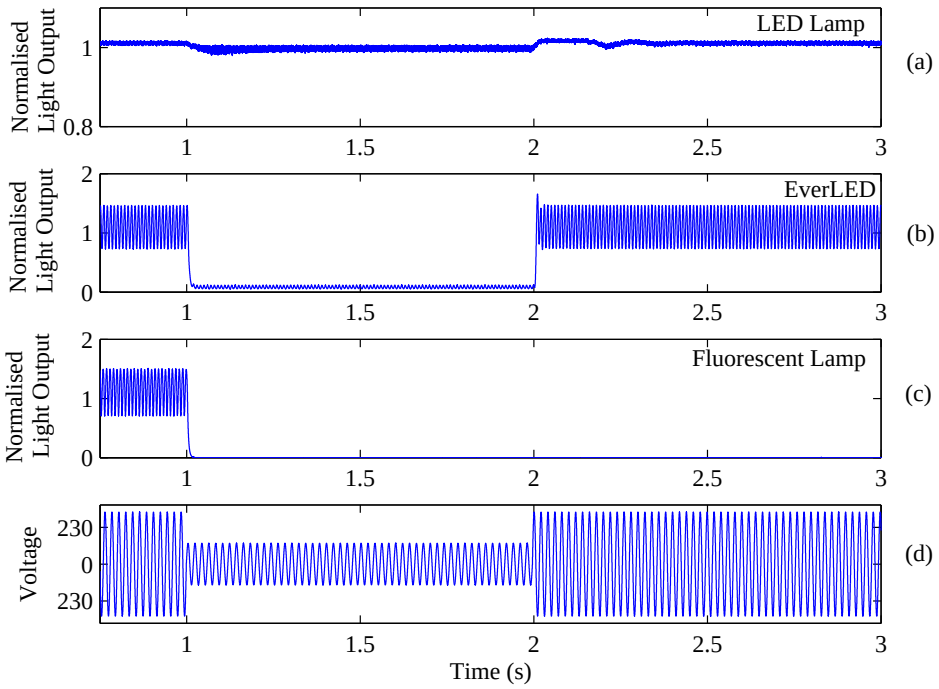

Figure 5.8: Normalized light output and supply voltage during dip to 40% nominal voltage for 1s

	0% 0.02s			40% 1s			120% 0.5s		
Number of events	1	3	5	1	3	5	1	3	5
Incandescent	1.32	2.57	3.01	1.32	2.57	3.07	1.53	2.98	3.35
New LED Lamp	0.09	0.14	0.15	0.06	0.07	0.09	0.14	0.21	0.23
EverLED	1.32	2.57	3.01	1.94	3.04	3.41	2.13	2.99	3.46
Fluorescent	1.35	3.17	3.69	1.95	2.72	3.14	2.17	3.18	3.69

Table 5.4: P_{st} levels for 1, 3 & 5 occurrences of event over a ten minute period

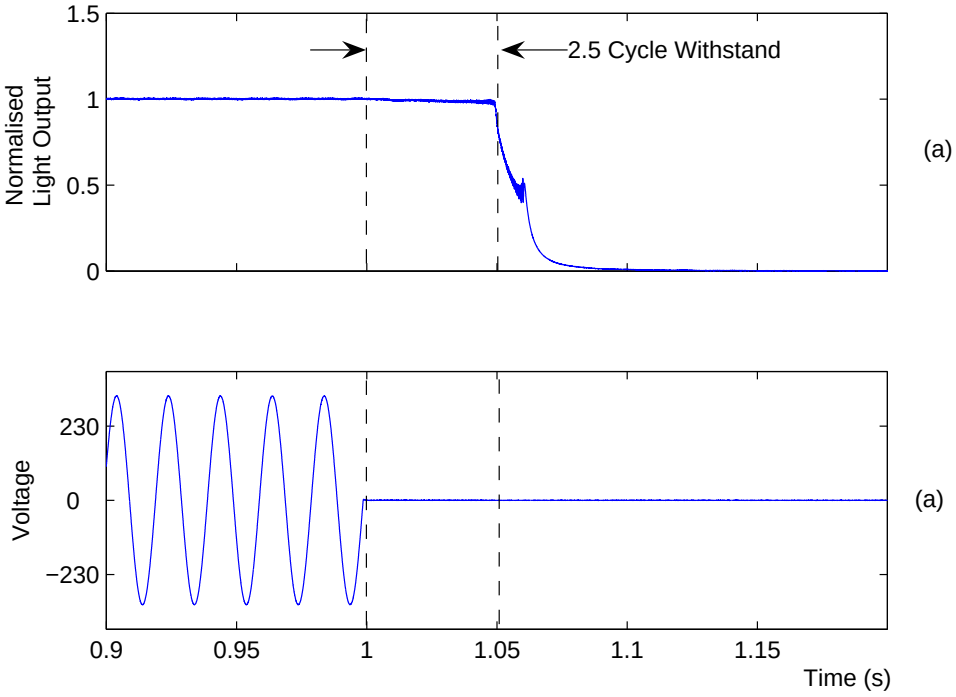

Figure 5.9: Light Output hold-up of LED lamp to Voltage Drop to 0%

5.4.3 Discussion

The practical results show that existing fluorescent lighting suffers from a number of drawbacks, including quality of light spectrum, frequency of tube replacement, flicker sensitivity, either poor power factor or, with PFCC fitted, as is usual, the potential for non-compliance. Nonetheless the efficiency of converting electrical energy to light is still good. A commercially available LED tube replacement tackles the frequency of tube replacement issue, but fails to offer significant improvements on all other counts. A new LED lamp, with colour correction and UPFC drive circuitry, designed to be retrofitted into existing fluorescent fittings, improves on all aspects of the fluorescent performance. Nevertheless the cost of the new lamp is still too high, and its efficiency increase is still too modest to allow its adoption on economic grounds. It is possible that its improved performance, and potential for further power savings when used as a dimmable lamp, remote controlled by a building management system, coupled with other added value features, such as local energy storage for integrated emergency lighting and mood lighting, may earn it a niche market. As LED efficiencies continue to increase, whilst their price is falling and whilst

the price of electricity continues to rise and carbon markets come on stream, the viability of such lamps for widespread adoption comes closer.

5.5 CONCLUSION

The chapter demonstrates how the Light Flickermeter developed in chapter 4 is used in practical situations, and highlights how the existing IEC flickermeter methodology fails to measure flicker accurately for lamps of different technology. The results showed how CFLs are sensitive to a wider range of interharmonic and modulated frequencies. Yet under voltage dips and swells there performance is practically identical. Whether fluorescent, compact fluorescent or LED lighting, the fact that the sensitivity greatly differs from that of the incandescent lamp modelled by the IEC flickermeter emphasises that the standard fails to quantify light flicker as experienced throughout network.

In the case study example the Light Flickermeter was utilised in the design of emerging lighting, an LED Fluorescent replacement lamp. A LED replacement lamp and driver circuitry was developed with flicker minimisation a primary objective. The LED design showed that with careful consideration, an electrical lamp can be made virtually flicker free and immune to common voltage distortions. In aid the light flickermeter was used to characterise the lamps performance and compare it to existing lamp technologies at the design stage.

Chapter 6

HARMONIC DOMAIN STATE-SPACE REPRESENTATION OF NON-LINEAR LOADS

6.1 OVERVIEW

This chapter develops a design methodology for modelling of non-linear electronic devices within a Harmonic State-Space (HSS) Framework. The Harmonic State-Space extends from Linear Time Invariant State-Space (LTISS) systems using Linear Time Periodic (LTP) description of the transfers across the switching device. From basic circuit analysis theory and the use of harmonic transfer functions (HTF) to model the switching components (including Switching Instant Variation (SIV)) the device model is suitable for both transient and steady state simulation.

As part of the linearisation, the models are optimised to include only the strongest relationships or couplings around the operating conditions. This reduces computational burden and develops a model suitable for both detailed study and, through aggregation, large scale system studies. The analytical models presented for three electrical lamps, explore the theoretical and mathematical techniques involved in the HSS formulation.

6.2 INTRODUCTION

The extension of the Harmonic Domain in to linear time periodic system with Laplace operators has been referred to under many titles: Dynamic Harmonic Domain (DHD) [15], Extended Harmonic Domain (EHD)[56], and more generally as the Harmonic State-Space [59] to model the operation of power system components. The approach provides the direct solution for transient and steady-state of harmonics and being based on orthogonal and operational matrices, is computationally efficient. Non-linear and linear network components

There also exists other electrically non-linear devices that can be described by switching functions yet do not include the traditional AC-DC transformation. Lisboa [35], described the saturation of a transformer in a harmonic model by allowing the transform to switch characteristics between non-saturated and saturated states. The fluorescent lamp is also a naturally switching device without the transfer from AC to DC sub-systems.

6.3 REVIEW OF LINEAR TIME PERIODIC/FREQUENCY DOMAIN MODELLING

The modelling of electrical systems through linearised frequency domain techniques has been a continuing research area at the University of Canterbury. Smith [52] developed harmonic domain model and using iterative algorithms solved the system mismatch equations for a detailed model of an HVDC converter. An interesting discovery was that the model often produced a solution after a single iteration, this observation gives an indication that the HVDC converter is reasonably linear in the harmonic domain. Wood [60] adopted Persson [44] the analytical approach to describe the frequency coupling across the HVDC converter through the use of switching functions. More importantly, Wood modelled the dynamics associated with commutation period and firing angle variation.

Perhaps the most notable single phase model was developed by Laird [33], who modelled the transfers through the rectifier circuit bridge, including the linearisation of the distorted switching instant variation on the circuit. His model included the DC side impedance (capacitive) with a load (constant current) and included the small signal transfers of voltage and current across the rectifier switchings. This correctly included the small signal distortion effects across the base case switching and distortion from large signal due to variation of the autonomous switching instants. The effect of switching instant variation observed either side of the rectifier was linearly approximated. However, it was concluded that the effect of switching instant variation was negligibly small compared to the other effects of the distortion. Laird also assumed a ripple free DC side voltage simplifying the modelling operating conditions.

Small signal input distortions were added to the AC side as a voltage source and to the DC side as a current source and formed a necessary part of the frequency transfer matrices. His model included a small dc side smoothing reactor, which could have also been incorporated on the AC side. His single phase modelling theory was extended to three phase shunt active filter design [33].

Wereley [59] developed the Harmonic State Space (HSS) Framework for the study of LTP systems. Wereley described a new signal class, the exponentially modulated periodic domain (or EMP domain) to represent time varying harmonically periodic signals. Wereley's work was in analogous to the LTI State Space, allowing for the full system dynamics to be modelled and many of the stability robustness results of LTI systems to be generalised and hold for LTP systems.

Love [36] examined the use of *jumps sets*, changing the entire set of system equations for each switched circuit configuration and mapping energies from the previous state to the jumped state. Later, Love adopted the HSS framework, producing models for the buck-boost converter and full-bridge rectifier. In parallel studies, Hwang [25] and Orillaza [40] developed HSS models for an HVdc converter and 3-phase Thyristor Controlled Reactor (TCR), respectively.

6.3.1 Frequency Coupling of Convertors

In general, the converter action has been modelled as voltage AC to DC switch, switching voltage from the AC side to the DC side and a current DC to AC switch, switching DC current to the AC side. In other words, the converter action switches the voltage from the AC side to the DC side, the voltage was subjected to the DC side admittance drawing a DC side current and

the DC side current is modulated again the switching function back to current on the AC side. The relationship can be described as $V_{ac} => Ts => V_{dc} => Y_{dc} => I_{dc} => Ts => i_{ac}$ where Ts represents the transformation. The switching functions and admittances form the system transfer. In forming the equations to observe additional system variables, outputs can be added as unknown variables into the matrix equation.

The previously developed models generally all contain a single switching mechanism from an AC side to a DC side. Whether they are single or three phase switched to a common DC bus or single switchings of a 3-phase TCR, they all switch to a single system. With the advent modern electronics it is found that circuits are beginning to contain multiple switchings, connecting different parts of the circuit together in varying configuration at separate timings. The HSS framework facilitates the multi-system, multi-switching characteristics of these circuits. Moreover the HSS framework allows small parts of the circuits to consider standalone sub-systems, each with there own internal states and dynamics; connecting sub-systems in order to complete the overall system.

6.4 LINEAR TIME PERIODIC SYSTEMS

Firstly, the mathematical preliminaries of LTI and LTP systems are reviewed. This leads to the identification of the fundamental signal space for LTP systems. Transformation of the signal basis derives an equivalent signal set and solutions.

The state space form is adopted to make use of the toolsets readily available for LTI systems, and it is described in Definition 1.

Definition 1 (Linear time periodic state space model)**.** *The state space form of a linear time periodic system is given by the linear ordinary differential equation called the state* ***dynamic equation***

$$\dot{x}(t) = A(t)x(t) + B(t)u(t) \tag{6.1}$$

and an ***output equation*** *or* ***measurement equation***

$$y(t) = C(t)x(t) + D(t)u(t) \tag{6.2}$$

where the ***dynamic matrix****,* $A(t) \in P^{n\times n}[T]$*, the* ***control distribution matrix****,* $B(t) \in P^{n\times m}[T]$*,the* ***measurement matrix****,* $C(t) \in P^{m\times n}[T]$*, and the* ***feed-forward matrix****,* $D(t) \in P^{m\times m}[T]$*, are all time-periodic.*

6.4.1 Linear Time Periodic Systems: Sinusoidally Periodic Signal Set

The extended harmonic domain proposes an Exponentially Modulated Periodic (EMP) signal of the form:

$$x(t) = \sum_{m=-\infty}^{\infty} x_m e^{(jm\omega_0+s)t} \quad t > 0 \tag{6.3}$$

Formed by an infinite sum of orthogonal harmonic terms $e^{jm\omega_0 t}$, and it is used as the signal basis for the solution. They are each modulated by an e^{st} term, a laplace operator.

The property of the EMP signal is such that the derivative becomes:

$$\dot{x}(t) = \sum_{m=-\infty}^{\infty} (jm\omega_0 + s) x_m e^{(jm\omega_0+s)t} \tag{6.4}$$

$$\dot{x}(t) = \sum_{m=-\infty}^{\infty} (jm\omega_0 + s) x(t) \tag{6.5}$$

The derivative is a function of itself multiplied by $jm\omega_0 + s$ which is an important characteristic when it is use to formulate the HSS equations.

Through the linear combination of the state space equation (6.1), the output signal $y(t)$ is expressed in a similar EMP form,

$$y(t) = \sum_{m=-\infty}^{\infty} y_m e^{(jm\omega_0+s)t} \tag{6.6}$$

This is the frequency separation property of an LTI system that is realised in an LTP system by the use of EMP signal class [37].

6.4.2 State-Space Form for LTP Systems

The time domain input signal and the system transfer function are written using Fourier series expansion which converts them into the frequency domain and more importantly each element in its respective expansion is orthogonal to others in the series. This means that the output is also a set of elements that are formed over an orthonormal basis and linear independent equations can be written for each output element. This is the principal of harmonic balance [37].

Using the state-space form in Equations (6.1) along with the EMP signal class, the state variable derivative can be written as

$$\sum_{m=-\infty}^{\infty} (jm\omega_0 + s) x_m e^{(jm\omega_0+s)t} = A(t) \sum_{m=-\infty}^{\infty} x_m e^{(jm\omega_0+s)t} + B(t) \sum_{m=-\infty}^{\infty} u_m e^{(jm\omega_0+s)t} \tag{6.7}$$

6.4.2.1 System Signals

In solving for the steady state, the input EMP signals are constant hence this results in constant state variables as well as constant outputs. This denotes that the derivatives of all such signals are zero, hence

$$\dot{x} = 0 \tag{6.8}$$

Substituting this into the state-space equation set gives,

$$0 = Ax + Bu$$
$$y = Cx + Du \tag{6.9}$$
$$x = A^{-1}Bu \tag{6.10}$$
$$y = (CA^{-1}B + D)u \tag{6.11}$$

The system signal representations and system responses are summarised in Table 6.1 below.

Table 6.1: LTI System Signal Representation and System Responses

Signal Description	Symbol	Formula
Input, State, Output	$u(t)$, $x(t)$, $y(t)$	ue^{st}, xe^{st}, ye^{st}
Steady State Response	$x_{ss}(t)$	$(sI - A)^{-1}Bu(t)$
Transient Response	$x_{tr}(t)$	$e^{At}(x(t_0) - x_{ss}(t))$
State Transition	$x_{st}(t)$	$\Phi u(t)$
Steady State Output	$y_{ss}(t)$	$[C(sI - A)^{-1}B + D]u(t)$
Transient Output	$y_{tr}(t)$	$Ce^{At}(x(t_0) - x_{ss}(t))$
Transfer Function	$G_(s)$	$C(sI - A)^{-1}B + D)$

The evolution of the system states, x, and the outputs, y are formally described by the state transistion matrix $\Phi(t)$. The transient response evolves from the eigenvalues of the system space while the steady state transfer response evolves at the frequencies of the input. Importantly the complex exponential input produces a complex exponential output via the steady state output response. This steady state response is the transfer function of the LTI system forming a linear mapping between the inputs and outputs. Stability and robustness analysis can be carried out by matrix algebra and frequency domain analysis techniques. Stability of the LTI system is attained from the eigenvalues of the system matrix falling in the left hand plane. However, for linear time varying systems (i.e. those with time dependent system matrices), these properties of the LTI system fail to hold. Stability can not be assumed even if the eigenvalues remain in the left half plane.

6.4.3 Elementary Harmonic Transfer Matrices

A set of elementary harmonic transfer matrices are presented in this section.

Constant Multiplier For the constant, C, the elements of its HTF, $\mathcal{C}$, are described in Equation 6.12.

$$\mathcal{C}(m,n) = \left\{ \begin{array}{ll} C & m = n \\ 0 & m \neq n \end{array} \right\} \tag{6.12}$$

$$\begin{bmatrix} \vdots \\ x(-\check{j}1\omega_0) \\ x(j\check{0}\omega_0) \\ x(+\check{j}1\omega_0) \\ \vdots \end{bmatrix} = \begin{bmatrix} \ddots & \vdots & \vdots & \vdots & \\ \cdots & C & 0 & 0 & \cdots \\ \cdots & 0 & C & 0 & \cdots \\ \cdots & 0 & 0 & C & \cdots \\ & \vdots & \vdots & \vdots & \ddots \end{bmatrix} \begin{bmatrix} \vdots \\ \Delta x(-\check{j}1\omega_0) \\ \Delta x(j\check{0}\omega_0) \\ \Delta x(+\check{j}1\omega_0) \\ \vdots \end{bmatrix} \tag{6.13}$$

Linear Time Invariant Response

$$\mathcal{H}(m,n) = \left\{ \begin{array}{ll} H(jk\omega_0) & m = n \text{if} jk\omega_0 \ni \lambda_n \\ 0 & m \neq n \\ 0 & m \in \{\lambda_n\} \end{array} \right\} \tag{6.14}$$

$$\begin{bmatrix} \vdots \\ x(-\check{j}1\omega_0) \\ x(j\check{0}\omega_0) \\ x(+\check{j}1\omega_0) \\ \vdots \end{bmatrix} = \begin{bmatrix} \ddots & \vdots & \vdots & \vdots & \\ \cdots & H(-j\omega_0) & 0 & 0 & \cdots \\ \cdots & 0 & H(0) & 0 & \cdots \\ \cdots & 0 & 0 & H(+j\omega_0) & \cdots \\ & \vdots & \vdots & \vdots & \ddots \end{bmatrix} \begin{bmatrix} \vdots \\ \Delta x(-\check{j}1\omega_0) \\ \Delta x(j\check{0}\omega_0) \\ \Delta x(+\check{j}1\omega_0) \\ \vdots \end{bmatrix} \tag{6.15}$$

Differentiator

$$\frac{d}{dt}(m,n) = \left\{ \begin{array}{ll} jk\omega_0 & m = n \\ 0 & m \neq n \end{array} \right\} \tag{6.16}$$

$$\begin{bmatrix} \vdots \\ x(-\check{j}1\omega_0) \\ x(j\check{0}\omega_0) \\ x(+\check{j}1\omega_0) \\ \vdots \end{bmatrix} = \begin{bmatrix} \ddots & \vdots & \vdots & \vdots & \\ \cdots & -j\omega_0 & 0 & 0 & \cdots \\ \cdots & 0 & 0 & 0 & \cdots \\ \cdots & 0 & 0 & +j\omega_0 & \cdots \\ & \vdots & \vdots & \vdots & \ddots \end{bmatrix} \begin{bmatrix} \vdots \\ \Delta x(-\check{j}1\omega_0) \\ \Delta x(j\check{0}\omega_0) \\ \Delta x(+\check{j}1\omega_0) \\ \vdots \end{bmatrix} \tag{6.17}$$

The Harmonic Transfer

The Harmonic Transfer Function (HTF) matrix is essential to the HSS, it performs the switching action of the device. This is simply the multiplication of the input signal, $u(t)$, with the switching function, $h(t)$. The multiplication occurs in the time domain and equates to a convolution in the frequency domain. The HTF takes the form of a toeplitz matrix where the diagonal components are constant. A square toeplitz matrix performs the cyclic convolution of the Fourier components.

$$\begin{aligned} y(t) &= h(t)u(t) \\ \sum_{m=-\infty}^{\infty} Y_n &= \sum_{n=-\infty}^{\infty} H_n e^{jnw_0 t} \sum_{m=-\infty}^{\infty} U_m e^{jmw_0 t} \\ &= \sum_{n-m=-\infty}^{\infty} H_{n-m} \sum_{m=-\infty}^{\infty} U_m e^{jmw_0 t} \end{aligned} \tag{6.18}$$

$$H = \begin{bmatrix} \ddots & \vdots & \vdots & \vdots & \\ \cdots & H_0 & H_{-1} & H_{-2} & \cdots \\ \cdots & H_{+1} & H_0 & H_{-1} & \cdots \\ \cdots & H_{+2} & H_{+1} & H_0 & \cdots \\ & \vdots & \vdots & \vdots & \ddots \end{bmatrix} \tag{6.19}$$

6.4.4 Tensor Representation for Realisable Signals

For all realisable systems with real input signals, the output remains strictly real. Considering a real valued periodic signal of frequency, $n\omega_0$, in the time domain, its Fourier components become matched complex conjugate pairs at the frequencies $n\omega_0$ and $-n\omega_0$. This same symmetry is observed in the HTF Toeplitz transfer matrices. Hence the same symmetry exists in the output containing conjugate pairs in the harmonic domain; when transformed to the time domain the signal is real. The EMP HSS form results a computationally inefficient equation set that requires complex arithmetic to solve the matrix equations. [1]

6.4.4.1 Tensor representation

The similarity of the two system bases, and the orthonormal change of basis matrices leads to the convenient relationships between the EMP and sinusoidal representations. The realisation of the time domain signal from sinusoidal signal set does not require the transformation by T, from the sinusoidal signal basis to the EMP signal basis. The time domain signal in the periodic steady state can be obtained directly by the inverse Fourier transform of the sinusoidal set.

In the transient, the time domain solution is found from the state transition matrix and derived at each time step by the inverse Fourier transform of the harmonic spectra. The process appears

[1] The complex form of the EMP HSS form can be represented in tensor that reduces the need for complex valued arithmetic. As a consequence the vector and transfer matrix dimensions are doubled to represent scalar quantities.

computationally intensive due to the need to perform the entire inverse Fourier transform at each time step. A more practical method is to evaluate each sinusoidal term at each time step while summing the results for each variable.

6.5 THE HARMONIC STATE-SPACE MODEL FRAMEWORK

The HSS is an extension to the harmonic domain, it preserves the frequency coupling representation using frequency transfer matrices (FTMs) while encapsulating them in a state-space format. This allows the modelling of harmonic signals under transient conditions. Furthermore, the use of a state-space formulation enables the application of control theory for system stability studies. The HSS has recently been used to model power electronic devices such as a thyristor controlled reactor [41], an HVDC converter, and a STATCOM. The HSS generic control approach also extends the modelling beyond basic ohms law of electrical components to non-electrical signals. Of particular interest in this thesis is the modelling of the light emitted from electric light systems.

This section proposes a general framework for electronic circuits in order to realise a system model in the HSS form. This framework follows classical electronic circuit analysis, control realisation and conversion by elementary HTF to the HSS.

In summary, the formulation of HSS model is achieved by the following procedures,

1. Describe the circuit operation and identify each switched configuration including both conducting and non-conducting states.
2. Sectionise the circuit operation into subsystems, ideally linear components containing singular state variables and switching functions for switched components considering switching types at turn on and off,
   (a) Controlled - include controller system and SIV.
   (b) Autonomous - include SIV.
3. Identify system inputs - Consider voltage and current sources as inputs.
4. Construct equations based on Kirchoffs voltage law and current for each switched configuration using nodal or mesh analysis where applicable.
5. Generate a control block diagram from subsystems, including switching functions to define each switch configuration.
6. Develop subsystem matrices from elementary constructs and summation blocks accordingly with the control block diagram.
7. Implement the control diagram in software linking subsystems inputs and outputs to form the HSS model.

When determining the operation of most power electronic devices it becomes apparent that separating and naming internal state variables improve the understanding and operational clarity. These variables can be made observable by constructing their equations and including them into the transfer matrix. The top rows of the matrix equation are reserved for such variables.

6.5.1 Solution Variable Initialisation

To achieve reliable convergence it is critical that the solution variables are suitably initialised, in particular the fundamental frequency operating point for each PWM converter. While it is possible to initialise the system with a flat voltage profile and no harmonic distortion and then solve the system using the full solution immediately, this is highly inefficient since each full iteration is computationally intensive. The solution variables are therefore initialised using the three-phase power-flow solved with no harmonics included. When convergence is achieved the harmonic solution is added with all harmonics initialised to zero. This point typically generates an adequate estimate of the full Jacobian; making it unnecessary to re-calculate the Jacobian at subsequent iterations, while still achieving satisfactory convergence.

6.5.2 Harmonic Truncation

In order to implement a Fourier series expansion for simulation, the series must be truncated to a finite dimension in a digital model. In addition, the switching of a power electronic circuit can often be described by its set of characteristic harmonics. Thus it is sufficient to model a switching circuit with its characteristic harmonics up to a finite limit which correctly represents its switching behaviour. However, frequency truncation leads to oscillations in the time domain waveforms and the magnitude of error may be significant especially at the points of discontinuity. This error is often referred to as the Gibbs phenomenon.

6.5.3 Redundancy of State Variables

The redundancy of state variables or loss of generality plagues circuit analysis techniques. This occurs when one unknown variable is defined by other unknowns in the system. The classic examples are; three inductors tied at a node where the current following in an inductor is defined by the other two, or three capacitors in a loop where the voltage on a capacitor is defined by the other two. In the state-space form this results in A being singular and can not be inverted. To avoid the state variable redundancy a common method adds a shunt resistance to one of the inductors. This thereby forces the inductor to have a slightly different current flowing and a different state variable. The technique is also applicable to avoid redundant state variables formed by parallel capacitors.

6.5.4 Switching Instant Variation

Switching instant variation (SIV) was first described by Wood in 1993 [60]. At the time it was referred to as the commutation period variability of an HVDC converter. His work discussed the effects of SIV due to current and voltage distortions as well as a change in the control system. Although the effects associated are non-linear in frequency domain, Wood concluded that they can be linearised for small-signal analysis. More recently, Love [36] identified two categories of SIV, autonomous switching instant variation and controlled switching instant variation. Autonomous SIV occurs when there is a variation in an electrical signal in the system whereas controlled SIV is due to a disturbance in the control signal.

For example, the switching of a thyristor can be modelled by its switch-on instant which is determined by a control signal while its switch-off instant which occurs automatically when the thyristor current reaches zero. A variation in the system electrical signals may introduce a residual thyristor current beyond the linearised switch-off instant, and it must be reset to zero to produce a correct SIV model. Similarly, if a variation in the control signal induces a change in the switch-on instant, the system waveforms must be corrected accordingly to represent the true effect of SIV.

6.6 DEVICE EXAMPLES

6.6.1 Compact Fluorescent Lamp - Capacitor Smoothed Full Bridge Rectifier

The capacitively smooth full bridge rectifier design CFL is the simplistic illustration of the HSS model formation through the control block diagram method. The CFL circuitry blocks as shown in Figure 6.1 are firstly analysed and converted to a simplified circuit diagram (see Figure 6.3)

The fluorescent tube and high frequency resonant circuit are replaced by a constant current source. The typical operating frequency (15-50kHz) of the resonant circuit exceeds of power system harmonics of interest to study.

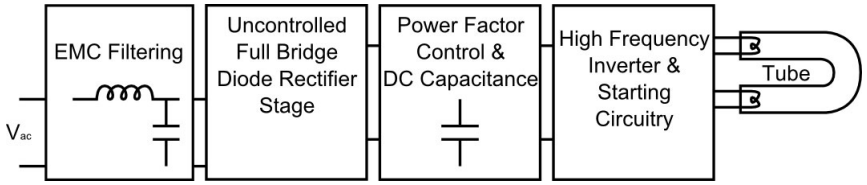

Figure 6.1: Circuit Diagram of the Capacitively Smoothed Full Bridge Rectifier CFL Ballast Design

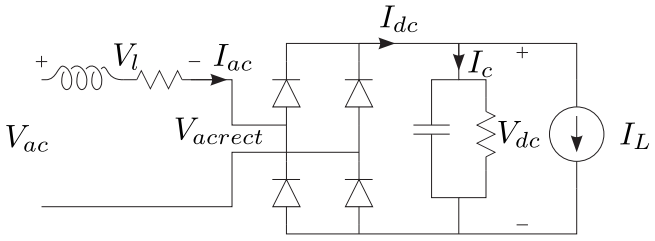

Figure 6.2: Circuit Partition of Capacitively Smoothed Full Bridge Rectifier CFL Ballast Design

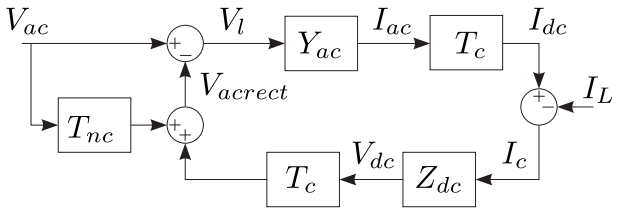

Figure 6.3: Control Diagram of Capacitively Smoothed Full Bridge Rectifier CFL Ballast Design

The primary input and output of interest to the device is the AC voltage and the AC current, respectively. The DC side current source adds one external input to the system. The next stage

is to apply Kirkchoffs circuit laws. Formulation the voltage loop equation on the AC side gives

$$v_{ac} = v_{zac} + v_{rect} \tag{6.20}$$

and the current nodal equation at gives

$$i_{ac} = i_{zdc} + i_L \tag{6.21}$$

The AC side current, i_{ac}, is a result of the voltage, v_{zac}, across the AC side impedance, $x_{ac}+r_{ac}$. The DC voltage is obtained from the current, i_c, following into the capacitor network on the DC side $x_c \parallel r_c$.

The conduction of the diode switches connects the voltage and current of the AC to DC side. Polarity is switched depending on the switching conditions. It explicitly states that during conduction the voltage either side of the diode rectifier are equal in magnitude of switched polarity. Similarly the currents either side of the rectifier are of the same magnitude of switched polarity.

During the non-conduction period of the rectifier, the diodes block the connection between AC and DC systems. Analytically switching functions describe non-conduction regions as a conduction of zero. However the conduction of zero states that the rectifier AC side voltage is zero times the DC side voltage. The zero voltage on the AC rectifier would act as a short and a substantial current would be drawn from the AC system. This is clearly not the case, the correct mode of non-conduction should be considered as a null connection stating that no connection exists between the two systems. The null conduction over the period can not be constructed by the analytical switching equation, instead the voltage and current must be additionally corrected over just the non-conducting period.

During non-conduction period, the voltage on the DC side is defined by the charge stored in the capacitor, on the AC rectifier side the voltage is actually equal to the input AC voltage, v_{ac}. As no current should be flowing into the rectifier during this stage, the voltage across the internal ac impedance should be forced to zero. These conditions follow the null conduction mode of the rectifier. The problem ceases to exist for the current transfer, as the current should have returned to zero on both AC and DC rectifier sides at the start of the non-condition period and remain zero throughout the non-conduction period. As both AC and DC side current should be zero the null connection mode is satisfied requiring no special correction.

During the transient or when the operational conditions are not met, the current either side of the rectifier may not completely return to zero at the beginning of the non-conduction period. In this case the state of the AC side inductor has not completely relaxed to zero, therefore a partial transient relaxation of the inductor current will take place on the AC side. Since the voltage is corrected on the AC rectifier, there is no voltage across the AC impedance. Hence the AC impedance is short circuited; for a substantial internal resistance the time constant is very short and in most cases the small error will decay to zero within the non-conducting period. Thereby state error at the beginning of the non-conduction period will have minimal to no effect on the transition to the conduction period.

6.7 CONCLUSION

The framework for the HSS connects the use of basic circuit analysis to the state-space form for LTP systems. This systematic method is applicable to both the development of small signal and large signal models for power electronic devices. The HSS provides the ability to capture system response under both steady state and transient conditions. More importantly, the HSS represents each harmonic as a state variable which allows the incorporation of harmonic transfer matrix.

The methodology proposed is intended as a pathway towards fully computer aided circuit analysis in the HSS. It presents the elementary formulation and components necessary, and illustrates the use of a generic LTI solver to perform transient simulations. The LTI environment grants the opportunity to use existing control theory such as root locus or pole-zero plots for design and stability analysis. In addition, the modular modelling approach allows subsystems to be formulated separately and connected via their respective inputs and outputs; a very useful feature for simplifying or extending models.

The example of modelling a CFL rectifier circuitry in the harmonic state-space shows that the framework which is usually associated with the modelling of high power converters is also suitable for low power devices. More specifically, the small-signal linearity observed in high power converters is also applicable for low power devices. Furthermore, the modelling technique allows the calculation of steady state solution through a single matrix multiplication using the inverted state matrix.

Chapter 7

HARMONIC DOMAIN MODELS BY AUTOMATED EXPERIMENTAL METHODS

7.1 OVERVIEW

Essential in the formulation of a HSS model shown in Chapter 6, is the extensive knowledge of the circuit characteristics and operation. This chapter develops an automated technique, with the aid of test system of Chapter 3, to experimentally derive a fully phase dependent Harmonic domain models for the device under test. The harmonic injection technique sequentially applies voltage distortions, varying in magnitude, phase and frequency, to measure the response and construct a linear frequency domain representation. The technique is used to develop models for a number devices including CFLs and LFTs. The models were utilised within a small network simulation and verified against an equivalent physical system.

7.2 INTRODUCTION

Perhaps the greatest disadvantage in developing a frequency domain model is the in-depth knowledge required of the device's full circuitry and operation. As is demonstrated in the previous chapter, even for a simple device model, a complete operational description of the circuit design and control modes is required. From this the analytical equations are developed and formulated into an HSS model.

Due to the complexity of many components, approximations are made when developing the model. These approximations are made by identifying those characteristics with minimal effect on the overall operation. In particular, the analysis of electrical systems using computerised microcontroller based control, the inclusion of the control actions become vitally important, yet the complexity increases. In most cases, however, the controller designs are generalised and can often become over-simplified. While simplified methods can provide insight, they may lack accuracy. Rarely would the control strategies match the commercial implementation. It becomes increasingly challenging to identify the aspects of the control and/or components that have the greatest influence that are required to be modelled.

This chapter presents an approach to form linear, phase dependent harmonic domain models of low power non-linear loads. A sequential harmonic injection technique is proposed and implemented on the experimental test system to develop the models from the physical non-linear device using small signal distortions. Since the actual non-linear device is tested no knowledge

of load circuit design or operation is required. Computational efficiency is gained when the matrices are used to simulate large numbers of non-linear loads distributed throughout electrical power systems. A tensor admittance representation is incorporated into the solution to accurately model the phase dependent behaviour. Moreover the physical realisation of the system signals warrants the concise real positive frequency representation.

7.3 HARMONIC DOMAIN MODELLING

Fauri [19] describes the alternative non-linear load model using a cross-coupling frequency admittance matrix. However the model lacks the full convertor action observed by Larsen [34], Smith [52] and many others, that necessitates a phase dependent relationship between the transfers of voltage and current.

In 1996, Smith performed a similar simulation study within PSCAD/EMTDC on an hvdc converter and successfully obtained a linearised cross coupled admittance [52]. The admittance lattice structure was sparse, and included the phase dependency by tensor representation.

7.4 LINEAR FREQUENCY DOMAIN MODEL

For the voltage to current relationship the transfer is termed the admittance.

$$I = TV \tag{7.1}$$

Recalling from the previous chapter, state-space model of a LTP system can be expressed by the following equations,

$$sx = (A - \mathcal{N})x + Bu \tag{7.2}$$
$$y = Cx + Du \tag{7.3}$$

and its steady state solution is found by

$$y = (-C(A - \mathcal{N})^{-1}B + D)u \tag{7.4}$$

where the time varying derivative is set to zero, $s = 0$. Observing the steady state solution, the system is represented by a constant matrix, $(-C(A - \mathcal{N})^{-1}B + D)$ and can be rewritten as

$$y = H_{ss}u \tag{7.5}$$

where H_{ss}, incorporates the entire system characteristics, including all electrical components, control and couplings of the convertor switchings. When the input/output is a voltage to current relationship, the transfer, H_{ss}, is referred to as the admittance matrix, Y.

$$i = Yv \tag{7.6}$$

The FTM terms model the linear relationships about the operating point of the device. As depicted in Figure 7.1, a general non-linear function can be linearised about a set point such that small deviations can be calculated with minimal error. This linear gradient is represented by the FTM.

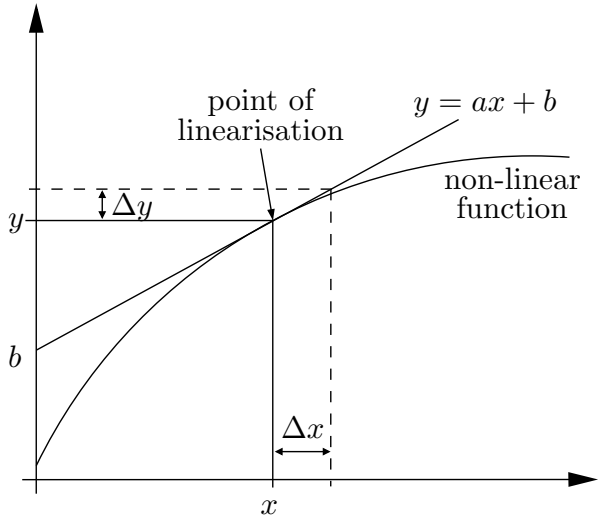

Figure 7.1: Linearisation of a non-linear relationship

The device's operating point can be defined by a number of parameters, for controlled devices, such as HVDC links the operating point is defined by the MW and MVAr and ultimately the firing angles, for uncontrolled devices such as full bridge rectifiers the turn on and turn off switching instants can define the operating point. Any deviation from this operating point can be linearised. The admittance matrix is not strictly limited to electrical transfers, for example it can be extended to include the control transfers of a device [42].

All devices considered hereafter are uncontrolled which allows a mathematical description in a general form,

$$\begin{bmatrix} I_1 \\ I_2 \\ \vdots \\ I_k \end{bmatrix} = \begin{bmatrix} Y_{11} & Y_{12} & \dots & Y_{1m} \\ Y_{21} & Y_{22} & \dots & Y_{2m} \\ \vdots & \vdots & \ddots & \vdots \\ Y_{k1} & Y_{k2} & \dots & Y_{km} \end{bmatrix} \begin{bmatrix} V_1 \\ V_2 \\ \vdots \\ V_m \end{bmatrix} + \begin{bmatrix} I_{b1} \\ I_{b2} \\ \vdots \\ I_{bk} \end{bmatrix} \tag{7.7}$$

where each FTM admittance term Y_{km}, relates the m^{th} harmonic order distortion voltage to the k^{th} order distorted current.

The base case current is obtained by applying the base voltage. The base voltage is not necessarily sinusoidal, but can contain arbitrary harmonic levels, around which the harmonic couplings

can be correctly linearised.

Accurate analytical models of devices with switching functions require consideration of both the positive and negative frequencies. For developing the cross coupling matrices the positive and negative frequencies may be considered independently [55], separated but within the same matrix or fully combined into the same matrix, such that only positive harmonics need to be considered. The latter is the most concise representation and is utilised in this paper. The inclusion of positive and negative frequencies results in phase dependent transfers between the voltage and currents. In other words, the magnitude and phase of the current, I_k, can be dependent on the phase of the applied voltage, V_m, requiring the admittance term Y_{km}, to model the behaviour. The remainder of this section describes the modelling of the phase dependency by a Tensor Admittance.

7.4.1 Tensor Representation

The phase dependent behaviour can be successfully modelled by expressing each Y_{km} as a 2×2 tensor matrix as shown in equation (7.8). 2×1 vectors are used to represent the positive frequency voltage and current. The vectors contain the real (direct in phase with the reference frame) and imaginary (quadrature or out of phase) components. This means the admittance tensor and vectors contain only real valued terms. The tensor structure retains the same complex number operations performed when using complex number representation.

$$\begin{bmatrix} \Delta I_r \\ \Delta I_i \end{bmatrix} = \begin{bmatrix} y_{11} & y_{12} \\ y_{21} & y_{22} \end{bmatrix} \begin{bmatrix} \Delta V_r \\ \Delta V_i \end{bmatrix} \tag{7.8}$$

This rank-2 tensor observed by Smith [53] effectively varies the gain and phase angle of the transfer depending on the phase of the voltage. The tensor can be visualized geometrically as a circle locus in a complex admittance plane (discussed further in section 7.5.1). Each tensor incorporates both the positive and negative frequency interactions by the summation of;

$$\begin{aligned} \text{the direct term} \quad & \begin{bmatrix} y_{da} & -y_{db} \\ y_{db} & y_{da} \end{bmatrix} \\ \text{(positive frequency)} \quad & \\ \text{and the conjugate term} \quad & \begin{bmatrix} y_{ca} & y_{cb} \\ y_{cb} & -y_{ca} \end{bmatrix} \\ \text{(negative frequency)} \quad & \end{aligned}$$

The conjugated term introduces the phase dependent behaviour into the tensor transfer. Therefore a linear non-phase dependent relationship is described by a tensor where the conjugate terms are zero and the direct terms, y_{da} and y_{db}, correspond electrically to the conductance and susceptance respectively.

The resultant positive frequency current vector contains the sum of the negative and positive frequency transfers in a concise manner. This has improved computational and memory efficiency over the other forms where additional steps are required to recombine the terms [55]. Using real valued tensor admittances and voltage and current vectors further improves the computational efficiency when performing general arithmetic multiplication/division. This is most notable when solving the impedance coupling matrix by inverting the admittance matrix.

7.5 SEQUENTIAL HARMONIC INJECTION TECHNIQUE

The sequential harmonic injection technique obtains the load FTM by sequentially applying small input (voltage) distortions to the load and measuring the change in the outputs (current). The frequency coupling matrix is formed in the small signal, linearising the load around a base case operating point. The process is applicable to both time domain simulations and physical time domain testing of the actual devices.

A single voltage distortion is applied at each of the frequencies of interest and the response measured at each output frequency. A single frequency injection permits any resultant current distortion to be directly related to the input voltage distortion.

The phase and magnitude of the distortion can be varied to investigate any phase dependent relationships and to confirm the device's linearity about the operating point.

An observant reader will quickly identify that for multi input/output systems, to obtain each transfer, all of the individual inputs need individually distorted. The most useful relationship for harmonic studies is the AC voltage to AC current transfer and is used here to illustrate the sequential harmonic injection technique. The transfers can equally be found between the AC voltage and DC bus voltage.

In the development of the model the following conditions are assumed;

- The load must be stationary, LTP. Required by the model, the load must be in steady state and its frequency characteristics be time invariant and not influence by uncontrollable inputs.
- The input must be independent of the device operation. For example, the input voltage must be independent of the load current, demanding a low supply impedance.
- The base case operating conditions must remain constant. Both base case inputs and outputs are held constant.

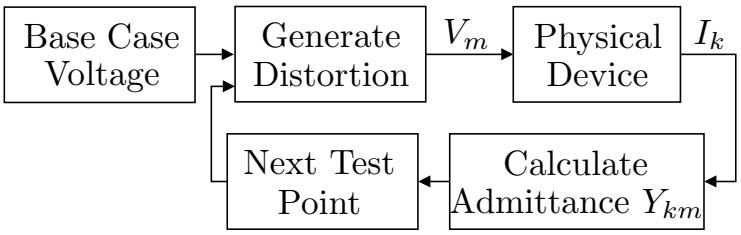

Figure 7.2: Sequential Harmonic Technique Process Flow Diagram

The sequential technique, shown in Figure 7.2 initially solves for the base case operation, I_b at base voltage V_b. It should be noted that the base voltage V_b can contain harmonics of any phase angle. V_b and I_b are subsequently assumed as the base case operating point, and therefore, must remain constant throughout the entire procedure. Next a single m^{th} order harmonic voltage distortion is added to the base case voltage and applied to the load terminals. Once the load reaches steady-state the current waveform is decomposed into the harmonic domain components I_k; and the admittance, Y_{km} is found using (7.9) at each k^{th} frequency of interest. In (7.9),

the base case voltages and currents are subtracted from the measured harmonic levels so as to consider only the contribution caused by the distortion.

$$Y_{km} = \frac{I_k - I_{bk}}{V_m - V_{bm}} = \frac{\Delta I_k}{\Delta V_m} \tag{7.9}$$

V_m and I_k are the measured harmonics at the load terminals and V_{bm} and I_{bk} are the base case m^{th} order voltage and k^{th} order current. ΔV_m is the m^{th} order applied distortion and ΔI_k is the resultant current distortion.

Sequentially the applied voltage distortions are varied in phase, magnitude and frequency. At each test frequency the vertical rows of the FTM are obtained. The phase dependent tensors are found by parameterising the calculated admittance as the phase of the distortion is varied. This process is given in detail in Section 7.5.1.

Although the technique is computationally straight forward, the freedom of the phase, magnitude, input and output frequency dimensions can lead to lengthy testing times. In saying this, the entire procedure only needs to be carried out once for a device at each operating point. The technique presents two key advantages; firstly the load can be treated as a 'black box' where no knowledge of the device operation or circuit design is required. The procedure combines all the interactions of the physical device's operation. Secondly, by forming the FTM model from the physical device, errors introduce by incorrect component modelling within an equivalent computer simulation are eliminated.

7.5.1 Tensor Parametrisation

The tensor components of each frequency relationship is found using the geometric properties of the phase dependant relationship. As the phase of the applied voltage distortion is varied from 0 to 2π, the phase dependent relationship causes the admittance, Y_{km} to change in the form of a double circle locus as shown in Figure 7.3. Geometrically the circle locus rotates about its centre $a + jb$, on the real and imaginary axis with a radius r. The locus contains a phase shift of θ about its own axis to correspond to the admittance relationship at a input distortion angle of zero degrees.

The four terms of the tensor can be found by an elegant method proposed by Smith [52] which uses only two admittance points. Although this method is efficient it is quite prone to experimental error and more suited for analytical or simulated models, thus a more robust method is proposed.

The method used in this analysis finds the double circle locus to best match the admittance points obtained from the measured data. The measured data contains measurement errors and an unknown level of non-linearity of the device. By simply increasing the number of admittance points the effects of system noise and data abnormalities can be reduced. For an admittance locus plotted by an even number of N voltage phase angles that are evenly spaced between $0 - 2\pi$ then a, b, r and θ are found by;

$$a = \frac{1}{N} \sum_{n=1}^{N} real(y(n)) \tag{7.10}$$

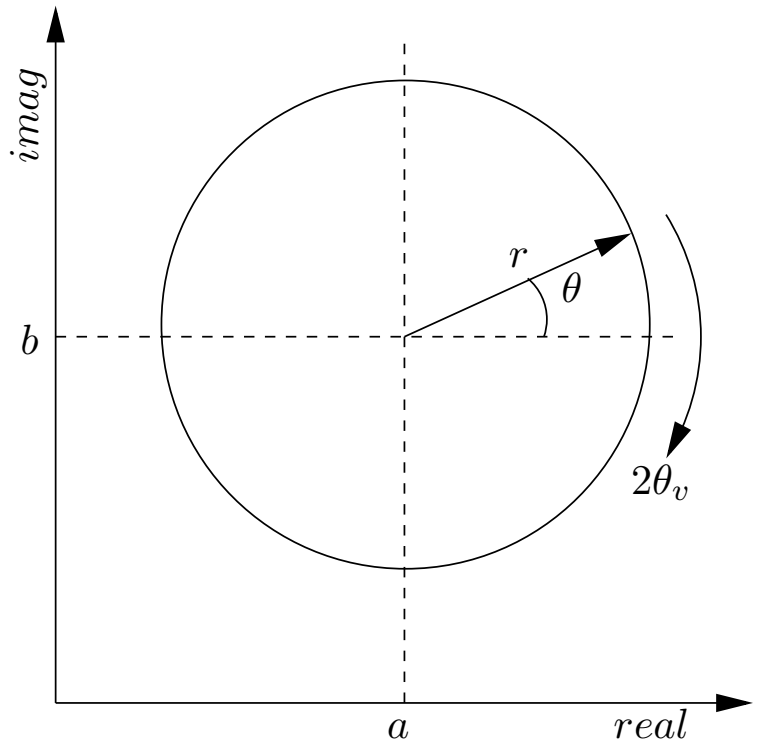

Figure 7.3: Parametrisation of a Phase Dependent Admittance Locus

$$b = \frac{1}{N}\sum_{n=1}^{N} imag(y(n)) \tag{7.11}$$

$$r = \frac{1}{N}\sum_{n=1}^{N} abs(y(n) - (a + jb)) \tag{7.12}$$

$$\theta = \frac{1}{N}\sum_{n=1}^{N} angle(y(n) - (a + jb)) + 2\theta_v(n) \tag{7.13}$$

where, $\theta_v(n)$ is the applied voltage angle at the n^{th} admittance component.

Likewise, four simultaneous equations can be written for each of the tensor values;

$$y_{11} = \frac{\alpha}{2}\sqrt{\frac{2r^2}{1 + tan^2(\theta)}} + a \quad \alpha = \begin{cases} 1, & \frac{-\pi}{2} < \theta \leq \frac{\pi}{2} \\ -1, & \frac{\pi}{2} < \theta \leq \frac{3\pi}{2} \end{cases} \tag{7.14}$$

$$y_{12} = \frac{\alpha}{2}\sqrt{\frac{2r^2}{1 + 1/tan^2(\theta)}} - b \quad \alpha = \begin{cases} 1, & 0 < \theta \leq \pi \\ -1, & \pi < \theta \leq 2\pi \end{cases} \tag{7.15}$$

$$y_{22} = 2a - y_{11} \tag{7.16}$$

$$y_{21} = 2b + y_{12} \tag{7.17}$$

The conditional fields are required as the assumed principal value of the trigonometric function and thus the circle radius may not correlate to the correct phase location of the admittance

locus.

For the cross-coupled model the tensors are derived from the calculated admittance Y_{km} at each phase angle of the voltage as it is varied from 0 to 2π. This calculated admittance is prone to experimental error and may also include higher order complex non-linearities. Proposed is the use of a robust Fourier descriptor to find the best tensor approximation to match the measured data. Fourier descriptors are commonly used in image recognition for the classification of closed looped objects. The double circle locus form of the tensor in Figure 7.3 is closed loop on a complex plane and its Fourier descriptor describes how the admittance varies as a function of the applied distortion angle.

The Fourier descriptor is the discrete Fourier transform of the complex admittance at N_p evenly spaced distortion phase angles and is described by;

$$Y_{fd}[k] = \frac{1}{N_p} \sum_{n_p=0}^{N_p-1} y(n_p) e^{\frac{-j2\pi k n_p}{N_p}} \tag{7.18}$$

where $Y_{fd}[k]$ is the Fourier descriptor and $y(n_p)$ is the admittance measures at the ${n_p}^{th}$ voltage phase angle.

Geometrically the tensor's direct term is the offset of the admittance circle from the real and imaginary axis and corresponds to the zero'th Fourier descriptor (comparative to the DC component of a Fourier transform). The conjugate, or negative frequency component rotates at twice the rate of the voltage angle in the opposite (clockwise) direction and corresponds to the -2 element of the Fourier descriptor. In other words the direct term is obtained from the constant offset of the waveform in Figure 7.3 and the conjugate term is the -2 order complex rotating component. Therefore both the direct and conjugate terms are obtained from the Fourier descriptor;

$$\begin{aligned} y_{da} + jy_{db} &= Y_{fd}(0) \\ y_{ca} + jy_{cb} &= Y_{fd}(-2) \end{aligned} \tag{7.19}$$

and combined to form the full 2×2 tensor for each Y_{nm}.

Smith's [53] observation requiring two only admittance points to determine tensor relationship meets the nyquist sampling criterion for the tensor admittance.

7.6 AUTOMATED EXPERIMENTAL SYSTEM

The sequential injection technique was automated using the Universal PQ Test System, described in Chapter 3, to validate and develop the proposed FTM models. The automation is performed by the National Instruments Labview software environment, carrying out the sequential control, signal generation and signal processing.

7.6.1 System Overview

The test system (depicted in Figure 7.4) was designed to carry out the sequential harmonic technique to validate the proposed FTM model. The process has been automated within the experimental system described in Chapter 3. The user specifies the voltage distortion harmonics, m to be applied and the current harmonics, k that are of interest. The magnitude and phase of voltage distortion are also both configurable within the software.

The technique relies on a voltage source capable of accurately producing the base case conditions and superimposing the required distortion. This is achieved by creating the waveforms within software and using a Programmable/Arbitrary Waveform AC Power Source for amplification up to rated voltage.

The Chroma is a single phase AC source capable of delivering up to 500VA at 300Vrms to a bandwidth of 2400Hz. This restricts the test devices to relatively low power and single phase loads, even though the described technique is applicable to three phase loads. Ideally the source should have zero internal impedance so as not to affect the test device's harmonic performance. This was minimised by setting the programmable output impedance as low as possible. The effect is further reduced by measuring the electrical waveforms directly at the load terminals. These time domain waveforms are sampled through a data acquisition card and are decomposed into their frequency domain components.

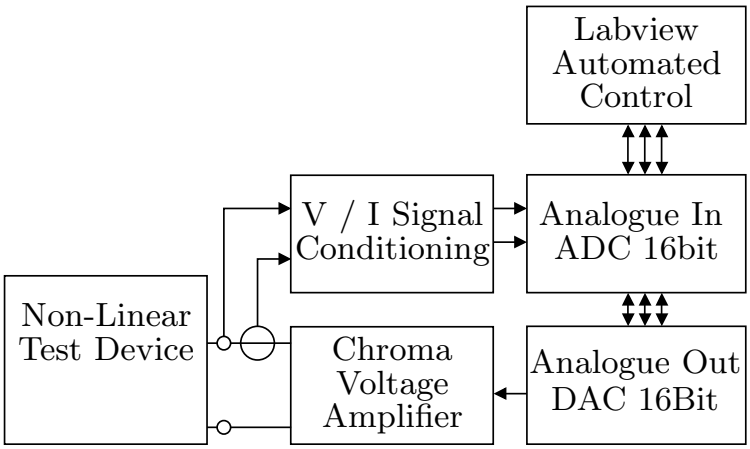

Figure 7.4: Test System Block Diagram

The admittances are calculated using (7.9) at each test point and are then parametrised by equations (7.19) and (7.18) within MATLAB. The 2×2 tensors are then combined to form the FTM for the device and associated with the base case to complete the harmonic model. Some terms of the FTM can be manifested by the presence of noise in the measurement system. These are identified by interactions which cause small current distortions less than the test systems noise floor (indicating low harmonic coupling) or those that incorrectly follow a circle locus.

7.7 AUTOMATED FREQUENCY DOMAIN DEVICE MODELS

The following results illustrate the sequential harmonic technique carried out on a capacitive smoothed full bridge rectifier, a compact fluorescent lamp and a linear fluorescent tube. For

practicality, only the integer harmonics up to the 20th harmonic have been modelled. For all loads the nominal supply is rated a 230V at 50Hz and linearisation is achieved using a 1% voltage distortion at phase angle steps of 7.5°. The system reference frame was synchronised to the fundamental voltage. The base case voltage used for all cases consists of 100% 1^{st} harmonic, 1.4% $\angle$ 80° 3^{rd} and 3% $\angle$ −162° 5^{th} harmonic. This generates a flat top waveform typical of the distortion caused by rectifier loads experienced at the author's workplace.

7.7.1 Single Phase Capacitor Smoothed Full-Bridge Rectifier

The full-bridge rectifier represents an uncontrolled load where the turn on and turn off instants are effectively defined by the terminal voltage waveform. These devices are not common as they do not conform to most harmonic limitation standards for medium power applications, however its simplicity is used for the validation of the process. The rectifier load is rated at 56W in parallel with a 33μF capacitor.

The effect of a 1% 3^{rd} harmonic voltage distortion on the 3^{rd}, 5^{th} and 7^{th} harmonic currents is illustrated in Figure 7.5. As the distortion phase is varied the measured current (marked '×') forms an ellipse around the base case current (marked '•') beginning from the zero degree distortion (marked '○'). This clearly demonstrates that the 3^{rd} harmonic voltage causes distortion of 3^{rd}, 5^{th}, 7^{th} (and all odd) order harmonic currents.

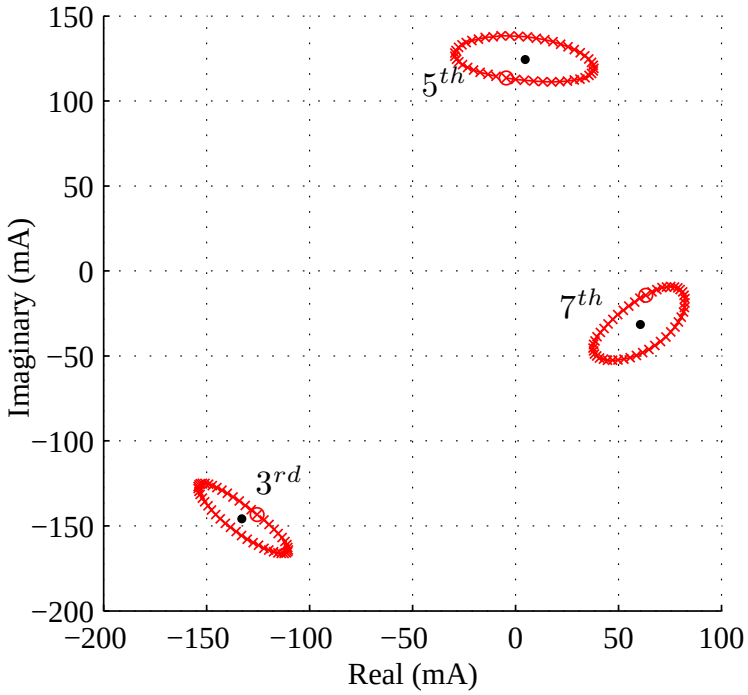

Figure 7.5: 3^{rd}, 5^{th}, 7^{th} Harmonic Current in the presence of 1% 3^{rd} Harmonic Terminal Voltage Distortion, Phase $0-2\pi$. '•' base case current, '×' measured current distortion, '○' 0° distortion

The elliptical shape of the current locus is due to the phase dependency of the admittance. The admittances for the same 3^{rd} harmonic distortion are shown in Figure 7.6. The points marked '×' are those obtained from the measured data and the solid locus is the circle created by the parametrisations described by the 2×2 tensor. The arrow indicates the radius and position of

the zero phase angle admittance. These admittance locus can also offer valuable insight into the angles of voltage distortion which result in the maximum or minimum distortion of the current.

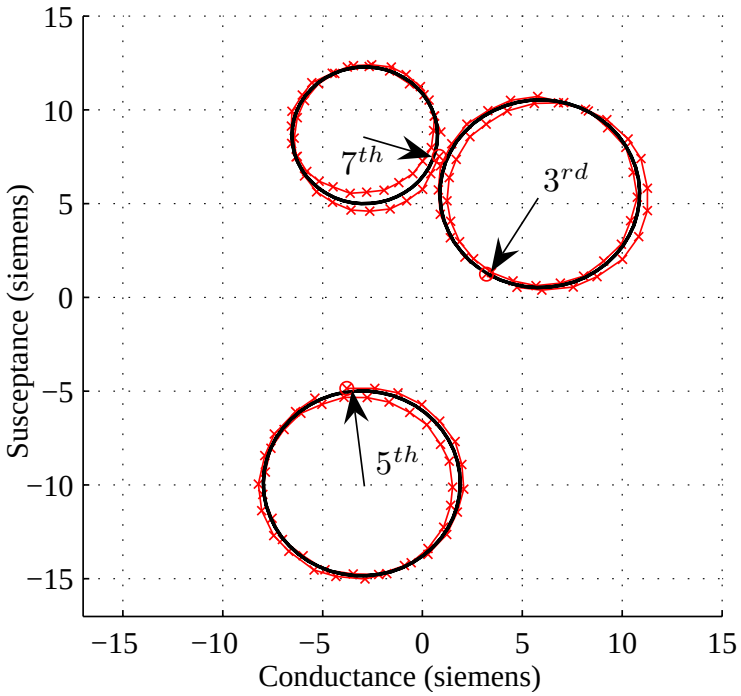

Figure 7.6: 3^{rd}, 5^{th}, 7^{th} Harmonic Admittance in the presence of 1% 3^{rd} Harmonic Terminal Voltage Distortion, Phase varied $0 - 2\pi$. '$\times$' calculated from measured data, 'solid circle' estimation for tensor parameterisation, 'arrow' radius of tensor pointing to 0° distortion

The FTM for the rectifier (Figure 7.7) forms a lattice structure showing significant coupling occurs between harmonics of different orders. Each coupling, represented by a 2×2 tensor is indicated by 4 dots. Strong coupling occurs between odd order voltage harmonics and odd order current harmonics, as is also the case with even order harmonics coupling to even order current harmonics.

7.7.2 Compact Fluorescent Lamp

The vast quantities of compact fluorescent lamps available on the market each employ various control strategies which define their harmonic performance. For demonstration purposes, only the model of a 20W 230V/50Hz Ecobulb CFL is presented. The base case was obtained under the same operating voltage as the rectifier drawing only odd order harmonics with a THD of 26%. Once again the FTM, shown in Figure 7.8 indicates the strong cross coupling formed a lattice structure.

An important aspect of the FTM is its validity in modelling large number of loads operating together. As one would expect the system harmonics may increase with additional non-linear loading. Table 7.1 presents the comparison of the FTM harmonic domain model with the actual measurements from the CFL under increased distortion. The voltage waveform is distorted by an additional $0.6\% \angle 80°$ 3^{rd} harmonic and $0.6\% \angle -162°$ 5^{th} harmonic. These distortions result in the distortion of only odd order harmonic currents as presented.

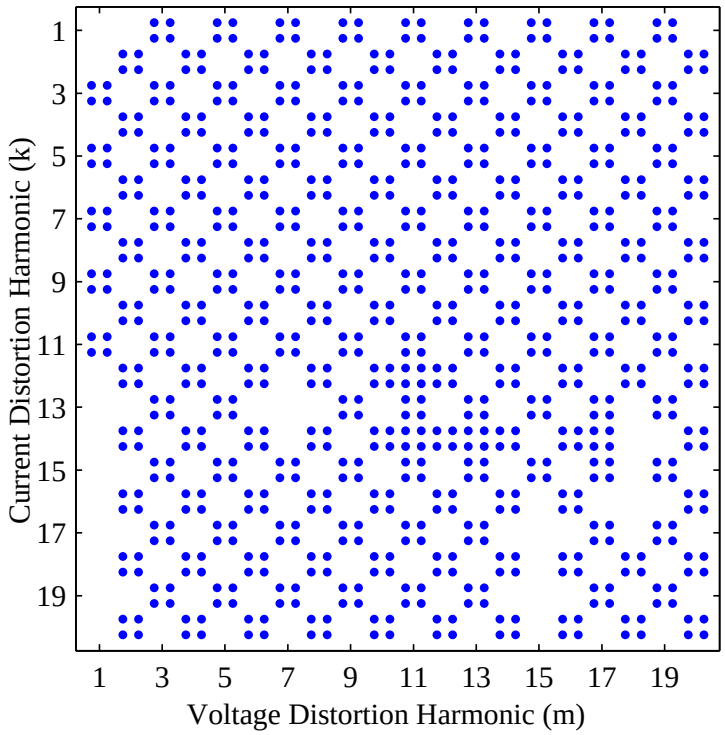

Figure 7.7: Lattice Structure of Admittance FTM for Capacitor Smoothed Rectifier 1% Voltage Distortion. Transfer terms less than 0.5 Siemens are ignored

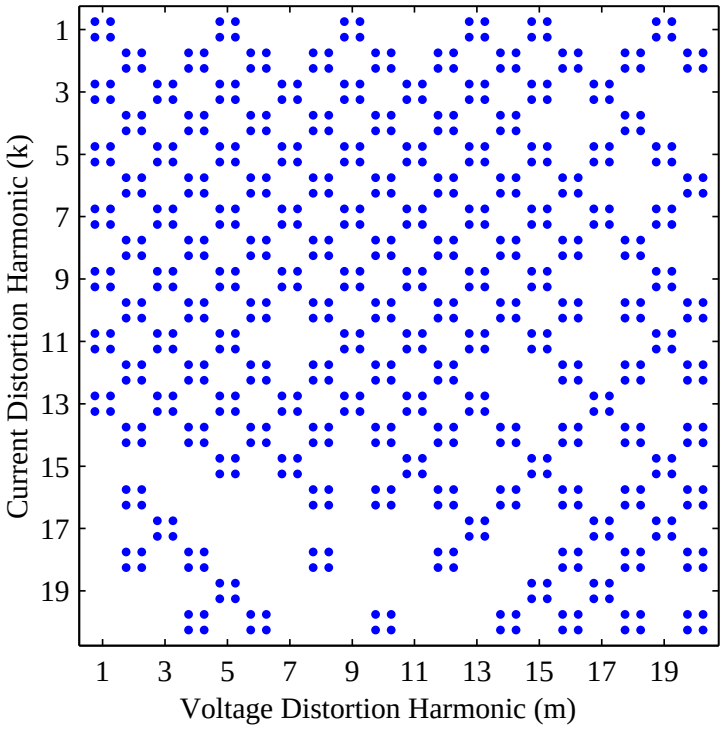

Figure 7.8: Lattice Structure of Admittance FTM for Ecobulb 20W CFL, 1% Voltage Distortion. Transfer terms less than 0.4 Siemens are ignored

Harmonic Order	Voltage (%)	FTM Model Current (mA)	Measured Current(mA)
1	100	83.7∠ 7	83.5∠ 7
3	2∠ 80	7.7∠-26	7.7∠-24
5	3.6∠ -162	16.0∠-23	16.1∠-21
7	0	4.6∠-50	4.7∠-44
9	0	6.8∠-25	7.3∠-22
11	0	2.5∠ 49	2.2∠ 65
13	0	1.5∠-32	2.4∠-32
15	0	3.1∠ 0	2.9∠ 7
17	0	0.6∠ 43	1.1∠ 6
19	0	1.9∠-12	1.6∠-5

Table 7.1: Comparison of CFL FTM Harmonic Domain Model and Measured Current under 3^{rd} and 5^{th} Voltage Distortion

Although these results are reasonable, it was found that the operation of the CFL was highly dependent on the temperature of the tube and electronic ballast. This leads to the device not always operating in the same base case and therefore limits the use of the harmonic domain model. The level and frequency of the applied distortion also had to be carefully selected to avoid the CFL from conducting multiple times during each half cycle. This causes a highly non-linear response for which the model is not designed.

7.7.3 Magnetic Ballast Fluorescent Lamp

The sequential harmonic technique was carried out on a 56W Philips single tube fluorescent fitting with a magnetic ballast. The fitting consists of a large inductor ballast in series with the tube and a capacitor connected parallel for power factor correction. The lamps are non-linear due to the electrical arc formed within the discharge tube and nominally draw small amounts of odd harmonics at 6% THD. The FTM shown in Figure 7.9 indicates that coupling predominantly occurs between harmonics of the same order as was observed in [19].

The diagonal couplings reveal that the LFT has a phase dependent admittance. Figure 7.10 shows the extent of the phase dependency and the magnitude and phase of the diagonal terms of the FTM. It is evident that the dependency reduces at higher order harmonics and that the admittance magnitude increases.

7.7.4 Harmonic Models

The three harmonic models for each CFL only include the odd order harmonics up to the 41^{st}. The base case conditions for the model was reproduced from low voltage 230V/50Hz supply at the author's work place supply consisting of 100% fundamental (used as the reference frame), $3\%\angle 80^\circ$ 3^{rd} harmonic and $1.4\%\angle -162^\circ$ 5^{th} harmonic. This produces a typical flat top voltage common in distribution systems with large numbers of computers and lighting. The harmonic Current Source model is given by the base case harmonic current generation, shown in Figure 7.18.

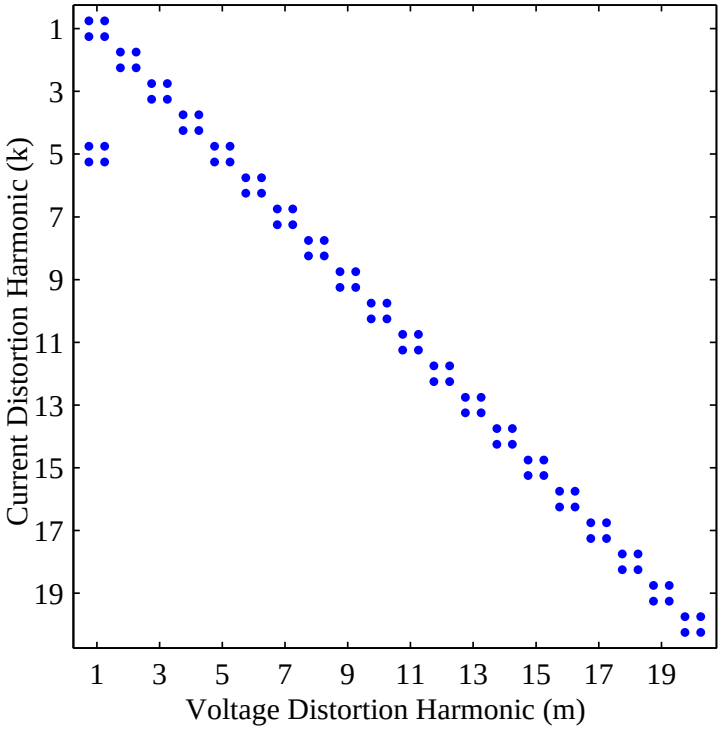

Figure 7.9: Structure of FTM for Magnetic Ballast Linear Fluorescent Tube. 2×2 tensor transfers are represented by 4 dots indicating high coupling

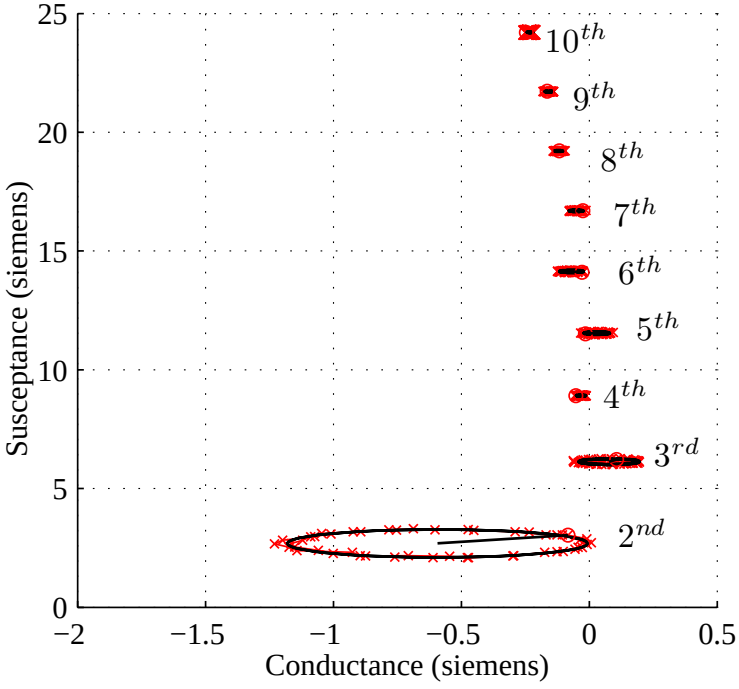

Figure 7.10: Diagonal Terms Harmonic Admittance Linear Fluorescent Tube Magnetic Ballast. '×' calculated from measured data, 'solid circle' estimation for tensor parameterisation, 'arrow' radius of tensor pointing to 0° distortion

The structure of the Harmonic Cross-Coupled admittance matrix is shown in Figures 7.11-7.15 for the 5 lamps linearised about a 0.5% distortion. From these graphs it is clear that the diagonal terms provide the strongest couplings, although they also indicate the off-diagonal terms are significant. In many cases coupling to the adjacent odd order harmonics can be as much as 80% of diagonal component. These off-diagonal couplings demonstrate the ability of the CFL to couple harmonics and the necessity for a cross-coupled model.

A single test is required to obtain the current source model and in this case is represented by 21 harmonic values. The Norton Equivalent model requires a 21 small signal voltage injection test and an admittance vector with 21 values to complete the model. While the cross-coupled model requires voltage injection at 21 harmonics $\times$ 48 phase angles equating to 1008 tests and an admittance tensor matrix of $21 \times 21 \times 2 \times 2 = 1764$ terms plus the base case current.

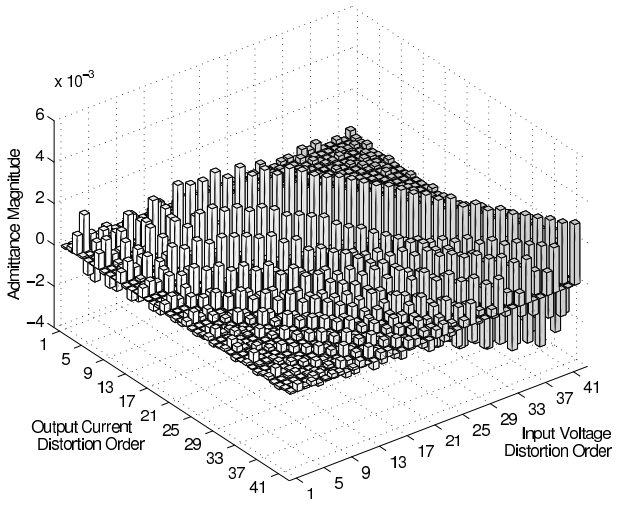

Figure 7.11: Ecobulb 20W Harmonic Cross-Coupled Admittance Matrix

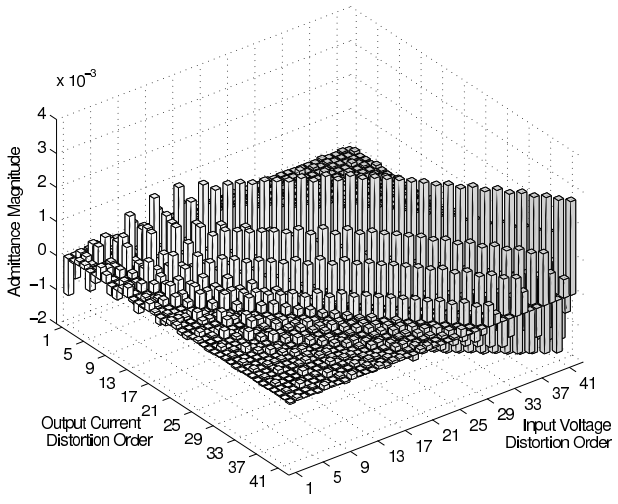

Figure 7.12: Ecobulb 13W Harmonic Cross-Coupled Admittance Matrix

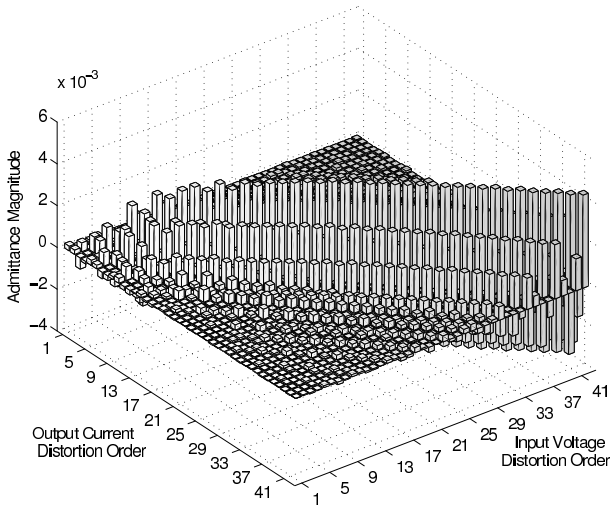

Figure 7.13: Elite 20W Harmonic Cross-Coupled Admittance Matrix

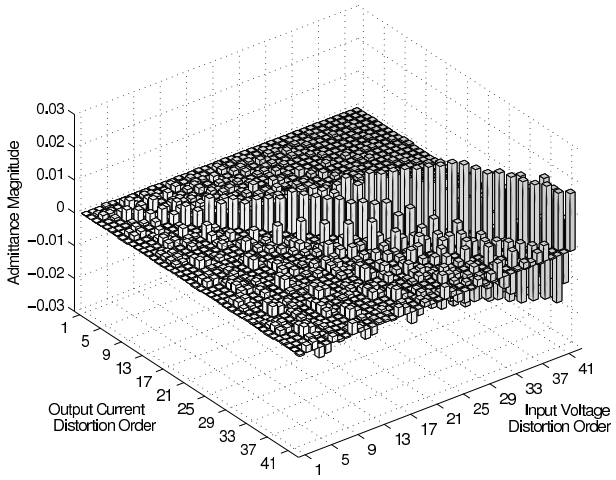

Figure 7.14: Philips 24W Harmonic Cross-Coupled Admittance Matrix

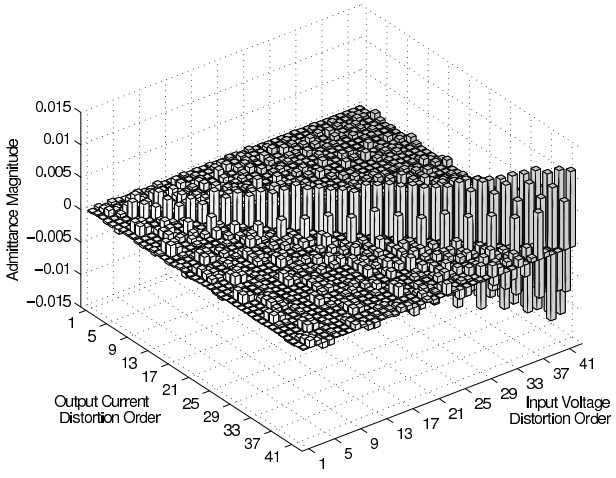

Figure 7.15: Signature 20W Harmonic Cross-Coupled Admittance Matrix

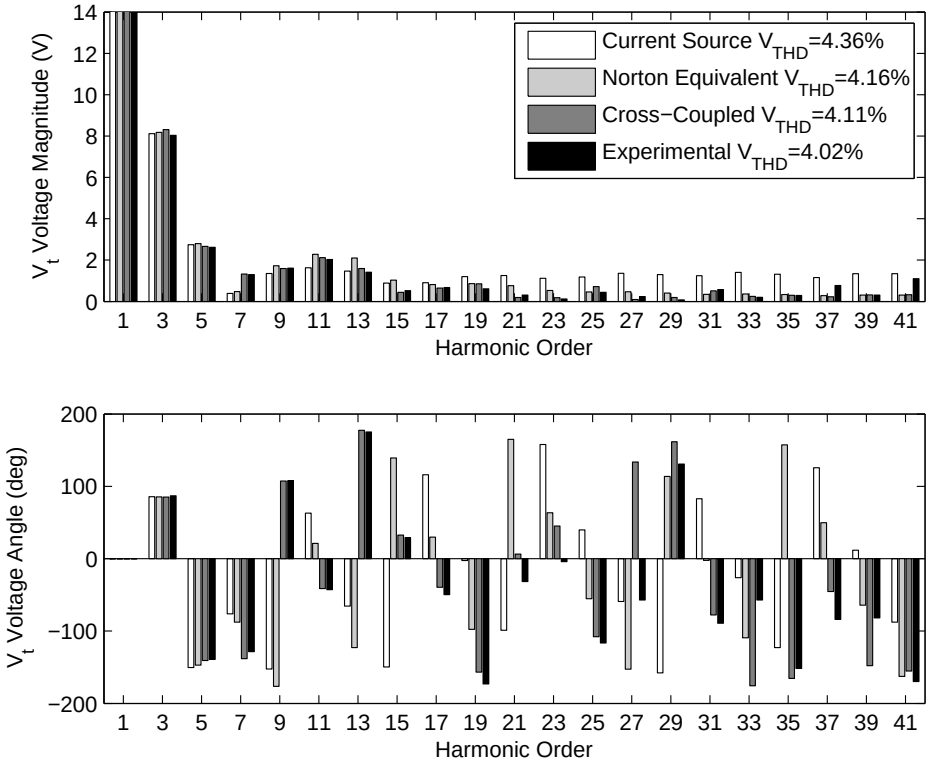

Figure 7.16: Terminal Voltage V_t Harmonics, Simulated and Experimental with all five lamps attached to the busbar

7.7.5 Simple System Simulation

To illustrate the interaction between the CFL and AC system via the system impedance, the small system shown in Fig. 7.17 was simulated in MATLAB using the three different harmonic models. The presence of a system impedance causes the current distortion from the CFLs to distort the terminal voltage. Since the CFL harmonic current is quite small the resulting voltage distortion will also be small. By setting the voltage source, V_s to the base case voltage, means it is likely the CFLs will be operating in the linear, or small signal region.

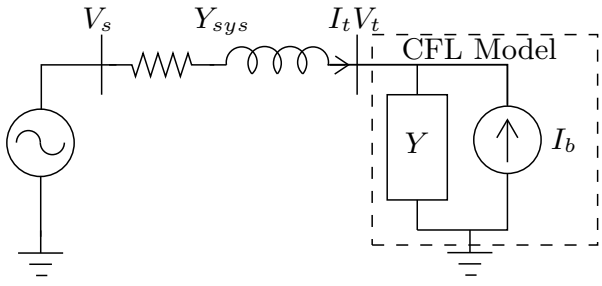

Figure 7.17: Simple System Network Model

The system impedance is modelled as a typical transmission line by a 13mH inductor with 2.4

of resistance. The experimental test was carried out in an isolated system with the Chroma as the voltage source and a ferrite core inductor and resistor. Due to the limited space only the results of connecting all five lamps to the busbar are given. The simulated terminal voltage and current form each of the harmonic models are compared to the experimental results in Figs. 7.16 & 7.18, respectively.

The harmonic Current Source model does not model either interaction between the non-linear load and ac system, or between harmonic non-linear loads, as the harmonic current injection is fixed. It is evident from Figure 7.18 that the harmonic current source model results in an under-estimation of the current injection at 7^{th} harmonic and over-estimation at the higher order harmonics ($> 19^{th}$). This is also reflected in the estimated harmonic voltages (in Figure 7.16). While the estimated magnitude for the $9^{th}, 11^{th} and 13^{th}$ appears good, it is important to match both the harmonic magnitude and angle to indicate an accurate result. The Norton equivalent gives a superior estimate of the harmonic current injection and busbar harmonic voltages, but it is clear from Figures 7.16 & 7.18 the most accurate results are produced by the cross-coupled model.

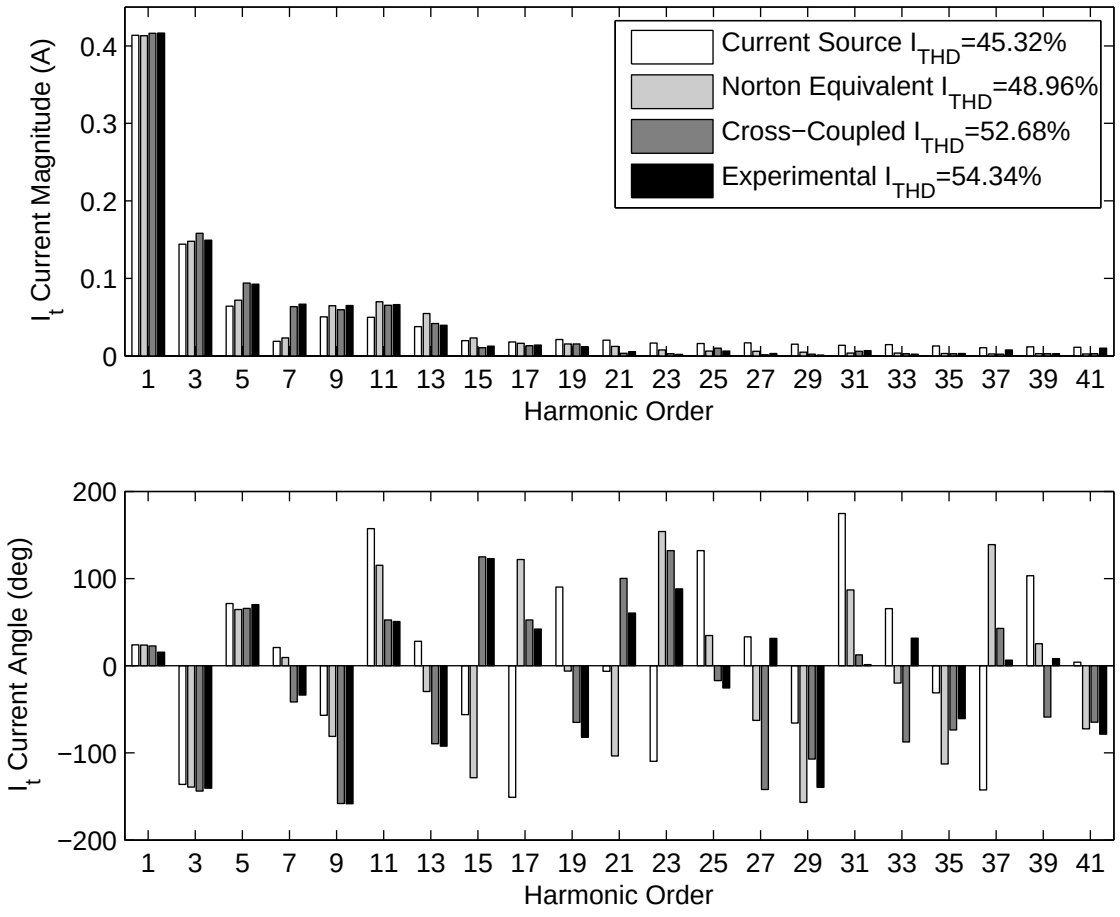

Figure 7.18: Terminal Current I_t Harmonics, Simulated and Experimental with all five lamps attached to the busbar

7.7.6 System Reference Shift of the Harmonic Domain Model

Previously, the development of analytical models of high power devices are constructed in a system sense, with predefined transmission lines, loads and generators. A fixed phase reference is then defined at the slack bus generator and used as the reference for all system signals (including switching instants) during the simulation. This is common with larger non-linear loads as the system is well defined as a practical study of a system.

This is not the case for the models developed in this chapter and in the following Automated Frequency Domain modelling chapter. The models are derived using the terminal conditions as the system reference (typically the fundamental voltage as the zero phase reference angle). Thus all phasors are referenced to this reference. It is important to note that the developed linear harmonic models are not dependent on this system reference nor are they confined to a system with this reference frame. The techniques used in forming the model are for the specific operating conditions.

Modelling of the device with reference to its terminal is more appropriate for low power distribution loads (1-phase and 3-phase). Distribution type loads are typically locked to the terminal voltage as a reference.

7.8 CONCLUSION

The linearisation of electrical devices in the harmonic domain is generally well understood, however the phase dependency of the transfers is not widely appreciated. This chapter clearly shows the implementation of a phase dependent admittance into a computationally efficient tensor based frequency transfer matrix, and demonstrates the importance of doing so via practical tests and results.

Automating the formation of harmonic domain models by an experimental process enables the extensive testing of consumer based devices. The wide range of distortion frequencies, phase shifts and magnitudes can lead to lengthy testing times. The sequential harmonic technique allows the device to be treated as a ‘black box’ such that the knowledge of the complex internal circuit design and operation is not required. The robust parametrisation of the admittance utilises the tensor’s geometric properties to form the 2×2 tensor elements of the FCM.

The FCM models for a number of CFLs demonstrated the variability of the circuit response. These models were connected to a simple network and compare with the experimental results. This showed the interactions between the lamps and the system impedance and importantly the interaction between devices. The FCM models were utilised in the model generation. The measured results allow us to observe the device’s linearity.

This work paves the way towards analysing the effects of large numbers of distributed harmonic generating loads by efficient and accurate models using matrix methods. This could be used to determine performance requirements of devices as to avoid harmonic issues or for optimising mitigation measures if problems arise.

Chapter 8

CONCLUSION AND FUTURE WORK

8.1 CONCLUSIONS

The adoption of energy efficient lighting technologies, dominated particularly by CFLs and soon to be followed by LEDs, are fundamentally changing the procreation of flicker within the power system. This rapid transition also raises concern regarding their level of harmonic distortion and the combined effect it will have on the network. Little consideration has been given to wide-scale use of energy efficient lighting and it's effect on power quality of the system. Likewise there is limited knowledge of how the lamps technology, construction, or use, alters its flicker performance and how they contribute to harmonic distortion.

The main original contributions of this thesis are:

- The light flickermeter, for the accurate quantification of light flicker from all present and future lighting technologies,
- Application of the Harmonic State-Space to low power devices for the study of steady state and transient operation,
- Automated development of Harmonic Domain models, to characterise and improve the representation of loads in MV and LV networks.

The light flickermeter proposed in this thesis provides the objective measurement method for light flicker by measuring the instantaneous light level produced by the lamp. By removing the reference lamp from the IEC flickermeter, the light flickermeter can quantify flicker from any lighting source independent of its; operation, power rating, or underlying technology. Aligning with the IEC methodology, enabled the direct calibration of the light flickermeter and ensures its future use and coordination with the supporting power quality standards. This reconsideration of the flicker quantification method correctly allows power quality to be better managed on electrical networks.

Exploring the procreation of light flicker with the light flickermeter provides greater understanding of modern lamps sensitivity to voltage fluctuations. The experimental system constructed as part of this research enabled any lamp type, to be stimulated by an extensive range of power quality distortions and to measure the light flicker produced. The closed test system gave complete isolation from the electrical network and blocked external lighting to test under precise conditions and control. The light flickermeter, useful in its own right, has many

applications: product development, as was illustrated in Chapter 5, comparison of emerging technologies (LEDs) performance, the establishment and compliance of performance standards, or case specific disturbances such as light flicker caused by ripple control.

While the effect of CFLs and other modern lighting systems, as many researchers conclude, will be minimal on harmonic levels it is the ongoing accumulation of non-linear loads that will continue to push harmonic levels higher, eventually exceeding regulatory limits and leading to greater reports of harmonic problems. There is still much research needed to comprehend the combined affect and interaction of such loads. The application of the HSS presented in this research paves the way to modelling of low powered devices. This enables deeper understanding and extends the viewpoint that the HSS provides.

The procedural formation of a device model in the HSS framework aligns with computer aided simulation of electrical circuits. The circuit dissection enables the realisation to be visualised as control diagram, lending itself to the incorporation of controller actions. The model formulation is based on Kirchhoff's voltage and current laws, and constructs sub-systems from elementary matrices. The HSS framework built on the LTP basis allows for many of LTI analysis tools and techniques to be readily utilised. This is particularly useful to investigate electrical resonance or control aspects of a converter.

Automated development of harmonic domain models using the sequential harmonic injection technique provides a robust experimental method. The technique reduces the laborious task of model identification of traditional HD or HSS methods, and eliminates the development of analytical equations and the errors associated with circuit or control simplification. The process produces a phase dependent tensor representation from the actual device. The model can then be employed directly in steady state HD system simulations. With the replacement of incandescent lamps reaching saturation, the focus should be placed on other devices such as heat pumps and solar panel inverters.

8.2 FUTURE WORK

The emphasis of power quality assessment has in the past been the effect of the supply system non-linearities on the distribution voltage waveform on the assumption that the loads were reasonably linear. As the modern utilisation systems have become more controllable and efficient, this assumption does not hold. This thesis has shown the distorting effect that modern lighting loads have on the supply system with reference to flicker and harmonics. This needs to be extended to the other domestic loads. Although the added rating of the loads is almost the same as the generation and transmission ratings, it is not practical to represent them individually in the global system power quality assessment. Their accumulated effect is already used in power flow studies in terms of fundamental frequency active and reactive power derived from experience for the time of day and whether conditions. Further work is needed to relate the real and reactive load patterns of the load flow to their combined effect on the waveform assessment at point of common coupling. Such information could then be used in approximate harmonic analysis or combined with sophisticated Harmonic-Power Flow assessment. Also the effect of renewable sources at utilization points on the linearisation process should be investigated.

The automated harmonic domain modelling technique needs to be applied to other devices in order to gain a wider knowledge. The aim is to collect a library of device characteristics that can be called upon. This requires investigating the interactions between devices and their aggregation

to derive suitable models for system studies. It is important to conduct real world measurements for different levels in the system to identify the statistics and hence a measure of confidence that can be placed on the model of the aggregated load. This may also be extended by the use of the harmonic state-space framework to develop models suitable for transient simulation.

A portable test system could be developed using the proposed automated modelling algorithm. This would help to derive the Norton equivalent models of loads at various locations in the network by performing a similar sequential current injection technique. This could be useful for determining the performance requirements of devices to avoid harmonic issues.

The possibility of damped resonances occurring in distribution systems is very likely, even at the low voltage level. These resonance conditions are not widely reported most likely due to sufficient damping. There is valuable merit in studying this behaviour and modelling to predict harmonic levels.

The next stage for the light flickermeter research is to develop a portable version of the measurement device used in situ. However, as discussed in Chapter 4, the light flickermeter is highly susceptible to external light sources. Therefore, the portable light flickermeter must be designed to provide a controlled environment to produce useful measurements. The solution to this could be in the form of a portable enclosure which prevents other light sources from affecting the measurement of the light source in question. Furthermore, for the light flickermeter to produce comparable measurements from different sites, a suitable reference light source is required. Selecting an "average" lamp as the reference light source requires a broad comparison between existing lamp technologies; considerations need to be placed on the physical design, electrical characteristics, and its level of uptake.

REFERENCES

[1] CIE 1988 2° spectral luminous efficiency function for photopic vision. Technical Report 86, CIE, 1990.

[2] IEEE recommended practice for measurement and limits of voltage fluctuations and associated light flicker on AC power systems. *IEEE Std 1453-2004 (Adoption of CEI/IEC 61000-4-15:1997+A1:2003)*, 2005.

[3] IEC 61000-4-15, Electromagnetic compatibility (EMC) - part 4-15: Testing and measurement techniques - flickermeter - functional and design specifications. *IEC 61000-4-15 ed2.0*, 2010.

[4] *IEEE Std 1453-2010 (Adoption of CEI/IEC 61000-4-15:1997+A1:2003)*, 2011.

[5] Incandescent lamps for general lighting services - Minimum Energy Performance Standards (MEPS) requirements. *AS 4934.2*, 2011.

[6] AS/NZS 61000.4.15:2005. Electromagnetic Compatibility (EMC), part 4.15: Testing and measurement techniques – Flickermeter – function and design specifications. 2005. Equivalent to IEC 61000-4-15, Ed. 1.1 (2003).

[7] ComLaw Australian Government. Customs (prohibited imports) amendment regulations 2008 (no. 7), select legislative instrument 2008 no. 256,'import control on certain incandescent light bulbs'. *Governor-General of the Commonwealth of Australia*, Dec. 2008.

[8] Australian States NSW, QLD, SA, VIC. Energy labelling and MEPS program regulatory ruling, 30c. 2010.

[9] HB Barlow. Temporal and spatial summation in human vision at different background intensities. *The Journal of physiology*, 141(2):337–350, 1958.

[10] Soo-Hwan Cho, Young-Soo Jang, Gilsoo Jang, Sae-Hyuk Kwon, Young-Soo Jeon, No-Hong Kwak, and Sung-Woo Lee. Application of IEC flicker standards to Korean distribution systems. In *Power Engineering Society General Meeting, 2006. IEEE*, pages 6 pp.–, 2006.

[11] Chroma ATE Inc. *Programmable AC Source 61500 Series User's Manual*.

[12] CIGRE 36.05/CIRED WG 2/UIE PQ Joint Working Group CCU2 on Voltage Quality. Test protocol IEC flicker meter used in power system voltage monitoring draft. (11), July 2004.

[13] Dataforth. *Signal Condition Module Voltage Attenuator System, SCMVAS*, 2009.

[14] Dataforth. *Signal Condition Modules 5B series, SCM5B40/41 Analog Voltage Input Modules, Wide Bandwidth*, 2009.

[15] J. de Jesus Chavez, A.I. Ramirez, V. Dinavahi, R. Iravani, J.A. Martinez, J. Jatskevich, and G.W. Chang. Interfacing techniques for time-domain and frequency-domain simulation methods. *Power Delivery, IEEE Transactions on*, 25(3):1796 –1807, 2010.

[16] Disturbances Working Group. Flicker measurement and evaluation. *1992: Montreal, Canada - XII International Congress on Electroheat*, 1992.

[17] H. De Lange Dzn. Experiments on flicker and some calculations on an electrical analogue of the foveal systems. *Physica*, 18(11):935 – 950, 1952.

[18] E3, Australian Government, Department of Climate Change and Energy Efficiency, New Zealand, Energy Efficiency and Conservation Authority. Equipment energy efficiency. *http://www.energyrating.gov.au*, 2006.

[19] M. Fauri. Harmonic modelling of non-linear load by means of crossed frequency admittance matrix. *Power Systems, IEEE Transactions on*, 12(4):1632–1638, Nov 1997.

[20] Robert S. Fisher, Graham Harding, Giuseppe Erba, Gregory L. Barkley, and Arnold Wilkins. Photic- and pattern-induced seizures: A review for the Epilepsy Foundation of America Working Group. *Epilepsia*, 46(9):1426–1441, 2005.

[21] D. Gallo, C. Landi, and N. Pasquino. An instrument for the objective measurement of light flicker. In *Instrumentation and Measurement Technology Conference, 2005. IMTC 2005. Proceedings of the IEEE*, volume 3, pages 1942 –1947, May 2005.

[22] Gigahertz-Optik. *Light detectors - Photopic and Scotopic Illuminance Detectors, VL-3701 pg. 59-64, Optometers, Instruments P-9202-4 Current to Voltage Amplifier pg. 53-54.*

[23] B. Heffernan, L. P. Frater, and N.R. Watson. LED replacement for fluorescent tube lighting. In *Power Engineering Conference, 2007. AUPEC 2007. Australasian Universities*, pages 1–6, Dec 2007.

[24] D.J. Hume, A.R. Wood, and C.M. Osauskas. The effect of AC system impedance on the cross-modulation of distortion in HVDC links. pages 196–201 vol.1, Oct. 2002.

[25] S.P. Hwang. *Harmonic State-space Modelling of an HVdc Converter with Closed-loop Control*. PhD thesis, Electrical and Computer Engineering at the University of Canterbury, Christchurch, New Zealand, 2014.

[26] IEEE. IEEE Std 1453-2011, IEEE Recommended Practice–Adoption of IEC 61000-4-15:2010, Electromagnetic compatibility (EMC)–Testing and measurement techniques–Flickermeter–Functional and design specifications. pages 1–58, Oct 2011.

[27] IES. *Lighting Handbook*. 1984.

[28] CIE International Commission on Illumination. The measurement of luminous flux. (No. 84), 1989. 1st Edition.

[29] GDT Perturbations International Union for Electro-Heat, WG Disturbances. Flicker measurement and evaluation. Technical report, UIE, 1992.

[30] N.R. Watson J. Arrillaga, B.C. Smith and A.R. Wood. *Power System Harmonic Analysis*. John Wiley and Sons Inc, Chichester, UK, 1997.

[31] D. H. Kelly. Visual responses to time-dependent stimuli. I. Amplitude sensitivity measurements. *J. Opt. Soc. Am.*, 51(4):422–429, Apr 1961.

[32] D. H. Kelly. Frequency doubling in visual responses. *J. Opt. Soc. Am.*, 56(11):1628–1632, Nov 1966.

[33] Hamish Duncan Laird. *Modelling and measurement of diode rectifiers and their interaction with shunt active filters*. PhD thesis, University of Canterbury, 2001.

[34] E. V. Larsen, D. H. Baker, and J. C. McIver. Low-order harmonic interactions on AC/DC systems. *Power Delivery, IEEE Transactions on*, 4(1):493–501, 1989. 0885-8977.

[35] Maria L. V. Lisboa. *Three-phase three-limb transformer models in the harmonic domain*. PhD thesis, University of Canterbury, 1996.

[36] Geoffrey Neal Love. *Small signal modelling of power electronic converters, for the study of time-domain waveforms, harmonic domain spectra, and control interactions*. Ph.d. thesis, Electrical and Computer Engineering, University of Canterbury, N.Z., 2007.

[37] E. Mollerstedt and B. Bernhardsson. Out of control because of harmonics-an analysis of the harmonic response of an inverter locomotive. *Control Systems, IEEE*, 20(4):70–81, Aug 2000.

[38] National Instruments. *DAQ M Series User Manual - NI 6229 Device*, 371022k-01 edition, July 2008.

[39] Yoshi Ohno. Detector-based luminous-flux calibration using the absolute integrating-sphere method. *Metrologia*, 35(4):473, 1998.

[40] Jordan Rel C. Orillaza. *Harmonic state space model of three phase thyristor controlled reactor*. PhD thesis, Electrical and Computer Engineering at the University of Canterbury, Christchurch, New Zealand, 2012.

[41] J.R. Orillaza, M.S. Hwang, and A.R. Wood. Switching instant variation in harmonic state-space modelling of power electronic devices. In *Universities Power Engineering Conference (AUPEC), 2010 20th Australasian*, pages 1–5, Dec 2010.

[42] C. M. Osauskas, D. J. Hume, and A. R. Wood. Small signal frequency domain model of an HVDC converter. *Generation, Transmission and Distribution, IEE Proceedings-*, 148(6):573–578, 2001. 1350-2360.

[43] James M Palmer, 1957 Grant, Barbara G. (Barbara Geri), and Knovel (Firm). *The art of radiometry*. Bellingham, Wash. : SPIE Press, 2010. Includes bibliographical references and index.

[44] Erik V. Persson. Calculation of transfer functions in grid-controlled convertor systems. with special reference to h.v. d.c. transmissions. *Electrical Engineers, Proceedings of the Institution of*, 117(5):989–997, May 1970.

[45] M. Piekarz, M. Szlosek, Z. Hanzelka, A. Bien, A. Stankiewicz, and M. Hartman. Comparative tests of flickermeters. In *Harmonics and Quality of Power, 2002. 10th International Conference on*, volume 1, pages 220–227 vol.1, Oct 2002.

[46] T. C. Porter. Contributions to the study of flicker. Paper II. *Proceedings of the Royal Society of London*, 70(459-466):313–329, 1902.

[47] C. Rashbass. The visibility of transient changes of luminance. *The Journal of Physiology*, 210(1):165–186, 1970.

[48] M. Sakulin and H. Renner. Strategy for worldwide applicability of the UIE/IEC flickermeter. 1994.

[49] M. Sakulin, H. Renner, R. Bergeron, T. Key, and D. Nastasi. International recommendation for universal use of the UIE/IEC flickermeter. 1996.

[50] M.S. Shur and A. Zukauskas. Solid-state lighting: Toward superior illumination. *Proceedings of the IEEE*, 93(10):1691–1703, Oct 2005.

[51] K. Simons. Das flackern des lichtes in elektrischen beleuchtungsanlages. *ETZ*, (38):465–468, 1917.

[52] B.C. Smith. *A Harmonic domain model for the interaction of the HVdc convertor with ac and dc systems*. Ph.d. thesis, Electrical and Computer Engineering, University of Canterbury, N.Z., 1996.

[53] B.C. Smith, N.R. Watson, A.R. Wood, and J. Arrillaga. Harmonic tensor linearisation of HVDC converters. *Power Delivery, IEEE Transactions on*, 13(4):1244–1250, Oct 1998.

[54] D.A. Steigerwald, J.C. Bhat, D. Collins, Robert M. Fletcher, M.O. Holcomb, M.J. Ludowise, P.S. Martin, and S.L. Rudaz. Illumination with solid state lighting technology. *Selected Topics in Quantum Electronics, IEEE Journal of*, 8(2):310–320, Mar 2002.

[55] Y. Sun, G. Zhang, W. Xu, and J.G. Mayordomo. A harmonically coupled admittance matrix model for AC/DC converters. *Power Systems, IEEE Transactions on*, 22(4):1574–1582, Nov. 2007.

[56] B. Vyakaranam, M. Madrigal, F.Eugenio Villaseca, and R. Rarick. Dynamic harmonic evolution in facts via the extended harmonic domain method. In *Power and Energy Conference at Illinois (PECI), 2010*, pages 29–38, Feb 2010.

[57] Michael K. Walker. Electric utility flicker limitations. *Industry Applications, IEEE Transactions on*, IA-15(6):644–655, Nov 1979.

[58] Z. Wei, N.R. Watson, and L. P. Frater. Modelling of compact fluorescent lamps. In *Harmonics and Quality of Power, 2008. ICHQP 2008. 13th International Conference on*, pages 1–6, Sept 2008.

[59] N. Wereley. *Analysis and Control of Linear Periodically Time Varying Systems*. PhD thesis, Massachusetts Institute of Technology, 1991.

[60] Alan Ruthven Wood. *An analysis of non-ideal HVDC convertor behaviour in the frequency domain, and a new control proposal*. Ph.d. thesis, Electrical and Computer Engineering, University of Canterbury, N.Z., 1993.